Institut für Nutzpflanzenwissenschaften und Ressourcenschutz (INRES)

der

Rheinischen Friedrich-Wilhelms-Universität Bonn

Identification and functional characterization of *ENHANCED GRAVITROPISM 2* controlling the root setpoint angle in barley (*Hordeum vulgare* L.)

Dissertation

zur Erlangung des Grades

Doktorin der Agrarwissenschaften (Dr. agr.)

der Landwirtschaftlichen Fakultät

der Rheinischen Friedrich-Wilhelms-Universität Bonn

von

Li Guo

aus

Sichuan, China

Bonn, 2023

Referent: Prof. Dr. Frank Hochholdinger

Korreferent: Prof. Dr. Andreas Meyer

Tag der mündlichen Prüfung: 24. Februar 2023

Angefertigt mit Genehmigung der Landwirtschaftlichen Fakultät der Universität Bonn

Abstract

Root gravitropism is a prerequisite for the sessile growth of plants. Gravitropism allows roots to penetrate deep into the soil and is one of the main factors determining the root setpoint angle. Root setpoint angle is the determining factor for the three-dimensional growth of roots in soil, thereby affecting the ability of the plant to capture water and nutrients. Thus, understanding the molecular mechanisms underlying the root setpoint angle of crop species can help to reshape root system architecture to improve adaptation to changing environmental conditions, especially to climate change.

The *enhanced root gravitropism 2* (*egt2*) mutant was identified in a sodium azide-mutagenized barley population based on the hypergravitropic phenotype of its root system. The mutant shows a steeper root system compared with wild type due to the narrower growth angle of the seminal and lateral roots. Gravistimulation assays showed that the *egt2* mutant responded faster and adjusted at a larger angle to gravity compared to wild type plants. Anatomical analyses displayed no differences in the structure and size of the meristem and the elongation zone between *egt2* and wild type, nor in amyloplast content and sedimentation rate. Phytohormone treatments revealed that the auxin response of *egt2* was not disrupted.

The *EGT2* gene was mapped and cloned by a combination of single nucleotide polymorphism-based bulked-segregant analysis and whole genomic sequencing. The candidate gene was validated by a novel CRISPR/Cas9 mutant allele. Expression was studied by *in situ* hybridization and real time quantitative PCR analysis, which demonstrated that *EGT2* is expressed in the whole root tip including the root cap, the meristem and the elongation zone. *EGT2* encodes a sterile alpha motif (SAM) containing protein. Phylogenetic analyses showed that the SAM domain is highly conserved in wheat, Arabidopsis, peach and barley. Mutations of the two *EGT2* orthologs in tetraploid durum wheat resulted in the similar hypergravitropic phenotype of the wheat root system as observed in barley, suggesting that the function of EGT2 is evolutionarily conserved.

Root zone-specific transcriptome analyses of gravistimulated wild type roots in a time-course experiment revealed transcriptome regulation at different phases of the gravity response. These results demonstrated that the largest transcriptome changes in response to gravistimulation occurred in the elongation zone, the zone where root gravitropic bending occurs. This suggests that gravity perception and signal transduction are unlikely mediated on the transcriptome level. Gene Ontology analyses suggested that genes involved in reactive oxygen species metabolism, cytoplasmic microtubule organization and carbohydrate metabolism were differentially expressed in the root cap after gravistimulation. Cell wall organization-, oxidative stress- and

protein phosphorylation-related terms were significantly enriched in differentially expressed genes in the elongation zone.

By comparing *egt2* and wild type in the root cap, the meristem and the elongation zone before and after gravistimulation, we demonstrated that 33% of graviregulated genes in the elongation zone were also regulated by *EGT2*. This suggests that *EGT2* plays a key role in controlling the molecular network associated with gravitropic bending. Gene Ontology analyses suggested that terms associated with biological processes are related to cell wall, reactive oxygen species and protein modification are related to genes regulated by both gravity and *EGT2* in the elongation zone. This is consistent with the results of weighted gene co-expression network analyses, in which we identified a number of modules strongly correlated with genotype and gravistimulation in each root zone. In all three root zones, plant cell wall- and reactive oxygen species-related biological process terms were significantly enriched in the most strongly correlated modules, suggesting a role for *EGT2* in these biological processes.

A number of interaction candidates of EGT2 were identified by yeast-two-hybrid screening. Significantly more interaction candidates encoded by gravity-regulated genes were observed than expected by chance, highlighting the role of EGT2 in the regulation of root gravitropism. Validation of selected proteins encoded by gravity- and *EGT2*-regulated genes by bimolecular fluorescence complementation identified three direct interaction partners of EGT2 that are involved in cell wall organization and flavonoid metabolism. This is consistent with a role of *EGT2* in the elongation zone, where gravity perception is executed by asymmetric cell elongation on the upper and lower sides of the root tip, leading to gravitropic bending.

In summary, in this study we cloned and characterized *EGT2*, an evolutionarily conserved regulator of root setpoint angle in barley and demonstrated a substantial role of *EGT2* in controlling the molecular networks underlying root gravitropic bending in response to gravistimulation.

Zusammenfassung

Wurzelgravitropismus ist eine Voraussetzung für das sessile Wachstum von Pflanzen. Der Gravitropismus ermöglicht es den Wurzeln, tief in den Boden einzudringen, und ist einer der Hauptfaktoren, die den Wurzelansatzwinkel bestimmen. Der Wurzelansatzwinkel ist der entscheidende Faktor für die dreidimensionale Verteilung der Wurzeln im Boden und wirkt sich somit auf die Fähigkeit der Pflanze aus, Wasser und Nährstoffe aufzunehmen. Das Verständnis der molekularen Mechanismen, die den Wurzelansatzwinkel von Nutzpflanzen bestimmen, kann daher dazu beitragen, die Architektur des Wurzelsystems neu zu gestalten, um die Anpassung an sich ändernde Umweltbedingungen, insbesondere an den Klimawandel, zu verbessern.

Die Mutante *enhanced root gravitropism 2* (*egt2*) wurde in einer mit Natriumazid mutagenisierten Gerstepopulation aufgrund des hypergravitropischen Phänotyps ihres Wurzelsystems identifiziert. Die Mutante weist im Vergleich zum Wildtyp ein steileres Wurzelsystem auf, was auf den geringen Wachstumswinkel der Seminal- und Seitenwurzeln zurückzuführen ist. Gravistimulationsexperimente zeigten, dass die *egt2*-Mutante schneller reagierte und sich mit Hilfe eines größeren Wurzelwinkels an die Schwerkraft anpasste als Wildtyp-Pflanzen. Anatomische Analysen zeigten keine Unterschiede in der Struktur und Größe des Meristems und der Elongationszone zwischen *egt2* und dem Wildtyp sowie im Amyloplastengehalt und der Sedimentationsrate. Phytohormonbehandlungen zeigten, dass die Auxinreaktion von *egt2* nicht gestört war.

Das *EGT2*-Gen wurde durch eine Kombination aus SNP (single nucleotide polymorphism)-basierter BSA (*bulked-segregant* analysis) und vollständiger Genomsequenzierung kartiert und kloniert. Das Kandidatengen wurde durch ein neues CRISPR/Cas9-Mutanten-Allel validiert. Die Expression wurde mittels *in-situ*-Hybridisierung und quantitativer Echtzeit-PCR-Analyse untersucht. Dabei zeigte sich, dass *EGT2* in der gesamten Wurzelspitze einschließlich der Wurzelhaube, dem Meristem und der Elongationszone exprimiert wird. *EGT2* kodiert für ein Protein, das ein steriles Alpha-Motiv (SAM) enthält. Phylogenetische Analysen zeigten, dass die SAM-Domäne in Weizen, Arabidopsis, Pfirsich und Gerste hoch konserviert ist. Mutationen der beiden *EGT2*-Orthologe in tetraploidem Hartweizen führten zu einem ähnlichen hypergravitropischen Phänotyp des Weizenwurzelsystems, wie er in Gerste beobachtet wurde, was darauf schließen lässt, dass die Funktion von EGT2 evolutionär konserviert ist.

Wurzelzonenspezifische Transkriptomanalysen von gravistimulierten Wildtypwurzeln in einem Zeitverlaufsexperiment zeigten eine Transkriptomregulierung in verschiedenen Phasen

der Schwerkraftreaktion. Die Ergebnisse zeigten, dass die größten Transkriptomveränderungen als Reaktion auf die Gravitationsstimulation in der Elongationszone auftraten, der Zone, in der die gravitropische Biegung der Wurzeln stattfindet. Dies deutet darauf hin, dass Schwerkraftwahrnehmung und Signaltransduktion wahrscheinlich nicht auf Transkriptomebene vermittelt werden. Gen-Ontologie-Analysen ergaben, dass Gene, die am Stoffwechsel reaktiver Sauerstoffspezies, an der zytoplasmatischen Mikrotubuli-Organisation und am Kohlenhydratstoffwechsel beteiligt sind, in der Wurzelhaube nach Gravistimulation unterschiedlich exprimiert wurden. Begriffe, die mit Zellwandorganisation, oxidativem Stress und Proteinphosphorylierung zusammenhängen, waren bei den unterschiedlich exprimierten Genen in der Elongationszone deutlich angereichert.

Durch den Vergleich von *egt2* und dem Wildtyp in der Wurzelhaubee, dem Meristem und der Elongationszone vor und nach der Gravistimulation konnten wir zeigen, dass 35% der gravieregulierten Gene in der Elongationszone ebenfalls durch *EGT2* reguliert wurden. Dies deutet darauf hin, dass *EGT2* eine Schlüsselrolle bei der Kontrolle des molekularen Netzwerks im Zusammenhang mit der gravitropischen Biegung spielt. Gen-Ontologie-Analysen ergaben, dass Begriffe, die mit biologischen Prozessen in Verbindung stehen, mit Zellwand, reaktiven Sauerstoffspezies und Proteinmodifikation mit Genen assoziiert sind, die sowohl durch Schwerkraft als auch durch *EGT2* in der Dehnungszone reguliert werden. Dieses Ergebnis steht im Einklang mit den Analysen gewichteter Gen-Koexpressionsnetzwerke, durch die wir eine Reihe von Modulen identifiziert haben, die stark mit dem Genotyp und der Gravistimulation in jeder Wurzelzone korreliert sind. In allen drei Wurzelzonen wurden Begriffe aus den Bereichen Pflanzenzellwand und reaktive Sauerstoffspezies signifikant in den am stärksten korrelierten Modulen angereichert, was auf eine Rolle von *EGT2* in diesen Prozessen hindeutet.

Eine Reihe von Interaktionskandidaten von EGT2 wurden durch Hefe-Zwei-Hybrid-Screening identifiziert. Es wurden deutlich mehr Interaktionskandidaten beobachtet, die von durch die Schwerkraft regulierten Genen kodiert werden als zufällig erwartet, was die Rolle von *EGT2* bei der Regulierung des Wurzelgravitropismus unterstreicht. Bei der Validierung ausgewählter Proteine, die von durch Schwerkraft und *EGT2* regulierten Genen kodiert werden, durch bimolekulare Fluoreszenzkomplementierung wurden drei direkte Interaktionspartner von EGT2 identifiziert, die an der Zellwandorganisation und dem Flavonoidstoffwechsel beteiligt sind. Dies deutet auf eine Rolle von *EGT2* in der Elongationszone hin, wo die Schwerkraftwahrnehmung durch asymmetrische Zelldehnung an der Ober- und Unterseite der Wurzelspitze erfolgt, was zu einer gravitropischen Biegung führt.

Zusammenfassung

Zusammenfassend lässt sich sagen, dass wir in dieser Studie *EGT2* kloniert und charakterisiert haben, einen evolutionär konservierten Regulator des Wurzelansatzswinkels in Gerste, und dass wir eine wesentliche Rolle von *EGT2* bei der Kontrolle der molekularen Netzwerke nachgewiesen haben, die der gravitropischen Wurzelbiegung als Reaktion auf Gravistimulation zugrunde liegen.

List of Abbreviations

AGO	Anti-gravitropic offset
AS	Acetosyringone
AUX/IAAs	Auxin/indole-3-acetic acid family members
BiFC	Bimolecular fluorescence complementation
CO_2	Carbon dioxide
DEGs	differentially expressed genes
DRO1	DEEPER ROOTING 1
E	Elongation zone
EGT1/2	ENHANCED GRAVITROPISM 1/2
ER	Endoplasmic reticulum
FDR	False discovery rate
GO	Gene Ontology
GTF	Glycosyltransferase
GXM	Glucuronoxylan 4-O-methyltransferase
HMT	Heavy metal transport/detoxification
IAA	Indole-3-acetic acid
LB	Lysogeny broth
log_2FC	log_2 fold change
M	Meristem
MES	2-morpholinoethanesulfonic acid
NO	Nitric oxide
OMT	O-methyltransferase
PCA	Principal component analysis
PIN	PIN-FORMED
QC	Quiescent-center
qRT-PCR	Real-time quantitative RT-PCR
RC	Root cap
RIN	RNA integrity number
RNA-seq	RNA sequencing
ROS	Reactive oxygen species
SAM	sterile alpha motif
WGCNA	weighted gene co-expression network analysis

Table of contents

List of figures

List of Supplementary Data: Chapter 2

List of Supporting Information: Chapter 3

General Introduction

For decades, greenhouse gas emissions have been increasing as a result of global population growth. Carbon Dioxide (CO_2) is one of the most important greenhouse gases. Around half of the CO_2 generated by human activities is not absorbed by the ocean and ecosystems, but remains in the atmosphere (WMO, https://public.wmo.int). The rising concentration of greenhouse gases in the atmosphere is the first driver of global climate disruption, leading to an increase in global mean surface temperature (Wheeler & von Braun, 2013). Recent studies demonstrated that by 2021, the global mean surface temperature has increased by 1.1°C from the pre-industrial baseline (1850-1900, WMO).

There are ample indications that climate change will have a dramatic impact on agricultural production systems, including a negative impact on the yield of major crops (FAO, https://www.fao.org). The increasing demand for agricultural products due to population growth and the potential decline in agricultural productivity due to climate change makes the challenge of achieving food security for future generations one of the most important topics of agricultural research.

1.1 Barley is a promising model for studying agricultural adaptation to climate change

Barley (*Hordeum vulgare* L.) is one of the most important cultivated grains in the world. Modern barley was domesticated from wild barley (*H. vulgare ssp. spontaneum*) about 11,000 years ago (Fuller & Weisskopf, 2014). Barley is the fourth most productive crop in the world after maize, rice and wheat, with an annual world production of about 157 million tons in 2020. More than 60% of barley is produced in Europe (https://www.fao.org/faostat/en/#data/QCL). Barley contains many nutrients required by human and animals (Baik & Ullrich, 2008). In ancient times, barley was used as an important part of the basic diet and was a staple food in different regions of the globe, including Asia, North Africa and Europe. Over the centuries, since the popularity of wheat, rice and other cereals for human consumption increased, barley has been used mainly as animal fodder and as a fermentable material for beer and other non-alcoholic barley beverages. Recent studies on the health effects of barley have renewed interest in barley. Compared with other crops, barley grains are rich in dietary fibers, such as ß-glucan, which would protect humans from cardiovascular diseases (Newton *et al.*, 2011; Rani *et al.*, 2021; Geng *et al.*, 2022). Analyses in mice suggested that lifelong barley intake was beneficial for healthy aging (Shimizu *et al.*, 2019). In addition, barley has a number of uses that cannot be replaced by other crops, for instance, malt whisky can only be made from barley.

With a high degree of environmental adaptability, barley spread throughout Eurasia 4000 years ago and is now distributed throughout the world. Barley can be cultivated at high and low altitudes as well as in temperate and tropical areas, making it more widespread than almost any other crop species (Paulitz & Steffenson, 2010). Moreover, barley has a relatively short growth period and different sowing and harvesting dates compared to other major crops. Therefore, barley is an important component of crop rotation. In addition, barley has been shown to be more tolerant to drought and soil salinity compared with wheat and other small grain crops (Munns *et al.*, 2006). This allows barley to produce higher and more stable yields under unfavorable conditions than wheat and other small grains (Newton *et al.*, 2011). Therefore, barley is a promising model for studying agricultural adaptation to climate change (Dawson *et al.*, 2015).

Barley is diploid with seven pairs of chromosomes. The first reference genome of barley cultivar (cv.) Morex was published in 2012 (Mayer *et al.*, 2012) and has been updated three times to date (Mascher *et al.*, 2017, 2021; Monat *et al.*, 2019). As one of the crop species with a large genome, barley has a haploid genome size of approximately 5.3 Gb, more than twice the size of the maize genome and more than twelve times the size of the rice genome. In the newest reference genome (MorexV3, https://wheat.pw.usda.gov/GG3/content/morex-v3-files-2021) 81,687 gene models were predicted. Of these, 35,827 were identified as high confidence gene models.

1.2 Root setpoint angle is closely related to water and nutrient uptake by plants

As the “hidden-half” of plants, roots play a crucial role in development by anchoring the upper parts of the plant to the ground and by acquiring water and nutrients from the soil. In addition, roots act as the primary interface through which plants communicate with the changing environment, including sensing of abiotic and biotic stresses and responding accordingly. The distribution of the root system in the soil determines the resistance of the plant to external stimuli and their access to water and nutrients, thus affecting their ability to adapt to different environments (Wang *et al.*, 2018; Alahmad *et al.*, 2019).

The angle at which the root is placed relative to gravity is defined as the gravitropic setpoint angle, which is one of the most critical traits affecting the root distribution in different soil layers (Kawamoto et al., 2020). In general, a larger root setpoint angle leads to a deeper root system which facilitates access to water and mobile nutrients, including nitrogen, one of the most essential nutrients needed by plants (Feng *et al.*, 2020). A deeper root system is also beneficial for plants to grow in windy areas and for improving soil conditions (Uga *et al.*, 2015).

Conversely, smaller root setpoint angles result in a shallower root system that favors the uptake of immobile nutrients that tend to accumulate in the topsoil, such as phosphorus (Uga *et al.*, 2015). Therefore, the root setpoint angle is closely related to plant development and is now an important morphological trait for crop breeding (Toal *et al.*, 2018).

Root development is affected by a variety of environmental factors, including gravity, water, light, obstacles and soil density (Ramalingam *et al.*, 2017; Toal *et al.*, 2018; Alahmad *et al.*, 2019; Ober *et al.*, 2021). In response to these environmental stimuli, plants change their root setpoint angle accordingly, a phenomenon referred to as tropism. Among the different tropisms, root gravitropism directs root growth in response to gravity, and is therefore an important determinant of root setpoint angle (Toal *et al.*, 2018; Ober *et al.*, 2021; Fusi *et al.*, 2022).

1.3 Root gravitropism

Gravitropism allows plants to adjust the growth direction of their shoots and roots according to the direction of gravity. In general, gravitropism directs shoots to grow upward (negative gravitropism) and roots to grow downward (positive gravitropism). Therefore, shoots are able to use sunlight for efficient photosynthesis and resume upward growth after being reoriented by external factors such as wind and rain. Roots can penetrate deeply into the soil, thus contributing to plant anchoring and communication with the environment (Chen *et al.*, 1999; Jiao *et al.*, 2021).

Among the different species of vascular plants that possess true roots, two different patterns of root gravitropism have emerged during evolution. The root gravitropic response in lycophytes and ferns is slow, whereas the root gravitropism in seeds plants is faster and more efficient (Zhang *et al.*, 2019b). In flowering plants, root gravitropism can be divided into three spatiotemporally separated stages, including the perception of gravity signals primarily in the root cap, signal transduction through the root cap and the meristem and signal execution translated into a bending response in the elongation zone (Su *et al.*, 2017, 2020).

1.3.1 Root gravity perception

The essential role of the root cap in root gravity perception has been proposed by Ciesielski (1872) and Darwin (1880) based on the results of surgical experiments: de-capped roots with unaffected growth rate do not display gravitropic bending (Chen *et al.*, 1999). This hypothesis was further substantiated by other studies. Ablating the columella cells in the root cap by laser, genetics and heavy-ion microbeams all significantly altered the root gravitropic response (Blancaflor *et al.*, 1998; Tsugeki & Fedoroff, 1999; Tanaka *et al.*, 2002; Suzuki *et al.*, 2016).

In Arabidopsis, the first two layers of columella cells in the root cap play a predominant role in gravity perception (Blancaflor *et al.*, 1998). Columella cells are highly polarized with a peripherally localized endoplasmic reticulum (ER) and other organelles, centrally positioned vacuoles, and many amyloplasts located at the bottom of the cells (Figure 1.1; Stoker & Moore, 1984; Leitz *et al.*, 2009; Su *et al.*, 2020). From an evolutionary perspective, the fast root gravitropic response in seed plants is consistent with the exclusive localization of amyloplasts in the root cap. However, in roots of lycophyte, amyloplasts are distributed only in the cells above the root cap. In roots of ferns, amyloplasts are distributed in cells above the root cap in addition to the root cap cells (Zhang *et al.*, 2019b). This suggests that the unique localization of amyloplasts in the root cap is critical for fast gravitropism.

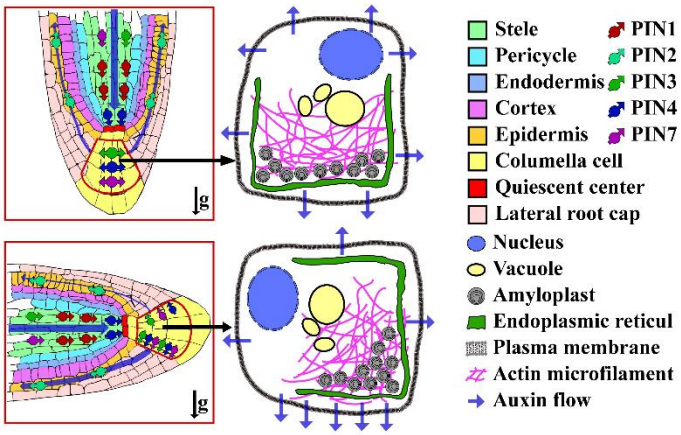

Figure 1.1: Model illustrating the cellular and molecular basis of root gravity perception. Before rotation (top), amyloplasts in columella cells localize to the bottom of cell and PIN (PIN-FORMED) proteins in columella cells are uniformly distributed. After rotating by 90° (bottom), the amyloplasts relocalize to the new bottom of the columella cells along with the direction of gravity vector, triggering polar localization of PINs within the columella cell. This allows auxin transport towards the new bottom side of the root tip (modified from Jiao *et al.*, 2021)

Based on the starch-statolith hypothesis, gravity perception is achieved by the repositioning of starch-filled amyloplasts in columella cells, which are relocalized to the new bottom side of the cell under gravity stimulus (Figure 1.1, Baldwin *et al.*, 2013). Studies of root gravitropism in starch-related mutants have shown a correlation between starch content of amyloplasts in columella cells and root gravitropic response (Caspar & Pickard, 1989; Kiss *et al.*, 1996; Li *et al.*, 2020; Su *et al.*, 2020). Displacement of amyloplasts in columella cells of vertical roots by magnetic force leads to root bending similar to that of gravistimulated roots (Kuznetsov & Hasenstein, 1996). These results support the starch-statolith hypothesis and make it the most widely accepted hypothesis regarding gravity perception. Modifying the stability of actin filaments by pharmacological treatments or genetic approaches revealed that the sedimentation

of amyloplasts in columella cells is fine-tuned by the actin filament network (Hou *et al.*, 2003; Mancuso *et al.*, 2006; Zheng *et al.*, 2015).

A secondary mechanism of gravity perception outside the root cap but in the distal elongation zone has been proposed. First, keeping the root cap in a vertical orientation and the distal elongation zone at a gravistimulated angle by the *rotato* system induced the root to continue bending (Wolverton *et al.*, 2002). This suggests that gravistimulation in the distal elongation zone alone can also induce a root gravitropic response. Second, decapped roots of maize seedlings still showed the ability to bend towards gravity (Mancuso *et al.*, 2006). Reasonable observations suggested that gravity perception in the distal elongation zone might be mediated by actin turnover (Mancuso *et al.*, 2006).

1.3.2 Root gravity signal transduction

Gravity perception in columella cells triggers the next gravity signal transduction process, in which the physical signal of amyloplast sedimentation is converted into a biochemical signal (Nakamura *et al.*, 2019). Applying [^{3}H]-labeled indole-3-acetic acid (IAA) asymmetrically to maize roots resulted in auxin movement across the root cap to the new lower side in response to gravistimulation (Figure 1.2; Young *et al.*, 1990). Further experiments demonstrated that the lateral auxin gradient generated across the root cap is transported through the meristem to the elongation zone to trigger the bending response (Figure 1.2; Su *et al.*, 2017, 2020). These results suggest that auxin is a central factor mediating root gravity signal transduction.

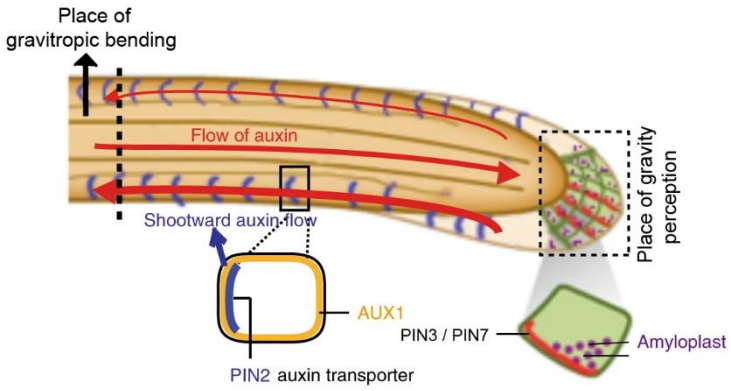

Figure 1.2: Schematic diagram showing polar auxin transport in the root tip in response to gravitropic stimulation. Asymmetrically distributed auxin across the root cap is transported towards the elongation zone via shootward localized PIN2, resulting in a higher auxin content on the lower side and a lower auxin content on the upper side of the root tip (modified form Zhang *et al.*, 2019b).

Auxin is synthesized mainly in the aerial parts of plants, including the apical meristems, young leaves, and flower buds (Band et al., 2012; Zhang et al., 2019a). In the root, auxin transported from the shoot mixes with root-produced auxin in the quiescent-center (QC) located above the

columella to form an auxin maximum. Auxin is then redistributed from the QC cells to the surrounding tissues of the root cap in response to the different demands (Ljung et al., 2005; Brumos et al., 2018). Auxin import from the apoplast into the cytoplasm is achieved by free diffusion (protonated auxin) or mediated by auxin influx carriers of the AUX1/LAX family (ionized auxin). The export of auxin from the cytoplasm is mediated by efflux carriers, including PIN-FORMED (PINs) proteins and P-glycoprotein-type transporters (Su *et al.*, 2020). Ingeniously, the polar localization of PINs allows them to determine the direction of auxin transport. In gravistimulated Arabidopsis roots, PIN3/7 are relocalized to the new bottom side of columella cells, facilitating downward auxin transport and the formation of a lateral auxin gradient across the root cap (Figure 1.2; Grones *et al.*, 2018). Once the asymmetric auxin gradient is established, the shootward-localized PIN2 directs auxin transport through the lateral root cap and epidermal cells towards the elongation zone. This results in higher auxin concentrations in the lower flanks of the elongation zone (Figure 1.2; Chen *et al.*, 1999; Abas *et al.*, 2006; Zhang *et al.*, 2019a; Su *et al.*, 2020). In addition, PIN2 also displays rootward localization in cortical cells in the distal elongation zone, which enables auxin to move back into the vasculature and root cap, which is also required for root gravitropism (Wisniewska *et al.*, 2006; Su *et al.*, 2020).

The polar localization of PINs is mainly modulated by reversible phosphorylation (Friml *et al.*, 2004; Michniewicz *et al.*, 2007). For instance, in Arabidopsis, phosphorylation facilitates rootward localization of PIN2, whereas dephosphorylated PIN2 localizes to the shootward direction of cells (Grones *et al.*, 2018; Su *et al.*, 2020). It has been demonstrated that type AGCVIII serine/threonine protein kinases regulate phosphorylation, while type-IIA protein phosphatase complexes modulate dephosphorylation of PINs (Friml *et al.*, 2004; Michniewicz *et al.*, 2007; Grones *et al.*, 2018). In addition, inositol trisphosphate (InsP3) played a role in modulating polar localization of PIN proteins and auxin transport, which was mediated by Ca^{2+} signaling (Zhang *et al.*, 2011), supporting the involvement of InsP3 and Ca^{2+} in mediating gravity signal transduction (Perera *et al.*, 2006; Toyota *et al.*, 2008; Salinas-Mondragon *et al.*, 2010; Zhao *et al.*, 2022).

1.3.3 Root gravitropic bending

Asymmetrically distributed auxin along the gravistimulated root tip triggers differential elongation of epidermal cells in the opposite flanks of the distal elongation zone (Chen *et al.*, 1999; Su *et al.*, 2020). In the upper flanks of the elongation zone of gravistimulated roots, the lower auxin content in the epidermal cells activates H^+ pumps, leading to a decrease in apoplastic pH. This activates members of the expansin and xyloglucan

endotransglucosylase/hydrolases (XTHs) protein families, two major cell wall modifying protein families and therefore increases cell elongation. In contrast, in the lower flanks of the gravistimulated elongation zone, higher auxin concentration in the epidermal cells activates H^+/OH^- antiporters. This results in an increase in cytoplasmic pH accompanied by increased cell wall rigidity, which ultimately inhibits cell elongation. Eventually, increased elongation of the upper flank and suppressed elongation of the lower flank lead to root bending along the gravity vector in the distal elongation zone (Singh *et al.*, 2017; Su *et al.*, 2017; 2020). A number of experiments suggested that other signaling factors, including nitric oxide (NO) and reactive oxygen species (ROS), are involved in the processes of root gravitropic bending (Liszkay *et al.*, 2004; Xiong *et al.*, 2015; Krieger *et al.*, 2016; Vembu, 2017).

1.4 Antigravitropic offset

Intriguingly, most roots grow with a non-vertical gravitropic setpoint angle, and even if these roots are placed in the direction of gravity, they will still grow back to their original gravitropic setpoint angle (Roychoudhry & Kepinski, 2015). This suggests that the root gravitropic setpoint angle is controlled by both gravitropism and an anti-gravitropic growth component, which is referred to as anti-gravitropic offset (Roychoudhry *et al.*, 2017). It has been shown that auxin is involved in the anti-gravitropic offset, mediated by the TIR1/AFB-Aux/IAA-ARF-dependent signaling pathway in columella cells (Figure 13; Roychoudhry *et al.*, 2013; Kawamoto *et al.*, 2020).

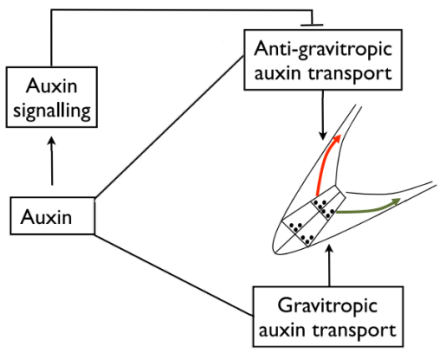

Figure 1.3: Model of the regulation of gravitropic setpoint angle by auxin. Auxin-dependent gravitropic (green arrow) and anti-gravitropic offset (red arrow) are indicated (Roychoudhry *et al.*, 2013).

In Arabidopsis, mutations in the *LAZY1-LIKE* (*LZY*) family genes resulted in an agravitropic phenotype (Kawamoto *et al.*, 2020). Phenotypic analysis of *lzy* mutants confirmed the important role of amyloplast-containing columella cells in maintaining the gravitropic response and anti-gravitropic offset (Kawamoto *et al.*, 2020). More recently, the barley gene, *ENHANCED GRAVITROPISM 1* (*EGT1*), has been proposed to function in anti-gravitropic offset-related

processes in an auxin-independent manner (Fusi *et al.*, 2022). Nevertheless, detailed knowledge about the anti-gravitropic offset remains largely unknown compared to the understanding of the mechanism underlying root gravitropic response (Roychoudhry *et al.*, 2013, 2017; Roychoudhry & Kepinski, 2015; Kawamoto *et al.*, 2020).

1.5 Genes involved in regulation of root setpoint angle in crop species

To date, several genes related to root setpoint angle have been cloned in crop species. The Rice Morphology Determinant (RMD) protein controls root growth angle by linking the statoliths and actin filaments in columella cells, allowing the shallower root system to respond to low phosphate conditions (Huang *et al.*, 2018). In contrast, the rice *DEEPER ROOTING 1* (*DRO1*) gene, involved in asymmetric cell elongation in the distal elongation zone upon gravity stimulus, controls a narrower and deeper root system (Uga *et al.*, 2013). This increases yield under water-deficient conditions (Uga *et al.*, 2013). Moreover, *qSOR1*, a homolog of *DRO1*, has been shown to function in modifying root angles, thereby increasing yield in saline paddy soils (Kitomi *et al.*, 2020). In wheat and barley, the *VERNALIZATION1* gene has been proved play a role in modulating root architecture (Voss-Fels *et al.*, 2018). Mutation of the maize *ZmCIPK15* gene, which encodes calcineurin B-like protein (CBL)-interacting serine/threonine-protein kinase 15, results in a steeper root system and increased nitrogen accumulation in the shoot (Schneider *et al.*, 2022). This suggests a role for *ZmCIPK15* in improving crop performance under low nitrogen conditions (Schneider *et al.*, 2022). Recently, the barley mutant *enhanced gravitropism 1* (*egt1*) with enhanced root gravitropism has been identified, and it is proposed that the causative gene *HvEGT1* encodes a putative anti-gravitropic offset component regulating cell wall stiffness (Fusi *et al.*, 2022).

1.6 Aims of this study

The overall objective of the study was cloning and functional characterization the *ENHANCED GRAVITROPISM2* (*EGT2*) gene to explore the role of *EGT2* in the control of barley seminal root setpoint angle. The hypotheses below were investigated:

1. The enhanced gravitropism of *egt2* mutant is caused by mutation of *EGT2* gene, which causes no other morphological defects compared to wild type.
2. The function of EGT2 in regulating the root setpoint angle is conserved between barley and wheat and similar to its homolog in Arabidopsis.
3. *EGT2* is expressed in the whole root tip and the mutation of *EGT2* in the *egt2* mutant

affects its expression.

4. Transcriptomic dynamics of wild type seminal roots in response to gravistimulation varies in distinct root zones.
5. *EGT2* plays a central role in remodeling the transcriptomic landscape of barley seminal roots in response to gravistimulation.
6. EGT2 functions in cell wall and reactive oxygen species-related processes.
7. EGT2 regulates root setpoint angle by mediating the expression of gravity responsive genes and interacts with proteins encoded by gravity- and *EGT2*-regulated genes.

1.7 References

Abas L, Benjamins R, Malenica N, Paciorek TT, Wiřniewska J, Moulinier-Anzola JC, Sieberer T, Friml J, Luschnig C. (2006). Intracellular trafficking and proteolysis of the Arabidopsis auxin-efflux facilitator PIN2 are involved in root gravitropism. *Nature Cell Biology*, 8, 249–256.

Alahmad S, El Hassouni K, Bassi FM, Dinglasan E, Youssef C, Quarry G, Aksoy A, Mazzucotelli E, Juhász A, Able JA, Christopher J, Voss-Fels KP, Hickey LT. (2019). A major root architecture QTL responding to water limitation in durum wheat. *Frontiers in Plant Science*, 10, 436.

Baik BK, Ullrich SE. (2008). Barley for food: Characteristics, improvement, and renewed interest. *Journal of Cereal Science*, 48, 233–242.

Baldwin KL, Strohm AK, Masson PH. (2013). Gravity sensing and signal transduction in vascular plant primary roots. *American Journal of Botany*, 100, 126–142.

Blancaflor EB, Fasano JM, Gilroy S. (1998). Mapping the functional roles of cap cells in the response of Arabidopsis primary roots to gravity. *Plant Physiology*, 116, 213–222.

Caspar T, Pickard BG. (1989). Gravitropism in a starchless mutant of Arabidopsis. *Planta*, 177, 185–197.

Chen R, Rosen E, Masson PH. (1999). Gravitropism in higher plants. *Plant Physiology*, 120, 343–350.

Dawson IK, Russell J, Powell W, Steffenson B, Thomas WTB, Waugh R. (2015). Barley: a translational model for adaptation to climate change. *New Phytologist*, 206, 913–931.

Feng H, Fan X, Miller AJ, Xu G. (2020). Plant nitrogen uptake and assimilation: regulation of cellular pH homeostasis. *Journal of Experimental Botany*, 71, 4380–4392.

Friml J, Yang X, Michniewicz M, Weijers D, Quint A, Tietz O, Benjamins R, Ouwerkerk PBF, Ljung K, Sandberg G, Hooykaas PJ, Palme K, Offringa R. (2004). A PINOID-dependent binary switch in apical-basal PIN polar targeting directs auxin efflux. *Science*, 306, 862–865.

Fuller DQ, Weisskopf A. (2014). Barley: origins and development. In *Smith, C. (eds) Encyclopedia of Global Archaeology*, Springer, New York, NY. https://doi.org/10.1007/978-1-4419-0465-2_2168.

Fusi R, Rosignoli S, Lou H, Sangiorgi G, Bovina R, Pattem JK, Borkar AN, Lombardi M,

Forestan C, Milner SG, Davis JL, Lale A, Kirschner GK, Swarup R, Tassinari A, Pandey BK, York LM, Atkinson BS, Sturrock CJ, Mooney SJ, Hochholdinger F, Tucker MR, Himmelbach A, Stein N, Mascher M, Nagel KA, De Gara L, Simmonds J, Uauy C, Tuberosa R, Lynch JP, Yakubov GE, Bennett MJ, Bhosale R, Salvi S. (2022). Root angle is controlled by *EGT1* in cereal crops employing an antigravitropic mechanism. *Proceedings of the National Academy of Sciences*, 119, e2201350119.

Geng L, Li M, Zhang G, Ye L.(2022). Barley: a potential cereal for producing healthy and functional foods. *Food Quality and Safety*, 6, 1–13.

Grones P, Abas M, Hajný J, Jones A, Waidmann S, Kleine-Vehn J, Friml J. (2018). PID/WAG-mediated phosphorylation of the Arabidopsis PIN3 auxin transporter mediates polarity switches during gravitropism. *Scientific Reports*, 8, 1–11.

Hou G, Mohamalawari DR, Blancaflor EB. (2003). Enhanced gravitropism of roots with a disrupted cap actin cytoskeleton. *Plant Physiology*, 131, 1360–1373.

Huang G, Liang W, Sturrock CJ, Pandey BK, Giri J, Mairhofer S, Wang D, Muller L, Tan H, York LM, Yang J, Song Y, Kim YJ, Qiao Y, Xu J, Kepinski S, Bennett MJ, Zhang D. (2018). Rice actin binding protein RMD controls crown root angle in response to external phosphate. *Nature Communications*, 9, 1–9.

Jiao Z, Du H, Chen S, Huang W, Ge L. (2021). *LAZY* Gene family in plant gravitropism. *Frontiers in Plant Science*, 11, 2096.

Kawamoto N, Kanbe Y, Nakamura M, Mori A, Morita MT. (2020). Gravity-sensing tissues for gravitropism are required for “anti-gravitropic” phenotypes of *lzy* multiple mutants in Arabidopsis. *Plants*, 9, 615.

Kiss JZ, Wright JB, Caspar T. (1996). Gravitropism in roots of intermediate-starch mutants of Arabidopsis. *Physiologia Plantarum*, 97, 237–244.

Kitomi Y, Hanzawa E, Kuya N, Inoue H, Hara N, Kawai S, Kanno N, Endo M, Sugimoto K, Yamazaki T, Sakamoto S, Sentoku N, Wu J, Kanno H, Mitsuda N, Toriyama K, Sato T, Uga Y. (2020). Root angle modifications by the *DRO1* homolog improve rice yields in saline paddy fields. *Proceedings of the National Academy of Sciences of the United States of America*, 117, 21242–21250.

Knight TA. (1806). On the direction of the radicle and germen during the vegetation of seeds. *Philosophical Transactions of the Royal Society of London*, 96, 99–108.

Krieger G, Shkolnik D, Miller G, Fromm H. (2016). Reactive oxygen species tune root tropic responses. *Plant Physiology*, 172, 1209–1220.

Kuznetsov OA, Hasenstein KH. (1996). Intracellular magnetophoresis of amyloplasts and induction of root curvature. *Planta*, 198, 87–94.

Leitz G, Kang BH, Schoenwaelder MEA. (2009). Statolith sedimentation kinetics and force transduction to the cortical endoplasmic reticulum in gravity-sensing *Arabidopsis* columella cells. *The Plant Cell*, 21, 843–860.

Li Y, Wang Y, Tan S, Li Z, Yuan Z, Glanc M, Domjan D, Wang K, Xuan W, Guo Y, Gong Z, Friml J, Zhang J. (2019). Root growth adaptation is mediated by PYLs ABA receptor-PP2A protein phosphatase complex. *Advanced Science*, 7, 1901455.

Liszkay A, Van Der Zalm E, Schopfer P. (2004). Production of reactive oxygen intermediates ($O^{2\cdot-}$, H_2O_2, and $^{\cdot}OH$) by maize roots and their role in wall loosening and elongation growth. *Plant Physiology*, 136, 3114–3123.

Mancuso S, Barlow PW, Volkmann D, Baluška F, Baluska F. (2006). Actin turnover-mediated gravity response in maize root apices gravitropism of decapped roots implicates gravisensing outside of the root cap. *Plant Signaling & Behavior*, 1, 52-8.

Mascher M, Gundlach H, Himmelbach A, Beier S, Twardziok SO, Wicker T, Radchuk V, Dockter C, Hedley PE, Russell J, Bayer M, Ramsay L, Liu H, Haberer G, Zhang XQ, Zhang Q, Barrero RA, Li L, Taudien S, Groth M, Felder M, Hastie A, Šimková H, Staňková H, Vrána J, Chan S, Muñoz-Amatriaín M, Ounit R, Wanamaker S, Bolser D, Colmsee C, Schmutzer T, Aliyeva-Schnorr L, Grasso S, Tanskanen J, Chailyan A, Sampath D, Heavens D, Clissold L, Cao S, Chapman B, Dai F, Han Y, Li H, Li X, Lin C, McCooke JK, Tan C, Wang P, Wang S, Yin S, Zhou G, Poland JA, Bellgard MI, Borisjuk L, Houben A, Doležel J, Ayling S, Lonardi S, Kersey P, Langridge P, Muehlbauer GJ, Clark MD, Caccamo M, Schulman AH, Mayer KFX, Platzer M, Close TJ, Scholz U, Hansson M, Zhang G, Braumann I, Spannagl M, Li C, Waugh R, Stein N, (2017). A chromosome conformation capture ordered sequence of the barley genome. *Nature*, 544, 427–433.

Mascher M, Wicker T, Jenkins J, Plott C, Lux T, Koh CS, Ens J, Gundlach H, Boston LB, Tulpová Z, Holden S, Hernández-Pinzón I, Scholz U, Mayer KFX, Spannagl M, Pozniak CJ, Sharpe AG, Šimková H, Moscou MJ, Grimwood J, Schmutz J, Stein N. (2021). Long-read sequence assembly: a technical evaluation in barley. *The Plant Cell*, 33, 1888–1906.

Mayer KFX, Waugh R, Langridge P, Close TJ, Wise RP, Graner A, Matsumoto T, Sato K, Schulman A, Langridge P, Platzer M, Fincher GB, Muehlbauer GJ, Sato K, Close TJ, Wise RP, Stein N. (2012). A physical, genetic and functional sequence assembly of the barley genome. *Nature*, 491, 711–716.

Michniewicz M, Zago MK, Abas L, Weijers D, Schweighofer A, Meskiene I, Heisler MG, Ohno C, Zhang J, Huang F, Schwab R, Weigel D, Meyerowitz EM, Luschnig C, Offringa R, Friml J. (2007). Antagonistic regulation of PIN phosphorylation by PP2A and PINOID directs auxin flux. *Cell*, 130, 1044–1056.

Monat C, Padmarasu S, Lux T, Wicker T, Gundlach H, Himmelbach A, Ens J, Li C, Muehlbauer GJ, Schulman AH, Waugh R, Braumann I, Pozniak C, Scholz U, Mayer KFX, Spannagl M, Stein N, Mascher M. (2019). TRITEX: Chromosome-scale sequence assembly of Triticeae genomes with open-source tools. *Genome Biology*, 20, 1–18.

Munns R, James RA, Läuchli A. (2006). Approaches to increasing the salt tolerance of wheat and other cereals. *Journal of Experimental Botany*, 57, 1025–1043.

Nakamura M, Nishimura T, Morita MT. (2019). Gravity sensing and signal conversion in plant gravitropism. *Journal of Experimental Botany*, 70, 3495–3506.

Newton AC, Flavell AJ, George TS, Leat P, Mullholland B, Ramsay L, Revoredo-Giha C, Russell J, Steffenson BJ, Swanston JS, Thomas WTB, Waugh R, White PJ, Bingham IJ. (2011). Crops that feed the world 4. Barley: a resilient crop? Strengths and weaknesses in the context of food security. *Food Security*, 3, 141–178.

Ober ES, Alahmad S, Cockram J, Forestan C, Hickey LT, Kant J, Maccaferri M, Marr E, Milner M, Pinto F, Rambla C, Reynolds M, Salvi S, Sciara G, Snowdon RJ, Thomelin P, Tuberosa R, Uauy C, Voss-Fels KP, Wallington E, Watt M. (2021). Wheat root systems as a breeding target for climate resilience. *Theoretical and Applied Genetics*,134, 1645–1662.

Paulitz TC, Steffenson BJ. (2010). Biotic stress in barley: disease problems and solutions. In *Barley: Production, Improvement, and Uses*; John Wiley & Sons, Inc.: Hoboken, NJ, USA, 2011; pp. 307–354.

Perera IY, Hung CY, Brady S, Muday GK, Boss WF. (2006). A universal role for inositol 1,4,5-trisphosphate-mediated signaling in plant gravitropism. *Plant Physiology*, 140, 746–760.

Poovaiah BW, McFadden JJ, Reddy ASN. (1987). The role of calcium ions in gravity signal perception and transduction. *Physiologia Plantarum*, 71, 401–407.

Ramalingam P, Kamoshita A, Deshmukh V, Yaginuma S, Uga Y. (2017). Association between root growth angle and root length density of a nearisogenic line of IR64 rice with DEEPER ROOTING 1 under different levels of soil compaction. *Plant Production Science*, 20, 162–175.

Rani M, Singh G, Siddiqi RA, Gill BS, Sogi DS, Bhat MA. (2021). Comparative quality evaluation of physicochemical, technological, and protein profiling of wheat, rye, and barley cereals. *Frontiers in Nutrition*, 8, 425.

Roychoudhry S, Del Bianco M, Kieffer M, Kepinski S. (2013). Auxin controls gravitropic setpoint angle in higher plant lateral branches. *Current Biology*, 23, 1497–1504.

Roychoudhry S, Kepinski S. (2015). Shoot and root branch growth angle control-the wonderfulness of lateralness. *Current Opinion in Plant Biology*, 23, 124–131.

Roychoudhry S, Kieffer M, Del Bianco M, Liao CY, Weijers D, Kepinski S. (2017). The developmental and environmental regulation of gravitropic setpoint angle in Arabidopsis and bean. *Scientific Reports*, 7, 1–12.

Salinas-Mondragon RE, Kajla JD, Perera IY, Brown CS, Sederoff HW. (2010). Role of inositol 1,4,5-triphosphate signalling in gravitropic and phototropic gene expression. *Plant, Cell and Environment*, 33, 2041–2055.

Schneider HM, Lor VSN, Hanlon MT, Perkins A, Kaeppler SM, Borkar AN, Bhosale R, Zhang X, Rodriguez J, Bucksch A, **Bennett MJ, Brown KM, Lynch JP. (2022)**. Root angle in maize influences nitrogen capture and is regulated by calcineurin B-like protein (CBL)-interacting serine/threonine-protein kinase 15 (ZmCIPK15). *Plant, Cell & Environment*, 45, 837–853.

Shimizu C, Wakita Y, Kihara M, Kobayashi N, Tsuchiya Y, Nabeshima T. (2019). Association of lifelong intake of barley diet with healthy aging: changes in physical and cognitive functions and intestinal microbiome in senescence-accelerated mouse-prone 8 (SAMP8). *Nutrients*, 11, 1770.

Singh M, Gupta A, Laxmi A. (2017). Striking the right chord: Signaling enigma during root gravitropism. *Frontiers in Plant Science*, 8, 1304.

Stoker R, Moore R. (**1984)**. Structure of columella cells in primary and lateral roots of *helianthus annuvs* (compositae). *New Phytologist*, 97, 205–212.

Su SH, Gibbs NM, Jancewicz AL, Masson PH. (2017). Molecular mechanisms of root

gravitropism. *Current Biology*, 27, R964–R972.

Su SH, Keith MA, Masson PH. (2020). Gravity signaling in flowering plant roots. *Plants*, 9, 1–23.

Suzuki H, Yokawa K, Nakano S, Yoshida Y, Fabrissin I, Okamoto T, Baluška F, Koshiba T. (2016). Root cap-dependent gravitropic U-turn of maize root requires light-induced auxin biosynthesis via the YUC pathway in the root apex. *Journal of Experimental Botany*, 67, 4581–4591.

Tanaka A, Kobayashi Y, Hase Y, Watanabe H. (2002). Positional effect of cell inactivation on root gravitropism using heavy-ion microbeams. *Journal of Experimental Botany*, 53, 683–687.

Toal TW, Ron M, Gibson D, Kajala K, Splitt B, Johnson LS, Miller ND, Slovak R, Gaudinier A, Patel R, de Lucas M, Provart NJ, Spalding EP, Busch W, Kliebenstein DJ, Brady SM. (2018). Regulation of root angle and gravitropism. *G3: Genes|Genomes|Genetics*, 8, 3841-3855.

Toyota M, Furuichi T, Tatsumi H, Sokabe M. (2008). Critical consideration on the relationship between auxin transport and calcium transients in gravity perception of Arabidopsis seedlings. *Plant Signaling & Behavior*, 3, 521.

Tsugeki R, Fedoroff N V. (1999). Genetic ablation of root cap cells in Arabidopsis. *Proceedings of the National Academy of Sciences of the United States of America*, 96, 12941–12946.

Uga Y, Kitomi Y, Ishikawa S, Yano M. (2015). Genetic improvement for root growth angle to enhance crop production. *Breeding Science*, 65, 111.

Uga Y, Sugimoto K, Ogawa S, Rane J, Ishitani M, Hara N, Kitomi Y, Inukai Y, Ono K, Kanno N, Inoue H, Takehisa H, Motoyama R, Nagamura Y, Wu J, Matsumoto T, Takai T, Okuno K, Yano M. 2013. Control of root system architecture by *DEEPER ROOTING 1* increases rice yield under drought conditions. *Nature Genetics*, 45, 1097–1102.

Vembu K. (2017). Interaction of nitric oxide with auxin and ethylene signalling in Arabidopsis root gravitropism. (Thesis). University of the West of England.

Voss-Fels KP, Robinson H, Mudge SR, Richard C, Newman S, Wittkop B, Stahl A, Friedt W, Frisch M, Gabur I, **Miller-Cooper A, Campbell BC, Kelly A, Fox G, Christopher J, Christopher M, Chenu K, Franckowiak J, Mace ES, Borrell AK, Eagles H, Jordan DR,**

Botella JR, Hammer G, Godwin ID, Trevaskis B, Snowdon RJ, Hickey LT. (2018). *VERNALIZATION1* modulates root system architecture in wheat and barley. *Molecular Plant*, 11, 226–229.

Wang L, Guo M, Li Y, Ruan W, Mo X, Wu Z, Sturrock CJ, Yu H, Lu C, Peng J, Mao C. (2018). *LARGE ROOT ANGLE1*, encoding OsPIN2, is involved in root system architecture in rice. *Journal of Experimental Botany*, 69, 385–397.

Wheeler T, **von Braun J. (2013**). Climate change impacts on global food security. *Science*, 341, 508-513.

Wisniewska J, Xu J, Seifartová D, Brewer PB, Růžička K, Blilou L, Rouquié D, Benková E, Scheres B, Friml J. (2006). Polar PIN localization directs auxin flow in plants. *Science*, 312, 883.

Wolverton C, Mullen JL, Ishikawa H, Evans ML. (2002). Root gravitropism in response to a signal originating outside of the cap. *Planta*, 215, 153–157.

Xiong J, Yang Y, Fu G, Tao L. (2015). Novel roles of hydrogen peroxide (H_2O_2) in regulating pectin synthesis and demethylesterification in the cell wall of rice (*Oryza sativa*) root tips. *New Phytologist*, 206, 118–126.

Young LM, Evans ML, Hertel R. (1990). Correlations between gravitropic curvature and auxin movement across gravistimulated roots of *Zea mays. Plant Physiology*, 92:792-6.

Zhang Y, He P, Ma X, Yang Z, Pang C, Yu J, Wang G, Friml J, Xiao G. (2019a). Auxin-mediated statolith production for root gravitropism. *New Phytologist*, 224, 761–774.

Zhang J, Vanneste S, Brewer PB, Michniewicz M, Grones P, Kleine-Vehn J, Löfke C, Teichmann T, Bielach A, Cannoot B, Hoyerová K, Chen X, Xue HW, Benková E, Zažímalová E, Friml J. (2011). Inositol trisphosphate-induced Ca^{2+} signaling modulates auxin transport and PIN polarity. *Developmental Cell*, 20, 855–866.

Zhang Y, Xiao G, Wang X, Zhang X, Friml J. **(2019b)**. Evolution of fast root gravitropism in seed plants. *Nature Communications*, 10, 3480.

Zhao R, Liu Z, Li Z, Xu S, Sheng X. (2022). Gravity induces asymmetric Ca^{2+} spikes in the root cap in the early stage of gravitropism. *Plant Signaling and Behavior*, 17, 2025325.

Zheng Z, Zou J, Li H, Xue S, Wang Y, Le J. (2015). Microrheological insights into the dynamics of amyloplasts in root gravity-sensing cells. *Molecular Plant*, 8, 660–663.

ENHANCED GRAVITROPISM 2 encodes a STERILE ALPHA MOTIF–containing protein that controls root growth angle in barley and wheat

Gwendolyn K. Kirschner[a,1], Serena Rosignoli[b,1], Li Guo[a,1], Isaia Vardanega[a,b], Jafargholi Imani[c], Janine Altmüller[d], Sara G. Milner[e], Raffaella Balzano[b], Kerstin A. Nagel[f], Daniel Pflugfelder[f], Cristian Forestan[b], Riccardo Bovina[b], Robert Koller[f], Tyll G. Stöcker[g], Martin Mascher[e,h], James Simmonds[i], Cristobal Uauy[i], Heiko Schoof[g], Roberto Tuberosa[b], Silvio Salvi[b,2], and Frank Hochholdinger[a,2]

[a]Institute of Crop Sciences and Resource Conservation, Crop Functional Genomics, University of Bonn, 53113 Bonn, Germany; [b]Department of Agricultural and Food Sciences, University of Bologna, 40127 Bologna, Italy; [c]Institute of Phytopathology, Research Centre for BioSystems, Land Use and Nutrition, Justus-Liebig-University Giessen, 35392 Giessen, Germany; [d]Cologne Center for Genomics, University of Cologne, 50931 Cologne, Germany; [e]Leibniz Institute of Plant Genetics and Crop Plant Research Gatersleben, 06466 Seeland, Germany; [f]Institute of Bio- and Geosciences, IBG-2: Plant Sciences, Forschungszentrum Juelich GmbH, 52425 Jülich, Germany; [g]Institute of Crop Sciences and Resource Conservation, Crop Bioinformatics, University of Bonn, 53115 Bonn, Germany; [h]German Centre for Integrative Biodiversity Research Halle-Jena-Leipzig, 04103 Leipzig, Germany; and [i]John Innes Centre, Norwich Research Park, Norwich NR4 7UH, United Kingdom

Edited by Philip N. Benfey, Duke University, Durham, NC, and approved July 13, 2021 (received for review January 25, 2021)

The root growth angle defines how roots grow toward the gravity vector and is among the most important determinants of root system architecture. It controls water uptake capacity, nutrient use efficiency, stress resilience, and, as a consequence, yield of crop plants. We demonstrated that the *egt2* (*enhanced gravitropism 2*) mutant of barley exhibits steeper root growth of seminal and lateral roots and an auxin-independent higher responsiveness to gravity compared to wild-type plants. We cloned the *EGT2* gene by a combination of bulked-segregant analysis and whole genome sequencing. Subsequent validation experiments by an independent CRISPR/Cas9 mutant allele demonstrated that *egt2* encodes a STERILE ALPHA MOTIF domain–containing protein. In situ hybridization experiments illustrated that *EGT2* is expressed from the root cap to the elongation zone. We demonstrated the evolutionary conserved role of *EGT2* in root growth angle control between barley and wheat by knocking out the *EGT2* orthologs in the A and B genomes of tetraploid durum wheat. By combining laser capture microdissection with RNA sequencing, we observed that seven expansin genes were transcriptionally down-regulated in the elongation zone. This is consistent with a role of *EGT2* in this region of the root where the effect of gravity sensing is executed by differential cell elongation. Our findings suggest that *EGT2* is an evolutionary conserved regulator of root growth angle in barley and wheat that could be a valuable target for root-based crop improvement strategies in cereals.

barley | CRISPR/Cas9 | EGT2 | gravitropism | root angle

The increase in human population and climate change are major challenges to food security (1, 2). A number of studies proposed to modify root system architecture to improve water and nutrient use efficiency, crop yield, and resilience to stress episodes (3, 4). Among the most important determinants of root system architecture is the root growth angle, i.e., the angle in which roots grow toward the ground.

Increased response to gravity, or hypergravitropism, and thereby a steeper root growth angle was shown to be associated to improved drought resistance in rice, probably by increased access to deep-soil water (5). At the same time, a deeper root system facilitates the uptake of N and other mobile nutrients that are more abundant in deeper soil layers (6). Root gravitropism is regulated by sensing the gravitropic stimulus and subsequent differential cell elongation to enable root growth toward the gravitropic vector. Removing the root cap mechanically or genetically substantially diminishes the gravitropic response (7–9), suggesting that gravity sensing occurs primarily in the root cap. However, there is evidence for a sensing site outside the root cap, located in the elongation zone (10, 11). There are different hypotheses on how the cells sense gravity, with the prevailing idea that the starch-containing plastids in the root cap act as statoliths and settle in response to gravity. In doing so, they trigger a signaling cascade, either by mechanosensitive channels or by direct protein interaction, on the organelle surface (12–14). This signaling pathway ultimately leads to a rearrangement of auxin export carriers and thereby to a reorganization of the auxin maximum in the root tip (15). At the same time, changes of pH in the root cap and an asymmetrical change of pH in the upper and lower side of the root meristem and elongation zone occur (16, 17). This finally leads to an increased elongation of the cells on the side averted to the gravity vector in the elongation zone of the roots so that the roots grow downward (18). To date, only single components of the signaling cascade regulating root gravitropism have been unraveled. Examples include the actin-binding protein RICE MORPHOLOGY DETERMINANT that localizes to the surface of statoliths in rice root cap cells and controls the root growth angle in response to external phosphate (19). Another protein involved in gravitropism is the membrane-localized ALTERED RESPONSE TO GRAVITY1 in *Arabidopsis*, which is expressed in the root cap and is involved in

Significance

To date, the potential of utilizing root traits in plant breeding remains largely untapped. In this study, we cloned and characterized the *ENHANCED GRAVITROPISM2* (*EGT2*) gene of barley that encodes a STERILE ALPHA MOTIF domain–containing protein. We demonstrated that *EGT2* is a key gene of root growth angle regulation in response to gravity, which is conserved in barley and wheat and could be a promising target for crop improvement in cereals.

Author contributions: G.K.K., S.R., S.S., and F.H. designed research; G.K.K., S.R., L.G., I.V., J.I., J.A., S.G.M., R. Balzano, D.P., C.F., R. Bovina, and J.S. performed research; G.K.K., K.A.N., R.K., T.G.S., M.M., C.U., H.S., R.T., S.S., and F.H. analyzed data; and G.K.K., S.R., S.S., and F.H. wrote the paper.

The authors declare no competing interest.

This article is a PNAS Direct Submission.

[1]G.K.K., S.R., and L.G. contributed equally to this work.

[2]To whom correspondence may be addressed. Email: hochhold@uni-bonn.de or silvio.salvi@unibo.it.

This article contains supporting information online at https://www.pnas.org/lookup/suppl/doi:10.1073/pnas.2101526118/-/DCSupplemental.

Published August 26, 2021.

the gravity-induced lateral auxin gradient (20). Both proteins seem to function in signaling immediately after gravity sensing in the root cap. In contrast, rice *DEEPER ROOTING1* (*DRO1*) acts as early auxin response gene later in the gravitropic signaling. The *DRO1* gene encodes for a plasma membrane protein that is expressed in the root meristem and was identified because of its influence on the root growth angle (5). The role of DRO1 may not be conserved in primary roots of different plant species since the *Arabidopsis* homolog does not affect the gravitropic response of the primary root but influences the growth angle of the lateral roots (21).

Barley (*Hordeum vulgare*) is the world's fourth most important cereal crop in terms of grain production, after wheat (*Triticum aestivum*), rice (*Oryza sativa*), and maize (*Zea mays*) (2019, http://www.fao.org/faostat/en/). It is cultivated over a broad geographical area because it can adapt to a wide range of climatic conditions and is therefore an excellent model to study responses to

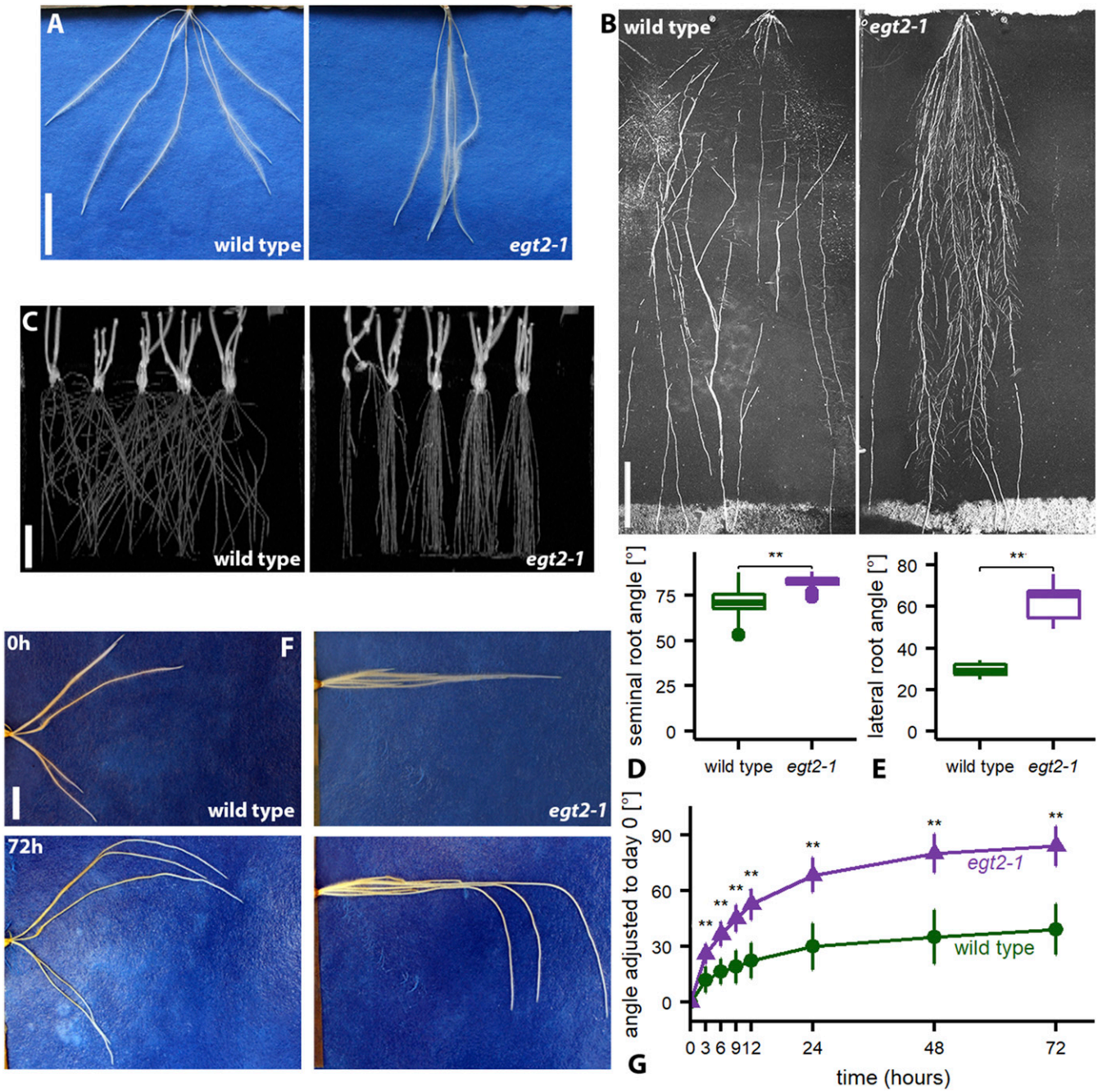

Fig. 1. Root phenotype of *egt2-1*. (*A*) Wild-type and *egt2-1* roots grown on germination paper, 7 d after germination (DAG). (Scale bar: 2 cm.) (*B*) Wild-type and *egt2-1* roots grown in rhizotrons 26 DAG. (Scale bar: 10 cm.) (*C*) MRI pictures of wild-type and *egt2-1* plants grown in soil 3 DAG. (Scale bar: 4 cm.) (*D*) Root angle of seminal roots 7 DAG; $n = 40$ per genotype in one experiment; two-tailed *t* test, $^{**}P < 0.01$. (*E*) Lateral root angle 14 DAG; n = 8 to 9 per genotype in two independent experiments; two-tailed *t* test, $^{**}P < 0.01$. (*F*) Wild-type and *egt2-1* roots after rotation (time point 0) at indicated time points. (Scale bar: 1 cm.) (*G*) Root tip angle after rotation; plants 5 DAG were rotated by 90° (time 0), and the root tip angle was measured over time; $n = 38$ per genotype in three independent experiments; the two genotypes were compared between each other at the respective time points by a two-tailed *t* test, $^{**}P < 0.01$. SD is depicted; to account for the different starting angles of the roots, all measurements were normalized to the starting angle of the roots at time 0.

climate change (22). In this study, we used a forward-genetics approach to clone *ENHANCED GRAVITROPISM2* (*EGT2*), a gene involved in barley root gravitropic response and whose effect is conserved in wheat. *EGT2* encodes a STERILE ALPHA MOTIF (SAM) domain–containing protein and likely acts in a regulatory pathway that counteracts the auxin-mediated positive gravitropic signaling pathway.

Results

The *egt2-1* Mutant Shows a Steeper Root Growth Correlated with an Enhanced Gravitropic Response. The *egt2-1* mutant was discovered in a sodium-azide mutagenized population of the barley cultivar Morex based on the hypergravitropic growth of its seminal root system in paper rolls and was shown to be inherited as a monogenic recessive Mendelian locus (23, 24). We investigated the phenotype in more detail in 2-D rhizoboxes, in which the plants grow vertically on flat filter paper. While in Morex wild type the seminal roots grow in a shallow angle toward the gravity vector and cover a larger area, the seminal roots in the *egt2-1* mutant grow steeply down (Fig. 1 *A* and *D* and *SI Appendix*, Fig. S1*A*). This phenotype was consistent in plants grown in soil-filled rhizotrons and pots, the latter visualized by MRI (Fig. 1 *B* and *C* and *SI Appendix*, Fig. S1 *E–G*). Furthermore, the lateral roots arising from the seminal roots also displayed a highly increased growth angle (Fig. 1 *B* and *E* and *SI Appendix*, Fig. S1 *A* and *H*). Apart from the increased root growth angle, we did not detect any other aberrant root phenotypes, neither a changed number of seminal roots nor a difference in root length (*SI Appendix*, Fig. S1 *B* and *C*). To further investigate the reason for the steep root phenotype, we tested the responsiveness of the root system to gravity. After rotation by 90°, we monitored the angle of the root tips over time (Fig. 1 *F* and *G*). Roots of the *egt2-1* mutant bent much faster and stronger than wild-type roots, approaching 90° after 3 d compared to just 30° in wild-type roots (Fig. 1*G*). Root growth rate, however, was not altered (*SI Appendix*, Fig. S1*D*). We concluded therefore that the steep root angle of the *egt2-1* mutant was likely caused by a higher responsiveness to gravity. Since gravity sensing and signal transduction was shown to take place in the root cap and meristem (16–18), we compared the root cap and meristem by microscopy and measuring the root meristem size, but we did not discover significant differences (*SI Appendix*, Fig. S2 *A–D*). Other mutants with disturbed root gravitropism exhibit different velocities of starch granule settling in the root cap cells than wild type (19). However, we did not detect such differences between wild type and the *egt2-1* mutant (*SI Appendix*, Fig. S2 *E* and *F*).

Auxin Response Is Unaffected in *egt2-1* Mutants. It was shown before that the phytohormone auxin is involved in gravitropic response signaling (15) and that auxin transport inhibitors or external supply of auxin influences the reaction of roots to rotation (25). To analyze if the *egt2-1* mutant is sensitive to manipulation of the auxin state in the roots, we treated wild type and mutant with auxin and an auxin transport inhibitor and recorded the reaction to 90° rotation and root elongation in a time course experiment. Application of the naturally occurring auxin indole-3-acetic acid led to a similar gravitropic response and root elongation at low concentrations in both wild type and the *egt2-1* mutant compared to mock treatment (*SI Appendix*, Fig. S3 *A–D*) and to an inhibition of root growth and thereby a slower response to the gravistimulus at higher concentrations (*SI Appendix*, Fig. S3 *E* and *F*). Treatment with low concentrations of the auxin transport inhibitor 1-*N*-naphthylphthalamic acid (NPA) resulted in a similar gravitropic response and root elongation within 48 h in both wild type and *egt2-1* compared to mock treatment (*SI Appendix*, Fig. S3 *G–J*), while high concentrations of NPA decreased the gravitropic response and root elongation significantly in wild type and *egt2-1* to a similar degree compared to mock treatment (*SI Appendix*, Fig. S3 *K* and *L*). In summary, we demonstrated that *egt2-1* reacts to auxin treatment to the same degree as the wild type, and we conclude that the mutation in *egt2-1* does not disrupt the major auxin signaling pathways. This notion is consistent with the results of a tissue-specific RNA sequencing (RNA-seq) analysis of wild-type and *egt2-1* seminal roots, where we did not find any auxin-related genes among the differentially expressed genes (see *Results*).

***EGT2* Encodes a SAM Domain–Containing Protein.** In order to map and clone the *EGT2* gene, single nucleotide polymorphism-based bulked-segregant analysis (BSA) was carried out using an F_2-population derived from the cross between the hypergravitropic *egt2-1* carrying line TM2835 (in Morex background) and cultivar (cv.) Barke, the latter showing a typical wild-type, shallow root architecture. *egt2* was mapped to a 312 Mbp interval on the short arm of chromosome 5H (Fig. 2*A*) between markers *SCRI_RS_222345* and *SCRI_RS_13395* (Dataset S1). Subsequently, TM2835 was subjected to whole genome sequencing, which led to the identification of seven genes within the *egt2* interval and which carried missense, splice site, or stop-codon gain mutations when compared with wild-type Morex sequence (*SI Appendix*, Table S1). Among these was a gene encoding for a 252 amino acid SAM domain–containing protein [*HORVU5Hr1G027890* (26) or *HORVU.MOREX.r2.5HG0370880.1* (27)] with a mutation (G447A) leading to a premature stop codon at the beginning of the functional domain (W149*) (Fig. 2*B* and *SI Appendix*, Fig. S4 *A* and *B*) (27). Apart from the SAM domain, no other functional domains were predicted (28). The sequence of the SAM domain between EGT2, and previously described SAM domains of other plant species is highly conserved (*SI Appendix*, Figs. S4*B* and S6) (29, 30).

To validate *HORVU.MOREX.r2.5HG0370880.1* as *EGT2*, we used CRISPR/Cas9 to create an additional mutant allele (*egt2-2*) in the barley cv. Golden Promise. We targeted two sites in the 5' untranslated region (5′ UTR) and exon 1, separated by 196 bp, and recovered a 215 bp deletion including the start codon, leading to the translation of a truncated protein (Fig. 2*B* and *SI Appendix*, Fig. S4*A*). We analyzed the root phenotype of the homozygous T_1-line and determined a significantly higher root angle of both seminal and lateral roots in the mutant in comparison to the wild type (Fig. 2 *C–E*). Hence, we confirmed that the altered root angle phenotype of *egt2-2* is caused by a truncation of *HORVU.MOREX.r2.5HG0370880.1*. Like in the *egt2-1* mutant in Morex background, the root length of *egt2-2* was similar to the wild type (*SI Appendix*, Fig. S4*C*). The reaction of the *egt2-2* roots after rotation was faster than in the wild type but not statistically significant (*SI Appendix*, Fig. S4*E*). It is notable that Golden Promise and Morex differ in seminal root angle growth although they both carry a wild-type *EGT2* allele (compare Figs. 1 *A* and *D* and 2 *C* and *D*). Additionally, the reorientation of the roots after rotation occurs much faster in wild-type Golden Promise than in Morex (compare Fig. 1*G* and *SI Appendix*, Fig. S4*E*). Thus, other genetic factors influence the root growth angle in addition to *EGT2*.

To further validate the function of the *EGT2* gene, we identified mutant lines carrying premature stop codons from a sequenced mutant population of tetraploid wheat (31). We combined mutations in the two durum wheat *EGT2* orthologs (homologs on A and B genomes) to generate complete *egt2* knockout lines. These double mutants showed narrower seminal root growth angle in rhizoboxes compared with the sibling lines carrying wild-type alleles in both homologs (Fig. 2 *F* and *G*). Similar to barley, the number and length of seminal roots was unaffected in 7-d-old seedlings (*SI Appendix*, Fig. S4 *G–I*).

***EGT2* Is Expressed in the Whole Root Tip.** To survey the spatial expression patterns of *EGT2* in roots, we performed RNA in situ hybridization experiments. *EGT2* is expressed in the whole root tip, including the root cap, meristem, and elongation zone (Fig. 3*A*). The negative (sense) control exhibited background staining, mainly in the root cap; therefore, we confirmed this expression pattern by surveying our RNA-seq data, where we found *EGT2* expressed in

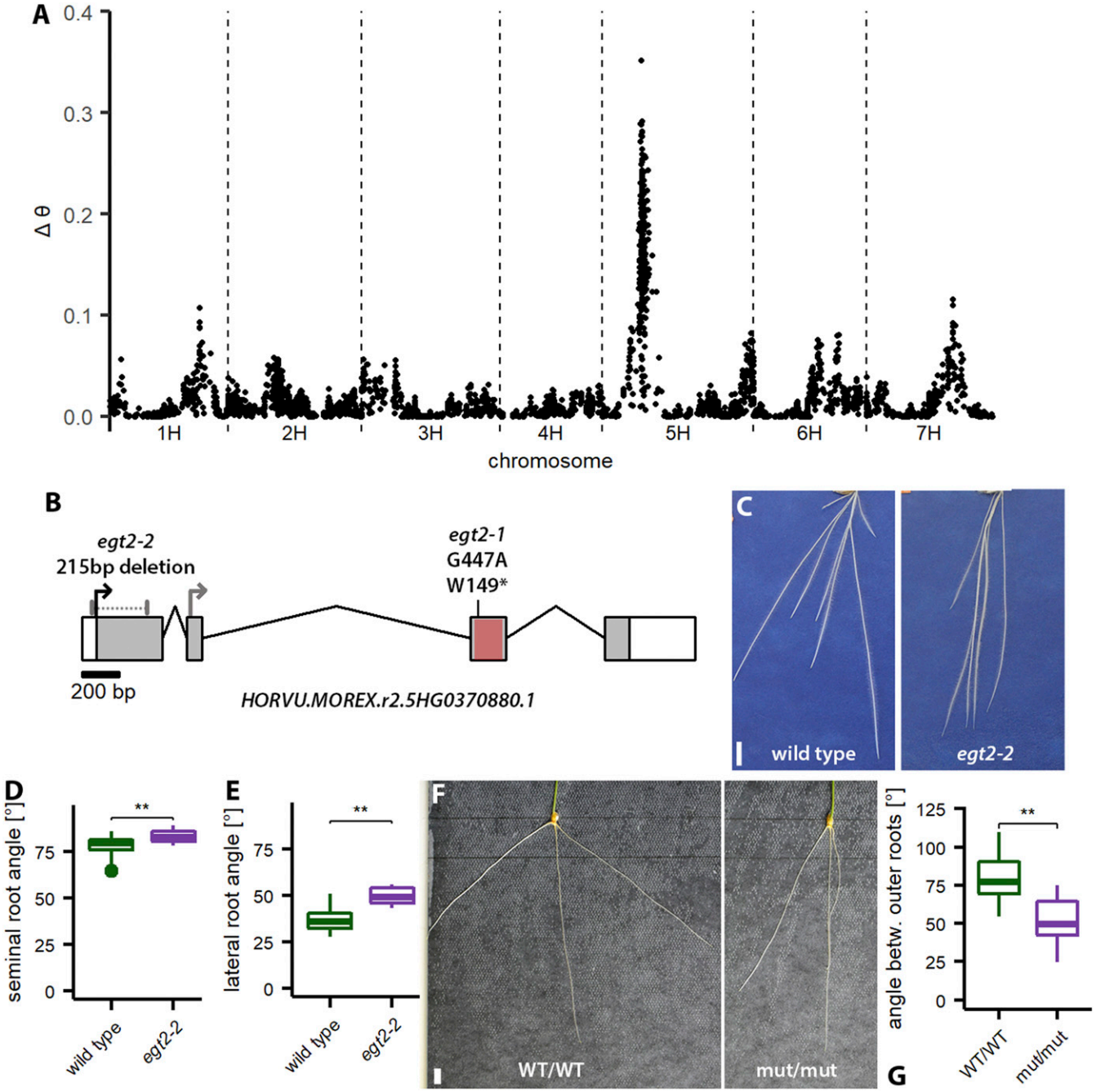

Fig. 2. *EGT2* encodes a SAM protein. (*A*) Association of SNP markers with seminal root angle across the barley genome as established by BSA in the F_2 cross TM2835 (*egt2-1,* hypergravitropic roots) × cv. Barke (wt roots). The *y*-axis reports $\Delta\theta$, an index accounting for the difference in allele-specific fluorescence signal between the two BSA DNA bulks, per SNP. (*B*) Gene structure of *EGT2* (HORVU.MOREX.r2.5HG0370880.1) with mutations in *egt2* (*egt2-1*: G to A transition and *egt2-2:* deletion); translational start site in wild type is shown as a black arrow and start site in the *egt2-2* mutant as a gray arrow; exons are depicted as a gray box, introns are depicted by lines, and UTRs are depicted as white boxes. The red box indicates the sequence encoding for the SAM domain. (*C*) Exemplary pictures of wild-type (cv. Golden Promise) and mutant *egt2-2* roots 7 DAG. (Scale bar: 2 cm.) (*D*) Seminal root angle of wild-type (cv. Golden Promise) and mutant *egt2-2* 7 DAG; $n = 15$ to 17 in two independent experiments. (*E*) Root angle of lateral roots 14 DAG; $n = 16$ to 18 in two independent experiments; two-tailed *t* test, $^*P < 0.05$, $^{**}P < 0.01$. (*F*) Exemplary pictures of wheat wild-type (WT/WT) and *egt2* (mut/mut) roots, 7 DAG. (Scale bar: 1 cm.) (*G*) Root angle between second and third seminal root of wild-type (WT/WT) and *egt2* (mut/mut) wheat seedling at 7 DAG; $n = 18$ and 39 for wild type and mutant, respectively. Wheat plants were derived from two independent segregating populations.

root cap, meristem, and elongation zone. qRT-PCR analysis of wild-type and *egt2* mutant root tips comprising root cap, meristematic, and elongation zone that were rotated by 90° for up to 9 h did not indicate any transcriptional regulation of *EGT2* with regard to gravistimulation (Fig. 3*B*). Furthermore, we measured *EGT2* expression in upper and lower flanks of the elongation zone 6 h after root rotation by 90° (Fig. 3*C* and *SI Appendix*, Fig. S5*A*) but did not detect any significant change. At all time points, *EGT2* expression was significantly down-regulated in the mutant, which is consistent which the observed premature stop codon in this gene likely leading to nonsense mediated decay of the transcripts (Fig. 3*B*). The control experiment with unrotated roots is depicted in *SI Appendix,* Fig. S8*B*.

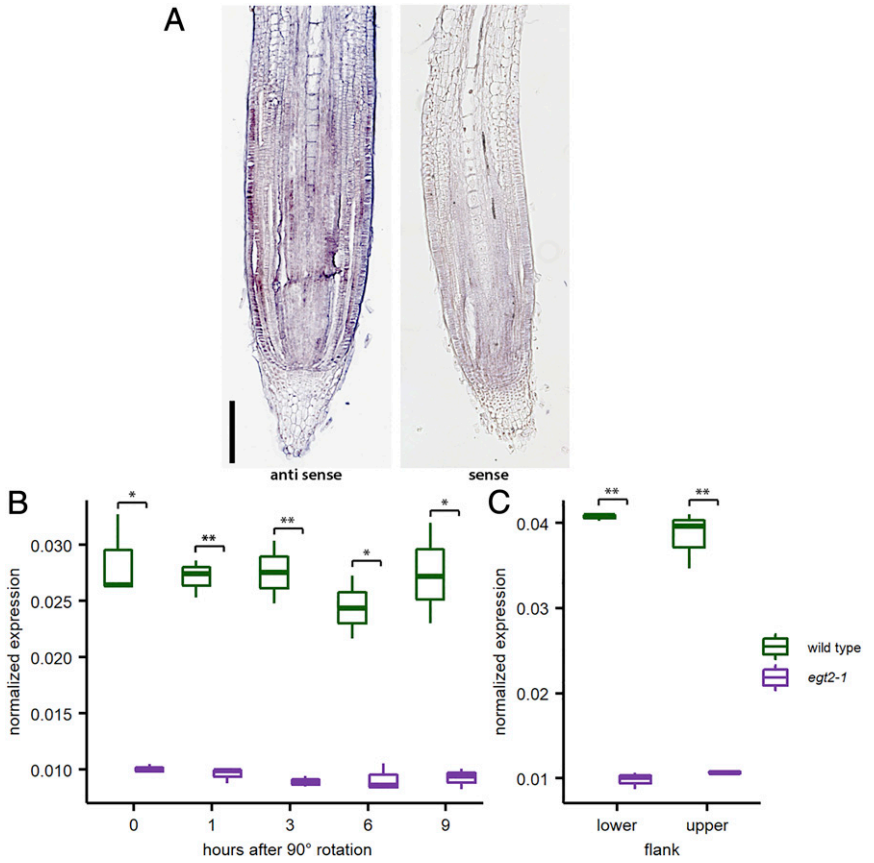

Fig. 3. Expression of *EGT2*. (*A*) RNA in situ hybridization of *EGT2*; negative controls (sense probes) are shown on the right. (Scale bar: 200 μm.) (*B*) qRT-PCR of *EGT2* expression in combined root cap, meristem, and elongation zone samples after rotation of 90°; normalized to *tubulin*; two-tailed *t* test, $*P < 0.05$, $**P < 0.01$. (*C*) qRT-PCR of *EGT2* expression in upper and lower flank of the elongation zone in roots after rotation by 90° for 6 h (as depicted in *SI Appendix*, Fig. S5*A*); normalized to *tubulin*; two-tailed *t* test, $**P < 0.01$.

In the *egt2-1* Mutant, Cell Wall–Related Processes Are Affected in the Elongation Zone. SAM domain–containing proteins from animals and plants have a plethora of different functions and act, among others, as transcription factors (29). To analyze the effect of the mutation in *EGT2* on the root transcriptome, we isolated RNA from different root tissues. For this, we applied laser capture microdissection to specifically separate root cap, meristem, and parts of the elongation zone from wild-type and *egt2-1* seminal roots. This allowed us to differentiate between gravity sensing (root cap), signal transduction (meristem), and signal execution (elongation zone) (Fig. 4*D* and *SI Appendix*, Fig. S5*B*). To this end, we selected the most vertically grown seminal roots in both genotypes that displayed a similar root growth angle (Fig. 4*A*). By doing so, we excluded secondary effects caused by different root growth angles. Moreover, we used roots of similar length to exclude differences in age since the barley seminal roots do not grow out simultaneously (32). The RNA-seq experiment yielded on average 41 million 100 bp paired-end reads per sample (*SI Appendix*, Table S2). We determined the transcriptomic relationships among the two genotypes and three tissues by a principal component analysis (PCA) (Fig. 4*B*). In the PCA, the two principal components PC1 and PC2 explained 82% of the total variance (Fig. 4*B*). The biological replicates per tissue included four wild-type and four mutant samples clustering closely together. This indicates small transcriptomic differences between the genotypes but large differences between the tissues. To identify differentially regulated genes, we computed pairwise contrasts between the genotypes of the respective tissues (false discovery rates [FDR] <5% and $\log_2$FC >|1|; see *Materials and Methods*) for genes that uniquely mapped to chromosomes 1 to 7 (33). This resulted in 67 differentially regulated genes among all tissues, some of which were shared between all or two tissues (Fig. 4*C* and *SI Appendix*, Fig. S7 and Table S3). Strikingly, we found seven genes encoding for expansins down-regulated in the elongation zone of the mutant *egt2* (*SI Appendix*, Figs. S7 and S8*A*). Among them, *HORVU3Hr1G076620* and *HORVU3Hr1G076650* are highly homologous, with a sequence identity of 99.5%. A time course experiment with the other five of these expansins did not display expression differences between wild type and *egt2* upon rotation of the roots by 90° (*SI Appendix*, Fig. S8 *C*–*G*). Gene ontology (GO) terms were only assigned to genes down-regulated in the elongation zone, all of them related to the term cell wall (Fig. 4*E*). At the same time, this validates our data set since expansins are expressed in the elongation zone and differentiated root tissue (34). Furthermore, we found that several genes categorized as peroxidase superfamily protein members were up-regulated in either the meristem or the elongation zone (*HORVU2Hr1G026420*, *HORVU7HR1G020300*, *HORVU3Hr1G036820*) (*SI Appendix*, Fig. S7). Differential regulation of a peroxidase superfamily protein-encoding gene was already found in a study in *Arabidopsis* related to agravitropic mutants (35). Moreover, we demonstrated that a gene encoding for calmodulin, a primary plant calcium receptor, down-regulated in meristem and elongation zone (*HORVU1Hr1G068440*) (*SI Appendix*, Fig. S7). Finally, we identified a gene annotated as exocyst complex component 7 up-regulated in the meristematic zone. Components of the exocyst are involved in directing exocytotic vesicles to fusion sites on the plasma membrane and might be involved in the distribution of the auxin transporter PINFORMED4 in *Arabidopsis* (36, 37).

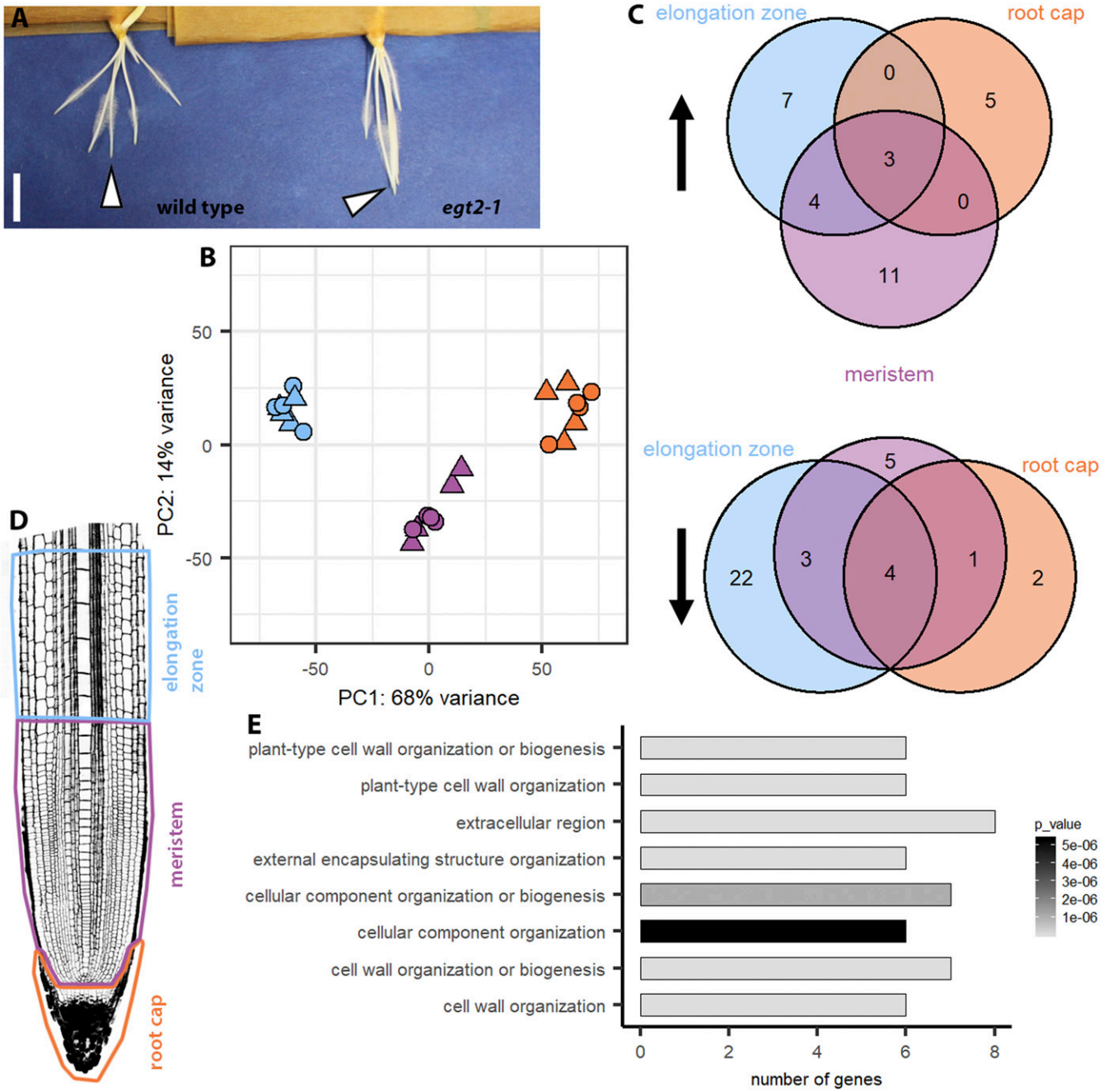

Fig. 4. RNA-seq reveals differences in cell wall-related processes in the elongation zone. (*A*) Wild-type and *egt2-1* plants 3 DAG used for RNA isolation. (Scale bar: 1 cm.) Arrow heads point to exemplary roots used for RNA isolation (most vertical ones). (*B*) PCA of the 24 RNA-seq samples of the two genotypes and three tissues; first and second principal components collectively explain 82% of the variance. (*C*) Venn diagram showing up-regulated (upward arrow) and down-regulated (downward arrow) differentially expressed genes (DEGs) in the respective tissue. (*D*) Experimental setup: RNA of root cap, meristem, and 900 μm of the elongation zone were isolated. (*E*) Enriched GO terms for DEGs down-regulated in the elongation zone.

Discussion

The optimization of root system architecture has been recognized as one of the most important objectives in current breeding programs aimed at increasing resilience and sustainability of crops and agricultural systems (4, 38). Variation of root growth angle can affect the way roots anchor to and explore different soil layers and capture nutrients and water and thus can influence drought tolerance, as shown for DRO1 in rice (4). Specifically, modeling and experimental evidence showed that steeper root angle growth can increase root system depth, thus helping plants in foraging for water and mobile nutrients, such as nitrogen (3–6). Possible tradeoffs are inefficient acquisition of less mobile, superficial nutrients such as phosphate or increased susceptibility to waterlogging and salinity (3, 39). Steeper root system is also expected to reduce the total volume of soil explored, alter intra- and interplant root competition, and contribute to root lodging, although these effects are strongly interconnected with crop management factors such as seeding rate (3, 40, 41). However, knowledge about genes, gene interactions, and regulatory networks in root development is currently limited in all major crops, including cereals.

Here, we cloned a key regulator of root gravitropism, *ENHANCED GRAVITROPISM2* (*EGT2*), in barley and wheat. Mutations in *EGT2* lead to enhanced gravitropic response and thereby to a steeper root growth angle of seminal and lateral roots. We did not find any other root or shoot morphological trait affected by this mutation, indicating that *EGT2* does not act in an ubiquitous signaling pathway but rather is specific for root gravitropism. In *Arabidopsis*, most gravitropic mutants were discovered because they show agravitropic root phenotypes (20, 42). In grasses, however, some mutants with hypergravitropic roots were discovered, for instance, *vln2* and *rmd*. The villin protein VLN2 facilitates microfilament bundling, while the actin-binding protein RMD links actin filaments with gravity-sensing organelles (19, 25).

The only predicted domain in EGT2 is the SAM domain. In animals, SAM domain–containing proteins function as transcription factors, receptors, kinases, or ER proteins (29). In plants, the best known protein containing a SAM domain is the transcription factor LEAFY (LFY), which is involved in flower and meristem identity formation. Modeling of *Arabidopsis* SAM proteins based on structure predictions and LFY characterization suggests that the majority of these proteins are able to form head-to-tail homo- or hetero-oligomers/polymers (29). The close phylogenetic relationship of EGT2 with AtSAM5 (At3g07760) indicates a similar potential of oligomerization for EGT2.

EGT2 is also closely related to WEEP, a SAM domain containing protein that was discovered because of the prominent shoot phenotype in peach tree mutants (30). Peach trees with deletions in *WEEP* show a weeping shoot growth phenotype; thus, the branches grow in a wider angle, and after gravistimulation by rotation by 90°, the branches do not orient their growth upward again (30). Therefore, EGT2 and WEEP are likely involved in a similar pathway that regulates gravitropism, but in different plant organs. Bud grafting experiments in peach implied that *WEEP* encodes an autonomous determinant of shoot orientation for each branch and that no mobile signals from other parts of the plants (like phytohormones) are necessary (30). Furthermore, no difference of auxin or abscisic acid concentration was detected in growing shoots between peach wild-type and *WEEP* mutants, nor were genes associated with auxin biosynthesis or perception differentially expressed (30).

Similarly, we did not find any expression changes of genes related to auxin biosynthesis or perception in our transcriptomic comparison between wild type and *egt2-1*. Treatments with auxins or an auxin transport inhibitor confirmed that the *egt2-1* mutant is as sensitive to disturbance of the auxin balance as the wild type (*SI Appendix*, Fig. S3), indicating that EGT2 works independently of auxin. Nevertheless, the auxin transport pathway could still be affected, as demonstrated for the rice mutant *villin2* (*vln2*) that exhibits a disturbed recycling of the auxin efflux carrier PIN-FORMED2 (PIN2) and thereby a hypergravitropic root response (25). However, auxin treatment of *vln2* mutants induced a restoration of the phenotype and the mutants were insensitive to auxin transport inhibitors which differs from *egt2-1*. On the other hand, exocyst complex component 7 was transcriptionally up-regulated in the *egt2-1* mutant. In *Arabidopsis*, disturbing the expression of *EXOCYST70A3* by knockout or overexpression leads to a higher agravitropic response upon auxin efflux inhibitors probably by regulating the PIN4 localization in columella cells and thereby auxin distribution in root tips (37). It is conceivable that disturbance of expression levels in *egt2-1* mutants might lead to a change in PIN localization and thereby a changed signal transduction; however, this hypothesis remains to be tested. The ubiquitous expression of *EGT2* in root cap, meristem, and elongation zone suggests a participation rather in the signal transduction of gravitropism than in the sensing or differential cell elongation. Since the *EGT2* expression does not change upon gravistimulus, neither in expression level nor in distribution, signal transduction most likely occurs on protein level.

In a split-ubiquitin yeast two-hybrid screen, the close homolog of EGT2, AtSAM5 interacted with the calcium-dependent protein kinase AtCPK13 (At3G51850) (43), putatively connecting AtSAM5 to calcium signaling pathways. Inhibition of the primary plant calcium receptor calmoldulin was shown to inhibit the response to gravity in *Arabidopsis* (42). In the *egt2-1* mutant, *Calmodulin 5* is transcriptionally down-regulated in the meristem and elongation zone, putatively connecting EGT2 with calcium-dependent signal transduction. It is still generally unknown, however, which role calcium plays in gravitropic signaling.

If we hypothesize a role for EGT2 in signal transduction, we would expect downstream targets in the elongation zone, where the effect of gravity sensing is executed by differential cell elongation (18). Here, we found a striking number of expansin genes transcriptionally down-regulated (*SI Appendix*, Fig. S7). Expansins are known as acid-induced cell wall loosening enzymes. However, most studies are based on the activity of bacterial enzymes and the function of expansins in plant cell walls is still unknown (34). Similarly, cell wall-related genes are differentially regulated in *weep* mutant peach trees, and the differentially regulated auxin response genes in *weep* mutants have roles in mediating cell expansion, or modulation of H^+ transport (30). Besides expansins, we found three genes encoding peroxidase superfamily proteins up-regulated in the meristem and elongation zone (*SI Appendix*, Fig. S7). Down-regulation of a peroxidase superfamily protein-encoding gene was already demonstrated in a study in *Arabidopsis* comparing inflorescence stems of wild type to *scarecrow* and *short root* mutant transcriptomes, which show no gravitropic response to rotation in the shoot (35). Peroxidases catalyze the consumption or release of H_2O_2 and reactive oxygen species (ROS). One class of peroxidases functions extracellularly, either for cell wall loosening or cell wall cross-linking (44), and the transcriptional regulation in *egt2* might be related to the regulation of the expansins. Moreover, it was shown that ROS work downstream of auxin signaling in root gravitropism, maybe as second messenger (45).

Based on the broad expression pattern of *EGT2* throughout root cap, meristem, and elongation zone, and the interaction of the *Arabidopsis* AtSAM5 homolog with CPK13, we can hypothesize that *EGT2* is involved in the signal transduction of gravitropic signaling. The missing interference in auxin-related processes on the transcriptomic level and the susceptibility to auxin treatments implies that EGT2 is not involved in any signal transduction related to changes in auxin levels and/or transport. It is possible that EGT2 acts in a pathway that counteracts the auxin-mediated positive gravitropic signaling pathway, since for the growth in an angle toward the gravity vector, a pathway counteracting the positive reaction to gravity is needed. By knocking it out, the downward growth of the roots would dominate and create the hypergravitropic phenotype.

In summary, our results suggest that *EGT2* is an evolutionary conserved check point of seminal and lateral root growth angle in barley and wheat. *EGT2* could be a promising target for root-based crop improvement in cereals.

Materials and Methods

Plant Material and Growth Conditions. The *egt2-1* mutation carrying line, TM2835, was derived from sodium-azide mutagenesis of the cv. Morex as previously described (23, 24). For growth in rhizoboxes and on agar plates, the seeds were washed in 1.2% sodium hypochlorite for 5 min and rinsed with distilled water. Then they were incubated in darkness at 30 °C overnight to induce germination and only germinating seeds were used for further experiments. Growth in rhizoboxes for plant phenotyping and rotation experiments were conducted as described before (46). For phytohormone treatments, plants were grown on half-strength Hoagland solution (47), pH 5.8, supplemented with 0.8% phytagel on square Petri dishes, which were placed at a 45° angle. The plants were grown in growth cabinets (Conviron) at 18 °C at night (8 h) and 22 °C at day (16 h). For growth in

rhizotrons filled with peat substrate, wild-type and *egt2* mutants were grown in the GrowScreen-Rhizo automated platform for 24 d as previously described (48). For the MRI measurements, the seeds were placed in a Petri dish on wet filter paper. The Petri dish was sealed with parafilm and stored lightproof for 24 h in the growth chamber (16 °C/20 °C night/day temperature, 14 h light per day) to induce germination and only germinated seeds were used for further experiments. Seeds were subsequently sown in field soil (Sp2.1, Landwirtschaftliche Untersuchungs- und Forschungsanstalt). Soil moisture was kept at 8.9%$_{m/m}$, corresponding to 40% of the maximal water holding capacity (49). Per genotype, 18 seeds were planted in one pot (Ø = 12.5 cm, 12 cm height) in a hexagonal grid with 2.5-cm seed spacing. Seedlings were imaged after 3 d in the growth chamber. For a longer experiment, single seeds were planted into larger pots (Ø = 9 cm, 30 cm height) and were grown for one week before imaging.

Durum wheat (*Triticum turgidum*) *egt2* mutants were identified from a TILLING population developed in tetraploid cv. Kronos (31). Two selected lines (Kronos2138 and Kronos3589) carrying premature termination codons in the two *EGT2* homeologous coding sequences (TraesCS5A01G102000 and TraesCS5B02G164200LC) were crossed and F_1 plants were self-pollinated. Progenies of selected wild-type and double mutant F_2 individuals derived from two independent initial crosses were grown in rhizoboxes for seminal root angle analysis. Seeds were washed in 70% ethanol for 1 min, then in 1% sodium hypochlorite + 0.02% TritonX-100 for 5 min and rinsed with distilled water. Sterilized seeds were pregerminated for 24 h at 28 °C in wet filter paper. Only germinating seeds were transferred in rhizoboxes for 7 d at 25 °C.

Phenotyping Experiments and Rotation Tests. For analysis of the root angles, plants were grown in rhizoboxes for 7 (seminal root angle) or 14 d (lateral root angle). The seminal root angle was measured as angle from the shoot to the root tip, in relation to the horizontal. For the angle of the lateral roots, the angle was measured from the outgrowth point of the main root to the lateral root tip in comparison to the horizontal. Twenty randomly chosen lateral roots were measured per plant. For the rotation tests, the plants were grown in rhizoboxes for 5 d and then rotated once by 90°. For phytohormone treatments, the plants were grown for 5 d on agar without phytohormones and then transferred to agar plates supplemented with phytohormones as indicated in the results. After 1 h recovery, the agar plates were rotated once by 90°. Pictures were taken at the time points indicated in the graphs. For analysis, the root angle of every single root tip was measured in relation to the horizontal and the angle right after rotation was set to 0. For all measurements, the average of all roots per plant was calculated, presented in the graphs, and compared in the statistical tests. For analysis of growth in the rhizotrons, root images were collected every 2 d, enabling to distinguish between seminal and crown roots. Images at 24 d were utilized for seminal, nodal, and lateral root angle analysis. Root angle values were collected with the software ImageJ (50).

RNA In Situ Hybridizations. Probes for *EGT2* (HORVU5Hr1G027890) mRNA were prepared from the whole coding sequence (start to stop codon). Cloning and RNA probe synthesis was performed as described before (32). RNA in situ hybridizations on roots of 7-d-old plants were performed as described before (32).

BSA and Whole Genome Sequencing. BSA (51) was carried out using plants from an F_2-population obtained starting from the cross TM2835 × cv. Barke and segregating for the *EGT2* locus. 106 F_2-seedlings were grown in flat rhizoboxes composed by two black plastic panels of 38.5 × 42.5 cm. Five pregerminated seeds (1 d, 20 °C, on wet filter paper, in the dark) were positioned between moist filter paper sheets within each rhizobox. Each rhizobox was placed vertically in a larger plastic tank containing deionized water to a level of 3 cm from the bottom, in growth chamber) at 18 °C at night (8 h) and 22 °C at day (16 h) for 13 d. At the end of the growing period, root growth angle of seedlings was visually evaluated and a segregation rate of 88:18 (wild type vs. hypergravitropic) recorded confirming that *egt2* segregates as a monogenic recessive Mendelian locus (χ^2 3:1 = ns). Immediately after this inspection, 15 plants showing wild-type root growth angle and 15 plants showing an hypergravitropic angle were chosen for DNA preparation on a single plant basis using 2 cm^2 leaf portions as previously described (23). DNA samples for BSA were obtained by mixing equal DNA amounts of each of the 15 bulk components, to a final concentration of 50 ng/ul. The two DNA bulks (in double) along with single plant DNA samples from 10 hypergravitropic plants were genotyped using the 9k Illumina Infinium iSelect barley SNP array (52). SNPs signal was analyzed using GenomeStudio (Illumina, San Diego, Inc.). For DNA bulks, SNPs signal was interpreted using the theta value approach as described in ref. 53, modified in order to integrate for each SNP the signals obtained from two bulks (wild type or $^{+/+}$ and hypergravitropic or $^{-/-}$) in the "delta theta" value score as follows "delta theta" = [(theta bulk$^{+/+}$)-(theta bulk $^{-/-}$)]^2.

Genomic DNA of TM2835 for whole genome shot gun sequencing was extracted from leaf samples using a commercial kit (Macheray-Nagel Nucleospin Plant II). The DNA was sequenced with Illumina HiSeq PE150, and 699,353,963 paired-end reads were produced corresponding to a coverage of approximately 40×. Reads were aligned to the first version of barley cv. Morex reference genome (26) with BWA v.7.12 (54) and variants in the genomic space were called with SAMtools v. 1.3 (55, 56), filtering for a minimum reads depth of 5×, PHRED quality >40. In order to discard background mutations due to the differences between the official Morex reference and the Morex parental seeds which had previously been used in the mutagenesis, the SNP calling considered further eight TILLMore mutants whole genome sequencing data that was available at that moment, filtering with a custom AWK script for a minimum ratio DV/DP of 0.8 for the *egt2* mutant and a maximum ratio of 0.2 in every other mutant, where DP is the coverage depth at the SNP position and DV is number of nonreference bases at the same position. SNP effects were predicted with SNPEff v.3.0.7 (57).

For coverage analysis, a minimum of 5× read depth was considered, resulting in a target region of 3.5 GB containing a total of 15,805 mutations, hence the estimated mutation load on the entire genome is 22,579 mutations, or approximately 1 mutation per 220 kb which is of the same order of magnitude of mutation density (1 per 374 kb) formerly estimated based on TILLING results from the same TILLMore population (23). For the provean analysis, values <−2.5 were considered deleterious and values >−2.5 were tolerated.

Modified Pseudo-Schiff Propidium Iodide and Lugol's Staining. The modified pseudo-Schiff propidium iodide staining was performed as described in ref. 32. For Lugol's staining, roots were fixed in 4% paraformaldehyde in phosphate-buffered saline (PBS) overnight, embedded in 13% agarose and sectioned at the vibratome with 40-μm thickness. Then, they were stained with Lugol's solution for 3 min and rinsed with PBS buffer.

Amyloplast Sedimentation Rate. After 1-d pregermination, wild-type and *egt2-1* plants were grown in rhizoboxes for 7 d and then rotated by 180° (shoots pointed downwards). The 0.5 cm root segments of the root tips were collected before rotation and 1 min, 2.5 min, 5 min, and 10 min after rotation. Eight plants were used for each genotype at each time point. Samples were fixed immediately in 4% PFA (diluted with PBS from 36% formaldehyde, VWR Chemicals), and placed in vacuum for 10 min. Subsequently, the solution was replaced and the samples were swirled at 4 °C overnight. Then, the fixed root samples were embedded in 13% low-melting agarose (peqlab) and sectioned longitudinally in a vibratome (Leica Biosystems) with a thickness of 40 μm. Root sections were stained with Lugol's solution (Roth) for 3 min and washed with PBS buffer, and pictures were taken with a light microscope (Zeiss).

Images of root sections were analyzed by ImageJ. The distance from the center of statoliths to the former distal cell wall and new lower cell wall were measured, respectively. Ten cells in the center of each root section were measured and the data of cells with a length of 25 μm to 40 μm were used for graphing.

Microscopy. RNA in situ hybridization and Lugol's-stained samples were examined using a Zeiss PALM MicroBeam microscope.

MRI. MRI images were acquired on a 4.7 T vertical magnet equipped with a Varian console (58). A multislice spin echo sequence was used. Sequence parameters were adapted to the different pot sizes. For the 9 cm pots, we used a birdcage RF coil with a 10 cm diameter and the following sequence parameters: 0.5 mm resolution, 1-mm slice thickness, 9.6 cm field of view, TE = 9 ms, TR = 2.85 s, Bandwidth = 156 kHz, two averages. For the 12.5 cm pots, the following parameters were changed: birdcage RF coil with 140 mm diameter, 14 cm field of view, and 0.55 mm resolution.

CRISPR. For CRISPR target sequences, we choose 20 base pair sequences with the protospacer adjacent motif PAM sequence NGG in the first exon of *EGT2* (HORVU5Hr1G027890) that we checked at http://crispr.dbcls.jp/ for off-targets in the barley genome (Barley [*Hordeum vulgare*] genome, 082214v1 [March 2012)]. We used sites with only one predicted target for a 20mer and only up to 3 predicted targets for the 12mer target sequence upstream of the PAM. The CRISPR guide sequences are marked in *SI Appendix*, Fig. S4*A*. The sgRNA shuttle vectors pMGE625 and 627 were used to generate the binary vector pMGE599 as described in ref. 59. Transformation was carried out with the spring barley cv. Golden Promise grown in a climate chamber at 18 °C/14 °C (light/dark) with 65% relative humidity, with a 16 h photoperiod and a photon

flux density of 240 μmol · m^{-2} · s^{-1}. The binary vector pMGE599 was introduced into *Agrobacterium tumefaciens* AGL-1 strain (60) through electroporation (*E. coli* Pulser; Bio-Rad). The scutella tissue of barley caryopsis was used for *Agrobacterium*-mediated transformation as described previously (61). The insert integration in the barley genome was confirmed by detection of hygromycin gene sequences via PCR in generated T0 lines and were analyzed for mutations in *EGT2* by PCR and Sanger sequencing and the seeds for T1 generation were used for experiments.

qRT-PCR. For the qRT-PCR, RNA from plants grown for 7 d after germination in rhizoboxes was extracted with the RNeasy Plant Mini Kit (Qiagen) and first strand complementary DNA (cDNA) was synthesized with the RevertAid First Strand cDNA Synthesis Kit (Thermo Fisher). Four plants were pooled per biological replicate, and samples were taken from the root tip containing the meristematic and elongation zone, ∼2 mm until the outgrowth of root hairs. For each genotype, three biological replicates and three technical replicates were used. For the reaction, 2 μL of PerfeCTa SYBR Green SuperMix (Quantabio), 1 μL primer mix of a concentration of 1 μM, and 1 μL cDNA was mixed. The primer efficiency of each oligonucleotide was calculated using the following dilution series: 1, 1/2, 1/4, 1/8, 1/16, 1/32, 1/64, and 1/128. The relative expression levels of the transcripts were calculated with reference to the housekeeping gene *TUBULIN* (*HORVU1Hr1G081280*) and according to the method described in ref. 62. Oligonucleotide primer sequences are listed in *SI Appendix*, Table S4. Significant differences in gene expression levels were determined by a two-sided Student's *t* test.

Laser Capture Dissection Microscopy and RNA-Seq. Root tips of the most vertically grown seminal root of 3-d-old plants were used and assigned as one biological replicate. Per genotype, four biological replicates were analyzed. Plants were grown in rhizoboxes and fixed with Farmer's fixative (EtOH:acetic acid 3:1) on ice for 15 min under 500 mbar vacuum and subsequent swirling at 4 °C for 1 h. The fixation solution was replaced, and the procedure was repeated twice before replacing the solution with 34% sucrose and 0.01% safranin-O in PBS. The samples were vacuum-infiltrated again for 45 min and incubated on ice at 4 °C for 21 h. Then the samples were dried carefully with tissue paper and embedded in tissue-freezing medium as described before (63). The medium blocks containing the tissue were stored at −80 °C and were acclimatized to −20 °C in the cryomicrotome (Leica CM1850). Longitudinal sections of 20-μm thickness were mounted on poly-L-lysine-coated glass slides (Zeiss), and the tissue-freezing medium was removed after 5:30 min by incubation in 50% EtOH and 1 min incubation each in 70% EtOH, 95% EtOH, 100% EtOH, and 100% xylol (RNase-free). The tissues (root cap, meristem, and 900 μm of the elongation zone adjacent to the meristem, *SI Appendix*, Fig. S5*B*) were cut with the following settings of the PALM Microbeam laser capture instrument (Zeiss, Germany): energy: 79; speed: 100; cutting program: "Center RoboLPC," picked up manually with a sharp needle and transferred to the cap of RNase-free adhesive caps (Zeiss). RNA was isolated with the Arcturus PicoPure RNA Isolation Kit (Thermo Fisher) according to the manufacturer's protocol for tissue, including the DNase treatment. RNA quality was determined with an Agilent 2100 Bioanalyzer using the Agilent RNA 6000 Pico kit and yielded RIN values between 7.1 and 8.9 and a concentration between 610 and 95,000 pg/μL. Preamplification and library preparation was carried out as described in ref. 64. Detection and sequencing were performed on an Illumina NovaSeq sequencing instrument with a PE100 protocol. Trimmomatic version 0.39 (65) was used to remove low-quality reads and remaining adapter sequences from each read dataset. Specifically, a sliding window approach was used, in which a read was clipped if the average quality in a window of 4 bp fell below a phred quality score of 15. Only reads with a length of ≥30 bp were retained for further analyses. Data are deposited at the sequence read archive (SRA), PRJNA589222. BBDuk of the BBTools suite (https://jgi.doe.gov/data-and-tools/bbtools/) was employed to remove rRNA reads from the datasets using a kmer length of 27 as a filtering threshold for decontamination. After removal of rRNA reads, on average, 8 million paired reads remained. The splice-aware STAR aligner v.2.7.2b (66) was used to align the remaining reads against a genome index of the barley reference sequence and annotation of genotype Morex (IBSC v2.0) (26). Multimapping reads that mapped to more than one position were excluded from subsequent steps by considering only reads, which mapped in a single location (–outFilterMultimapNmax 1). On average, 5 million reads per sample aligned to unique positions in the gene set of the IBSC v2.0 barley reference genome with 46,272 predicted coding and noncoding gene models [EnsemblPlants release 45 (26)]. The aligned paired-end reads were ordered according to their position and transformed to .bam files by the software SAMtools [version 1.3.1 (55)]. Alignment of sequences to the reference genome of Morex (release 45) (26) was performed using HTSeq [version 0.10.0 (67)] with the parameters "-r pos -i gene_id -s no–secondary-alignments ignore–supplementary-alignments ignore." The PCA was performed on the expression data using the normalization procedure rlog() implemented in the R package DESeq2 and the plotPCA() function [version 1.22.2 (33)]. Expression values were normalized with library size by calculating fragments per million (FPM) reads using the fpm() function of DESeq2, after removal of lowly expressed genes with less than 10 reads over all samples. Expression levels of genes were estimated by the variance-mean dependence in the count table based on a generalized linear model using the negative binomial distribution within the R package DESeq2 (33) calculating $\log_2$ fold change ($\log_2$FC) values between wild type and mutant in the respective tissues with the design ∼ genotype + tissue + genotype:tissue. Significance values for $\log_2$FC values were calculated as Wald test *P* value and were adjusted by the Benjamini-Hochberg procedure to obtain FDR (68). Genes with an FDR <5% and $\log_2$FC >|1| were considered differentially expressed. From this gene set, we excluded gene pairs that were assigned to chr0 and chr1, which had the same annotation, and the respective gene partner was the one with the closest related transcript after a BLAST search. GO term enrichment of the resulting gene set was performed using agriGo (69). The sequencing data have been deposited in the National Center for Biotechnology Information sequencing read archive (PRJNA589222).

Laser Capture Dissection Microscopy for Separating the Upper and Lower Flanks of Roots. Laser capture dissection microscopy was used to separate cells for the analysis of gene expression levels in the upper and lower flanks of rotated roots (*SI Appendix*, Fig. S5*A*). Six hours after rotating 7-d-old plants grown in rhizoboxes by 90°, 5-mm-long root tip segments of the initially most vertical roots were collected and then fixed, embedded, and sectioned as described. The cortical and epidermal cells of 1.5 mm of the elongation zone adjacent to the meristem were cut by a PALM Microbeam Platform (Zeiss) with the following settings: energy: 54; speed: 3; and cutting program: "Cut," picked up manually with a sharp needle and transferred to the cap of RNase-free adhesive caps (Zeiss).

RNA was isolated and analyzed as described. RIN values of RNAs were between 6.7 and 7.8, and concentrations were between 9 and 20 ng/μL. RNA of three roots from independent plants was used as one biological replicate; three biological replicates were analyzed for each genotype and flank.

Phylogenetic Analysis. The EGT2 (HORVU.MOREX.r2.5HG0370880.1) protein sequence was BLASTed on Phytozome v12.1 to the *Brachypodium dystachyon* proteome v3.1, the *Oryza sativa* proteome v7_JGI, the *Zea mays* proteome Ensembl-18, the *Arabidopsis thaliana* proteome TAIR10, the *Prunus persica* proteome v2.1, and the *Sorghum bicolor* proteome v3.1.1 with the default settings. Hits with E-values $<3.9 \times 10^{-77}$ were considered. The identified orthologs were then confirmed using the EnsemblPlants Compara Ortholog tool. Retrieved protein sequences were aligned by ClustalW in the software MEGA X, with default values (70): Ancestral states were inferred using the maximum likelihood method (71) and JTT matrix-based model (72). The tree shows a set of possible amino acids (states) at each ancestral node based on their inferred likelihood at site 1. The initial tree was inferred automatically by applying Neighbor-Join and BioNJ algorithms to a matrix of pairwise distances estimated using the JTT model and then selecting the topology with superior log likelihood value. The rates among sites were treated as being uniform among sites (Uniform rates option). This analysis involved 16 amino acid sequences.

Data Availability. RNA-seq data have been deposited in SRA (https://www.ncbi.nlm.nih.gov/bioproject/PRJNA589222).

ACKNOWLEDGMENTS. This work was funded by the Deutsche Forschungsgemeinschaft Grant HO2249/21-1 (to F.H.). K.A.N., D.P., and R.K. acknowledge support from the Helmholtz Association for the Forschungszentrum Jülich. The rhizotron study received funding from the European Union's Horizon 2020 research and innovation program under Grant Agreement No. 731013 (EPPN2020). Work described here is supported in part by the project "Rooty: A root ideotype toolbox to support improved wheat yields" funded by the IWYP Consortium (Project IWYP122) to C.U., J.S., R.T., and S.S. via the Biotechnology and Biological Sciences Research Council in the United Kingdom (BB/S012826/1). We thank Felix Frey (University of Bonn) for his advice on RNA-seq data analysis and discussion, Johannes Stuttmann (University of Halle) for sharing the CRISPR/Cas cloning vectors, and Shalima H. Orse for support throughout the project. We thank Anna Galinski, Jonas Lentz, Carmen Müller, Bernd Kastenholz, Ann-Katrin Kleinert, Roberta Rossi, and Kwabena Agyei (Forschungszentrum Jülich GmbH) for their assistance during the rhizotron study. R.K. and D.P. gratefully acknowledge Dagmar van Dusschoten and Johannes Kochs for support and maintenance of the MRI System.

1. T. Wheeler, J. von Braun, Climate change impacts on global food security. *Science* **341**, 508–513 (2013).
2. N. Ramankutty *et al*., Trends in global agricultural land use: Implications for environmental health and food security. *Annu. Rev. Plant Biol.* **69**, 789–815 (2018).
3. J. P. Lynch, Root phenotypes for improved nutrient capture: An underexploited opportunity for global agriculture. *New Phytol.* **223**, 548–564 (2019).
4. K. P. Voss-Fels, R. J. Snowdon, L. T. Hickey, Designer roots for future crops. *Trends Plant Sci.* **23**, 957–960 (2018).
5. Y. Uga *et al*., Control of root system architecture by DEEPER ROOTING 1 increases rice yield under drought conditions. *Nat. Genet.* **45**, 1097–1102 (2013).
6. A. P. Wasson *et al*., Traits and selection strategies to improve root systems and water uptake in water-limited wheat crops. *J. Exp. Bot.* **63**, 3485–3498 (2012).
7. R. Tsugeki, N. V. Fedoroff, Genetic ablation of root cap cells in *Arabidopsis*. *Proc. Natl. Acad. Sci. U.S.A.* **96**, 12941–12946 (1999).
8. E. B. Blancaflor, J. M. Fasano, S. Gilroy, Mapping the functional roles of cap cells in the response of *Arabidopsis* primary roots to gravity. *Plant Physiol.* **116**, 213–222 (1998).
9. H. Konnings, The significance of the root cap for geotropism. *Acta Bot. Sin.* **17**, 203–211 (1968).
10. S. Mancuso, P. W. Barlow, D. Volkmann, F. Baluska, Actin turnover-mediated gravity response in maize root apices: Gravitropism of decapped roots implicates gravisensing outside of the root cap. *Plant Signal. Behav.* **1**, 52–58 (2006).
11. C. Wolverton, J. L. Mullen, H. Ishikawa, M. L. Evans, Root gravitropism in response to a signal originating outside of the cap. *Planta* **215**, 153–157 (2002).
12. J. Z. Kiss, F. D. Sack, Severely reduced gravitropism in dark-grown hypocotyls of a starch-deficient mutant of *Nicotiana sylvestris*. *Plant Physiol.* **94**, 1867–1873 (1990).
13. F. Darwin, The statolith theory of geotropism. *Nature* **67**, 571–572 (1903).
14. N. Saether, T. H. Iversen, Gravitropism and starch statoliths in an *Arabidopsis* mutant. *Planta* **184**, 491–497 (1991).
15. J. Friml, J. Wiśniewska, E. Benková, K. Mendgen, K. Palme, Lateral relocation of auxin efflux regulator PIN3 mediates tropism in *Arabidopsis*. *Nature* **415**, 806–809 (2002).
16. G. B. Monshausen, H. E. Zieschang, A. Sievers, Differential proton secretion in the apical elongation zone caused by gravistimulation is induced by a signal from the root cap. *Plant Cell Environ.* **19**, 1408–1414 (1996).
17. J. M. Fasano *et al*., Changes in root cap pH are required for the gravity response of the *Arabidopsis* root. *Plant Cell* **13**, 907–921 (2001).
18. J. L. Mullen, H. Ishikawa, M. L. Evans, Analysis of changes in relative elemental growth rate patterns in the elongation zone of *Arabidopsis* roots upon gravistimulation. *Planta* **206**, 598–603 (1998).
19. G. Huang *et al*., Rice actin binding protein RMD controls crown root angle in response to external phosphate. *Nat. Commun.* **9**, 2346 (2018).
20. K. Boonsirichai, J. C. Sedbrook, R. Chen, S. Gilroy, P. H. Masson, ALTERED RESPONSE TO GRAVITY is a peripheral membrane protein that modulates gravity-induced cytoplasmic alkalinization and lateral auxin transport in plant statocytes. *Plant Cell* **15**, 2612–2625 (2003).
21. J. M. Guseman, K. Webb, C. Srinivasan, C. Dardick, DRO1 influences root system architecture in *Arabidopsis* and *Prunus* species. *Plant J.* **89**, 1093–1105 (2017).
22. I. K. Dawson *et al*., Barley: A translational model for adaptation to climate change. *New Phytol.* **206**, 913–931 (2015).
23. V. Talamè *et al*., TILLMore, a resource for the discovery of chemically induced mutants in barley. *Plant Biotechnol. J.* **6**, 477–485 (2008).
24. R. Bovina *et al*., Identification of root morphology mutants in barley. *Plant Genet. Resour.* **9**, 357–360 (2011).
25. S. Wu *et al*., VLN2 regulates plant architecture by affecting microfilament dynamics and polar auxin transport in rice. *Plant Cell* **27**, 2829–2845 (2015).
26. M. Mascher *et al*., A chromosome conformation capture ordered sequence of the barley genome. *Nature* **544**, 427–433 (2017).
27. C. Monat *et al*., TRITEX: Chromosome-scale sequence assembly of Triticeae genomes with open-source tools. *Genome Biol.* **20**, 284 (2019).
28. C. J. A. Sigrist *et al*., New and continuing developments at PROSITE. *Nucleic Acids Res.* **41**, D344–D347 (2013).
29. G. Denay, G. Vachon, R. Dumas, C. Zubieta, F. Parcy, Plant SAM-domain proteins start to reveal their roles. *Trends Plant Sci.* **22**, 718–725 (2017).
30. C. A. Hollender *et al*., Loss of a highly conserved sterile alpha motif domain gene (*WEEP*) results in pendulous branch growth in peach trees. *Proc. Natl. Acad. Sci. U.S.A.* **115**, E4690–E4699 (2018).
31. K. V. Krasileva *et al*., Uncovering hidden variation in polyploid wheat. *Proc. Natl. Acad. Sci. U.S.A.* **114**, E913–E921 (2017).
32. G. K. Kirschner, Y. Stahl, M. Von Korff, R. Simon, Unique and conserved features of the barley root meristem. *Front Plant Sci* **8**, 1240 (2017).
33. M. I. Love, W. Huber, S. Anders, Moderated estimation of fold change and dispersion for RNA-seq data with DESeq2. *Genome Biol.* **15**, 550 (2014).
34. D. J. Cosgrove, Plant expansins: Diversity and interactions with plant cell walls. *Curr. Opin. Plant Biol.* **25**, 162–172 (2015).
35. M. Taniguchi *et al*., The Arabidopsis LAZY1 family plays a key role in gravity signaling within statocytes and in branch angle control of roots and shoots. *Plant Cell* **29**, 1984–1999 (2017).
36. M. Hála *et al*., An exocyst complex functions in plant cell growth in *Arabidopsis* and tobacco. *Plant Cell* **20**, 1330–1345 (2008).
37. T. Ogura *et al*., Root system depth in *Arabidopsis* is shaped by EXOCYST70A3 via the dynamic modulation of auxin transport. *Cell* **178**, 400–412.e16 (2019).
38. N. Siddiqui, J. Léon, A. A. Naz, A. Ballvora, Genetics and genomics of root system variation in adaptation to drought-stress in cereal crops. *J. Exp. Bot.* **72**, 1007–1019. (2021).
39. Y. Kitomi *et al*., Root angle modifications by the *DRO1* homolog improve rice yields in saline paddy fields. *Proc. Natl. Acad. Sci. U.S.A.* **117**, 21242–21250 (2020).
40. G. Rubio *et al*., Root gravitropism and below-ground competition among neighbouring plants: A modelling approach. *Ann. Bot.* **88**, 929–940 (2001).
41. M. F. Dreccer *et al*., Genotypic variation for lodging tolerance in spring wheat: Wider and deeper root plates, a feature of low lodging, high yielding germplasm. *F. Crop. Res.* **258**, 107942 (2020).
42. W. Sinclair, I. Oliver, P. Maher, A. Trewavas, The role of calmodulin in the gravitropic response of the *Arabidopsis thaliana agr-3* mutant. *Planta* **199**, 343–351 (1996).
43. A. M. Jones *et al*., Border control–A membrane-linked interactome of *Arabidopsis*. *Science* **344**, 711–716 (2014).
44. F. Passardi, C. Penel, C. Dunand, Performing the paradoxical: How plant peroxidases modify the cell wall. *Trends Plant Sci.* **9**, 534–540 (2004).
45. J. H. Joo, Y. S. Bae, J. S. Lee, Role of auxin-induced reactive oxygen species in root gravitropism. *Plant Physiol.* **126**, 1055–1060 (2001).
46. A. Osthoff, P. Donà Dalle Rose, J. A. Baldauf, H. P. Piepho, F. Hochholdinger, Transcriptomic reprogramming of barley seminal roots by combined water deficit and salt stress. *BMC Genomics* **20**, 325 (2019).
47. D. C. Hoagland, D. I. Arnon, *The Water Culture Method for Growing Plant Without Soil* (College of Agriculture, University of California) (1950).
48. K. A. Nagel *et al*., GROWSCREEN-Rhizo is a novel phenotyping robot enabling simultaneous measurements of root and shoot growth for plants grown in soil-filled rhizotrons. *Funct. Plant Biol.* **39**, 891–904 (2012).
49. D. Pflugfelder *et al*., Non-invasive imaging of plant roots in different soils using magnetic resonance imaging (MRI). *Plant Methods* **13**, 102 (2017).
50. C. A. Schneider, W. S. Rasband, K. W. Eliceiri, NIH Image to ImageJ: 25 years of image analysis. *Nat. Methods* **9**, 671–675 (2012).
51. R. W. Michelmore, I. Paran, R. V. Kesseli, Identification of markers linked to disease-resistance genes by bulked segregant analysis: A rapid method to detect markers in specific genomic regions by using segregating populations. *Proc. Natl. Acad. Sci. U.S.A.* **88**, 9828–9832 (1991).
52. J. Comadran *et al*., Natural variation in a homolog of Antirrhinum CENTRORADIALIS contributed to spring growth habit and environmental adaptation in cultivated barley. *Nat. Genet.* **44**, 1388–1392 (2012).
53. D. L. Hyten *et al*., High-throughput genotyping with the GoldenGate assay in the complex genome of soybean. *Theor. Appl. Genet.* **116**, 945–952 (2008).
54. H. Li, R. Durbin, Fast and accurate short read alignment with Burrows-Wheeler transform. *Bioinformatics* **25**, 1754–1760 (2009).
55. H. Li *et al*.; 1000 Genome Project Data Processing Subgroup, The sequence alignment/map format and SAMtools. *Bioinformatics* **25**, 2078–2079 (2009).
56. H. Li, A statistical framework for SNP calling, mutation discovery, association mapping and population genetical parameter estimation from sequencing data. *Bioinformatics* **27**, 2987–2993 (2011).
57. P. Cingolani *et al*., A program for annotating and predicting the effects of single nucleotide polymorphisms, SnpEff: SNPs in the genome of *Drosophila* melanogaster strain w1118; iso-2; iso-3. *Fly (Austin)* **6**, 80–92 (2012).
58. D. van Dusschoten *et al*., Quantitative 3D analysis of plant roots growing in soil using magnetic resonance imaging. *Plant Physiol.* **170**, 1176–1188 (2016).
59. N. Kumar *et al*., Further analysis of barley MORC1 using a highly efficient RNA-guided Cas9 gene-editing system. *Plant Biotechnol. J.* **16**, 1892–1903 (2018).
60. G. R. Lazo, P. A. Stein, R. A. Ludwig, A DNA transformation-competent *Arabidopsis* genomic library in Agrobacterium. *Biotechnology (N. Y.)* **9**, 963–967 (1991).
61. J. Imani, L. Li, P. Schäfer, K.-H. Kogel, STARTS—A stable root transformation system for rapid functional analyses of proteins of the monocot model plant barley. *Plant J.* **67**, 726–735 (2011).
62. M. W. Pfaffl, A new mathematical model for relative quantification in real-time RT-PCR. *Nucleic Acids Res.* **29**, e45 (2001).
63. M. S. Anjam *et al*., An improved procedure for isolation of high-quality RNA from nematode-infected *Arabidopsis* roots through laser capture microdissection. *Plant Methods* **12**, 25 (2016).
64. A. Matei *et al*., How to make a tumour: Cell type specific dissection of Ustilago maydis-induced tumour development in maize leaves. *New Phytol.* **217**, 1681–1695 (2018).
65. A. M. Bolger, M. Lohse, B. Usadel, Trimmomatic: A flexible trimmer for Illumina sequence data. *Bioinformatics* **30**, 2114–2120 (2014).
66. A. Dobin *et al*., STAR: Ultrafast universal RNA-seq aligner. *Bioinformatics* **29**, 15–21 (2013).
67. S. Anders, P. T. Pyl, W. Huber, HTSeq—A Python framework to work with high-throughput sequencing data. *Bioinformatics* **31**, 166–169 (2015).
68. Y. Benjamini, Y. Hochberg, Controlling the false discovery rate: A practical and powerful approach to multiple testing. *R. Stat. Soc.* **57**, 289–300 (1995).
69. T. Tian *et al*., agriGO v2.0: A GO analysis toolkit for the agricultural community, 2017 update. *Nucleic Acids Res.* **45** (W1), W122–W129 (2017).
70. S. Kumar, G. Stecher, M. Li, C. Knyaz, K. Tamura, MEGA X: Molecular evolutionary genetics analysis across computing platforms. *Mol. Biol. Evol.* **35**, 1547–1549 (2018).
71. M. Nei, S. Kumar, *Molecular Evolution and Phylogenetics* (Oxford University Press, 2000).
72. D. T. Jones, W. R. Taylor, J. M. Thornton, The rapid generation of mutation data matrices from protein sequences. *Comput. Appl. Biosci.* **8**, 275–282 (1992).

New Phytologist

Research

ENHANCED GRAVITROPISM 2 coordinates molecular adaptations to gravistimulation in the elongation zone of barley roots

Li Guo[1], Alina Klaus[1], Marcel Baer[1], Gwendolyn K. Kirschner[1], Silvio Salvi[2] and Frank Hochholdinger[1]

[1]Institute of Crop Science and Resource Conservation, Crop Functional Genomics, University of Bonn, 53113 Bonn, Germany; [2]Department of Agricultural and Food Sciences, University of Bologna, 40127 Bologna, Italy

Author for correspondence:
Frank Hochholdinger
Email: hochholdinger@uni-bonn.de

Received: *11 October 2022*
Accepted: *11 December 2022*

New Phytologist (2023)
doi: 10.1111/nph.18717

Key words: barley, bimolecular fluorescence complementation (BiFC), EGT2, gravitropism, RNA-seq, WGCNA, yeast-two-hybrid.

Summary

- Root gravitropism includes gravity perception in the root cap, signal transduction between root cap and elongation zone, and curvature response in the elongation zone. The barley (*Hordeum vulgare*) mutant *enhanced gravitropism 2* (*egt2*) displays a hypergravitropic root phenotype.
- We compared the transcriptomic reprogramming of the root cap, the meristem, and the elongation zone of wild-type (WT) and *egt2* seminal roots upon gravistimulation in a time-course experiment and identified direct interaction partners of EGT2 by yeast-two-hybrid screening and bimolecular fluorescence complementation validation.
- We demonstrated that the elongation zone is subjected to most transcriptomic changes after gravistimulation. Here, 33% of graviregulated genes are also transcriptionally controlled by *EGT2*, suggesting a central role of this gene in controlling the molecular networks associated with gravitropic bending. Gene co-expression analyses suggested a role of *EGT2* in cell wall and reactive oxygen species-related processes, in which direct interaction partners of EGT2 regulated by *EGT2* and gravity might be involved.
- Taken together, this study demonstrated the central role of *EGT2* and its interaction partners in the networks controlling root zone-specific transcriptomic reprogramming of barley roots upon gravistimulation. These findings can contribute to the development of novel root idiotypes leading to improved crop performance.

Introduction

The gravitropic response plays an essential role in controlling plant growth direction and architecture under changing environmental conditions (Nakamura *et al.*, 2019). Root gravitropism enables plants to adjust their root growth direction, allowing them to penetrate deeply into the soil, thereby anchoring plants in the soil and optimizing the uptake of water and nutrients (Zhang *et al.*, 2019). In flowering plants, root gravitropic response is a three-step process: gravity perception, signal transduction, and curvature response (Singh *et al.*, 2017; Su *et al.*, 2017; Nakamura *et al.*, 2019; Jiao *et al.*, 2021).

The most prominent explanation of how roots sense gravity is the starch-statolith hypothesis: Upon root reorientation, the gravity signal is sensed by starch-filled amyloplasts sedimented to the new bottom-site of the columella cells in the root cap (Singh *et al.*, 2017; Su *et al.*, 2017). This results in the relocalization of auxin toward the bottom side of columella cells by downward auxin transport and a lateral auxin gradient across the root cap. Auxin is then transported to the lateral root cap and epidermal cells in a shootward direction toward the elongation zone, resulting in asymmetrical auxin distribution across the distal elongation zone with higher auxin levels on the lower flank and lower auxin content on the upper flank. In the epidermal cells on the lower flank of the elongation zone, elevated auxin levels increase the apoplastic pH and inhibit cell elongation. By contrast, on the upper side of the elongation zone, decreased auxin levels lead to a decrease in the pH of the apoplast, which increases cell elongation. The asymmetrical elongation of cells on the two sides of the gravistimulated root eventually leads to the gravitropic root bending in the direction of gravity (Su *et al.*, 2020). Nevertheless, cells within the root distal elongation zone have also been shown to play a role in gravity perception with an alternative mechanism (Wolverton *et al.*, 2002; Mancuso *et al.*, 2006; Su *et al.*, 2020).

In a previous study, we identified the barley mutant *egt2* (*enhanced root gravitropism 2*) that displays a narrower root system

than wild-type (WT) plants, with root angles at least 50% smaller than WT. Phytohormone treatment showed that *egt2* responds to auxin similarly as the WT, suggesting that the auxin response is unaffected in *egt2*. Moreover, we did not observe any significant differences between the structure and size of the meristem, the root cap, amyloplast content, and the amyloplast sedimentation velocities between *egt2* and WT. This suggests that *EGT2* is likely involved in root gravitropism after gravity perception. The *EGT2* gene encodes a STERILE ALPHA MOTIF (SAM) domain–containing protein (Kirschner *et al.*, 2021). STERILE ALPHA MOTIF domains are present in thousands of proteins in prokaryotes and diverse eukaryotes (Kim & Bowie, 2003; Qiao & Bowie, 2005; Denay *et al.*, 2017). The SAM domain was first considered as an evolutionarily conserved protein binding domain (Schultz *et al.*, 1997). Subsequently, a large diversity of SAM functions has been observed, including the binding of proteins, lipids, and RNAs (Denay *et al.*, 2017; Ray *et al.*, 2020). The best-characterized plant SAM domain-containing protein is LEAFY that functions as a master regulator of flower development in angiosperms (Eriksson *et al.*, 2006; Siriwardana & Lamb, 2012; Yamaguchi, 2021). The SAM domain at the N-terminus of LEAFY mediates oligomerization of LEAFY, which allows the LEAFY dimers to bind to DNA regions without LEAFY-binding sites or closed chromatin regions (Sayou *et al.*, 2016). AtSAM5, a homolog of EGT2 in Arabidopsis, has been shown to interact with the Ca^{2+}-dependent protein kinase CPK13 (Jones *et al.*, 2014), which is involved in the response to light by controlling the stomatal aperture (Ronzier *et al.*, 2014). Moreover, narrower lateral root angles were observed in mutants of *AtSAM5*, suggesting a role of *AtSAM5* in regulating lateral root angle in Arabidopsis (Johnson *et al.*, 2022). Another homolog of EGT2 is WEEP in peach trees (Hollender *et al.*, 2018). A 5′ deletion of the *WEEP* gene caused downward and wandering growth of the mutant shoots that did not bend upward after 90° reorientation. This suggests a role of WEEP in shoot gravitropism, which shows similarities to the function of EGT2 in roots (Hollender *et al.*, 2018). In barley, 17 SAM domain-containing proteins were annotated, and none of them has been functionally characterized thus far except for *EGT2* (Kirschner *et al.*, 2021).

In this study, the transcriptomes of the root cap, the meristem, and the elongation zone of gravistimulated WT and mutant *egt2* roots were studied by RNA sequencing (RNA-seq) in a time-course experiment. These experiments revealed that EGT2 is a central regulator of the gravitropism-regulated gene expression networks in barley seminal roots. Functional enrichment analyses of differentially expressed genes (DEGs) and weighted gene co-expression network analyses suggested the involvement of plant cell wall organization and reactive oxygen species (ROS) in *EGT2*-regulated root gravitropism. By a combination of yeast-two-hybrid experiments and bimolecular fluorescence complementation (BiFC), we demonstrated that a subset of the genes transcriptionally regulated by gravistimulation and by *EGT2* encoded proteins that directly interact with EGT2. The results of this study highlight the transcriptomic reprogramming of the gravitropic response of barley roots and provide new insights into the molecular function of *EGT2*.

Materials and Methods

Plant materials and growth condition

Wild-type barley plants (*Hordeum vulgare* L. cv Morex) and the *egt2* mutant (Kirschner *et al.*, 2021) were used for this study. Before germination, the seeds were washed in sodium hypochlorite (1.2% active chlorine) for 5 min and rinsed with distilled water. Then, seeds were incubated in dark at 30°C O/N, and only germinating seeds were used for further experiments. Plants used for RNA-seq were grown in growth chambers (Conviron, Winnipeg, MB, Canada) at 18°C at night (8 h) and 22°C at day (16 h).

Determination of root zones

To measure the length of the meristem, 3-d-old WT and *egt2* plants were rotated by 90° for 6 or 10 h. Root tip segments of 5 mm length of the most vertical roots before rotation were taken before and after rotation. Root tips were then embedded in 10% (w/v) agarose, and 40 µm sections were prepared with a vibratome. Images of root sections taken with a Zeiss PALM MicroBeam microscope (Zeiss) were analyzed by ImageJ. The zone between the first cell in the first cortical layer that doubled in size and the first cell that increased noticeably in length was considered as the transition zone. The length from root cap junction to the middle of transition zone was measured as the length of the meristem (Verbelen *et al.*, 2006; Baluška *et al.*, 2010). Eleven to nineteen roots were analyzed per genotype by time point combination (Supporting Information Fig. S1).

Sample collection and RNA isolation

For RNA sequencing, 3-d-old plants were rotated by 90° for 3, 6, and 12 h. The root cap, the meristem (1 mm; Fig. S1), and 1 mm of the distal elongation zone (Fig. 1a) of the most vertically grown seminal roots before rotation were separated by a razor blade under a binocular before (time point 0 h) and after rotation. Three roots were collected per seedling, and root zones from eight plants were pooled per biological replicate. Three biological replicates were used for each genotype by time point combination. After dissection, samples were immediately frozen in liquid nitrogen for RNA isolation. RNA extraction was performed with the RNeasy Plant Mini Kit (Qiagen) according to the manufacturer's protocol. RNA quality was assessed with an Agilent 2100 Bioanalyzer using the Agilent RNA 6000 Nano kit (Agilent, Santa Clara, CA, USA). The RNA integrity number was between 8.3 and 10 for all samples.

RNA-seq and data analyzing

Messenger RNA (mRNA) purified from total RNA using poly-T oligo-attached magnetic beads was used to prepare cDNA libraries for Illumina sequencing (Illumina, San Diego, CA, USA). Fragmented mRNA and random hexamer primers were used for reverse transcription. The cDNA library was prepared by ligating the cDNA product to adapter, followed by amplification

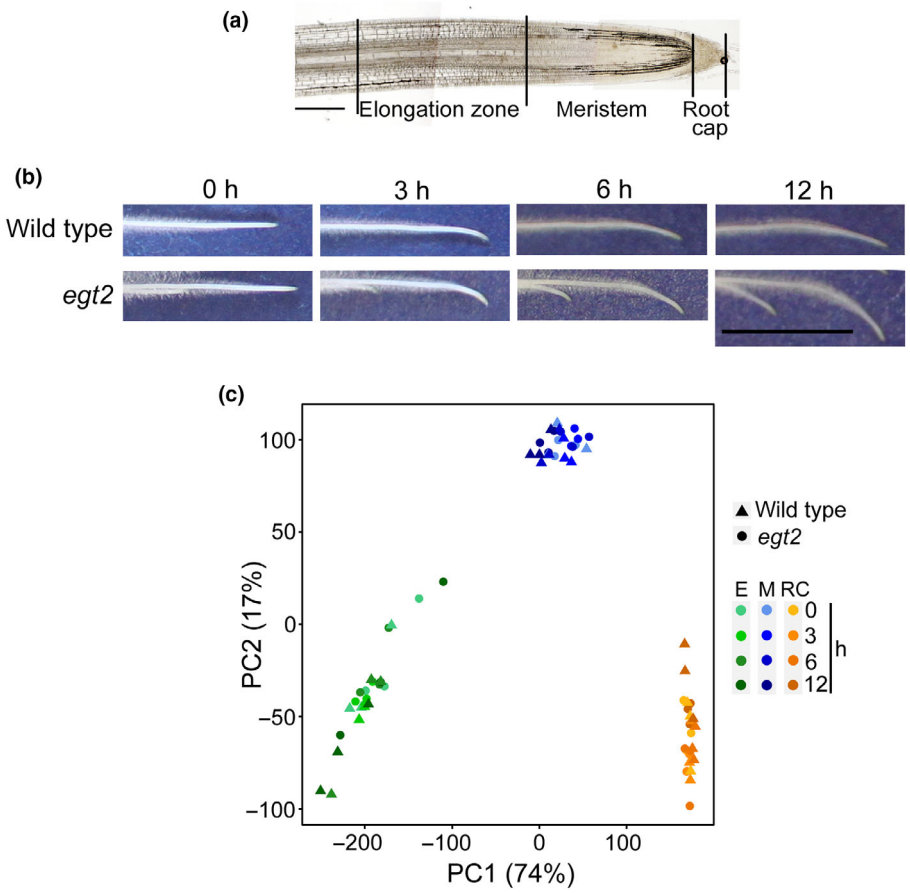

Fig. 1 Seminal roots upon rotation and RNA sequencing sample relationship of root zones. (a) Representative section for meristem length measurement, illustrating the elongation zone, the meristem, and the root cap harvested for RNA-seq. Bar, 300 μm. (b) Phenotype of wild-type and *enhanced gravitropism 2* mutant roots before (0 h) and after 3, 6, and 12 h of rotation. Bar, 1 cm. (c) Principal component analysis plot for the transcriptomes of the 72 RNA-seq samples of the two genotypes, three root zones, and four time points.

and purification (Novogene, Cambridge, UK). Cluster preparation and single read sequencing were performed according to the manufacturer's instructions (Illumina). Sequencing was performed in a NovaSeq 6000, S4 FlowCell using the paired-end 150 bp sequencing strategy. Raw RNA-seq reads were processed with CLC GENOMICS WORKBENCH (v.20.0.1) as previously described with some minor modifications (Osthoff *et al.*, 2019). Reads with a length < 40 bp were discarded, and the remaining reads were mapped to the barley reference genome (Hv_Morex.pgsb.Jul2020) with a similarity of 0.9 and a length fraction of 0.8. Reads mapped to more than one position were regarded as duplicate mapped reads and removed from further analyses (Mascher *et al.*, 2021).

Data generated by CLC GENOMICS WORKBENCH were analyzed using R. To remove lowly expressed genes, the cpm() function from the EDGER library was used to normalize the different sequencing depths for each sample (Robinson *et al.*, 2010). A CPM threshold of 1.2 was used and only genes that have at least three TRUES in each row of threshold were kept for further steps. A principal component analysis (PCA) was computed by R the functions prcomp() and visualized by the autoplot() function in the GGPLOT2 package. The contrasts.fit function of the R package LIMMA was used to calculate $\log_2$ fold change ($\log_2$FC) values between different root zones and time point combinations in the WT time-course experiment and in comparisons between the *egt2* mutant and WT (Ritchie *et al.*, 2015). The false discovery rate (FDR) was adjusted to < 5% to correct *P*-values of contrasts for multiple testing (Benjamini & Hochberg, 1995). Venn diagrams were produced by the VENNDIAGRAM package (Chen & Boutros, 2011). A hierarchical clustering analysis was conducted by the CLUSTER package with dynamic tree cutting (Maechler *et al.*, 2022). The upset() function in the UPSETR library was used for comparison between multiple gene sets (Conway *et al.*, 2017). Gene Ontology (GO) analyses were performed by the R function TOPGO (Alexa & Rahnenführer, 2022). Redundant GO terms were filtered by REVIGO with a similarity ≤ 0.5 (Supek *et al.*, 2011).

Weighted gene correlation network analysis

The R package weighted gene correlation network analysis (WGCNA) was used for gene co-expression analyses (Langfelder & Horvath, 2008). After filtering out lowly expressed genes with < 50 total reads in the 24 samples of each root zone, the read data generated by CLC GENOMICS WORKBENCH were used as input. Samples were clustered using the hclust function. The outlier samples were determined by setting the cutheight to 50 for the root cap, 40 for the meristem, and 75 for the elongation zone. After removing outliers, the co-expression modules of each root zone dataset were generated by the one-step network construction function blockwiseModules with a soft threshold of 4 for the root cap and elongation zone and 6 for the meristem, and setting

TOMtype to 'signed'. To avoid small clusters, modules with < 30 genes were merged with their closest larger module using the cutreeDynamic function. The eigengene calculation of each module was performed using the moduleEigengenes function followed by the calculation of the module dissimilarity of eigengenes. Modules whose eigengenes were correlated > 0.8 were merged via the mergeCutHeight function with a cutHeight of 0.20. A unique color was then assigned to each merged module via the plotDendroAndColors function. The edge weight determined by the topology overlap measure (TOM) reflected the connectivity between two genes. The weight values across all edges of each gene in each module were calculated and exported for gene network visualization, which was achieved by CYTOSCAPE (v.3.9.1). To determine the hub genes of each module, we sorted the weight values of each edge from the highest to the smallest, and nodes with the top 1%, 0.1%, or 0.01% of weight were considered as hub genes based on the size of the module. Gene networks were analyzed with the 'Analyze Network' tool in CYTOSCAPE and the 'degree' values were considered to reduce the numbers of hub genes.

We calculated relationships between module eigengenes and traits using Pearson's correlation coefficients in R. Significant *P*-values of each module and trait correlation were calculated using the corPvalueStudent function. Modules with *P*-values ≤ 0.05 were considered as significantly correlated modules.

Yeast-two-hybrid library construction

Total RNA extracted from the whole root system of ten 5-d-old seedlings was used to generate the cDNA library, which was conducted with the 'Make Your Own 'Mate & Plate™' Library System' according to the manufacturer's instructions with minor modifications (Clontech, Saint Germain en Laye, France). Oligo-dT primers provided in the kit were used for first-strand cDNA synthesis with 2 μg total RNA as input. Amplification of cDNA was performed by using long-distance PCR with 25 cycles to generate 6–7 μg of ds cDNA. After purifying with CHROMA SPIN + TE-400 columns, ds cDNA library was transformed into yeast (*Saccharomyces cerevisiae*) strain Y187.

Generation of competent yeast cells and library transformation were conducted using the LiAc/SS-DNA/PEG procedure (Gietz *et al.*, 1995). Transformed cell plating and library cell harvesting were conducted according to the manufacturer's instructions.

Toxicity and autoactivation testing

To test the toxicity and autoactivation of EGT2, the full-length coding sequence of EGT2 was amplified using the primers specified in Table S1 and then inserted into the vector pGBKT7 using *Eco*RI and *Bam*HI restriction endonucleases. Detection of EGT2 toxicity on yeast growth was performed according to Matchmaker® Gold Yeast Two-Hybrid System User Manual (TaKaRa, Saint Germain en Laye, France). Yeast cells expressing pGBKT7-EGT2 displayed a similar growth rate to yeast cells transformed with an empty pGBKT7 vector, indicating that EGT2 is not toxic (Fig. S2a). To test the autoactivation of EGT2, pGBKT7-EGT2 plasmid was co-transformed into Y2HGold yeast cells with pGADT7. pGBKT7-53 and pGBKT7-lam plasmids were transformed together with pGADT7-T as positive and negative controls, respectively. The transformed cells were grown on SD/−Trp/−Leu medium at 30°C for 4 d. Three clones of each combination were diluted in ddH_2O, and 1 μl of these diluted cells was dotted on SD/−Trp/−Leu/−His/−Ade medium and grown at 30°C for 4 d. Yeast cells transformed with pGBKT7-EGT2 plasmid cannot survive on SD−Trp/−Leu/−Ade/−His medium, suggesting that EGT2 does not display autoactivation (Fig. S2b). Therefore, pGBKT7-EGT2 was used as bait for yeast-two-hybrid screening.

Yeast-two-hybrid library screening

Yeast-two-hybrid library screening was performed according to the Matchmaker Gold Yeast Two-Hybrid System User Manual (Clontech).

Yeast colony PCR was performed with pGADT7 primers to eliminate duplicated positive colonies containing the same prey plasmid. Among the PCR products from all positive colonies, only DNA bands with different sizes were recovered and sequenced to identify the genes inserted. Subsequently, prey plasmids from library were rescued from yeast clones with 'Easy Yeast Plasmid Isolation Kit' (Clontech) and sequenced. By doing so, all prey plasmids contained in one positive colony were identified and further tested. These prey plasmids were further used in one-on-one yeast-two-hybrid assays to confirm the results of yeast-two-hybrid screening.

Subcellular localization

The vectors constructed using the 2in1 cloning system were used for the subcellular localization analyses (Grefen & Blatt, 2012). The full-length coding sequence of *EGT2* (*HORVU.MOREX.r3.5HG0447830.1*), *OMT* (*HORVU.MOREX.r3.3HG0330120.1*), *PBP* (*HORVU.MOREX.r3.7HG0709860.1*), *GXM* (*HORVU.MOREX.r3.7HG0749870.1*), *HMT* (*HORVU.MOREX.r3.2HG0126380.1*), and *HORVU.MOREX.r3.1HG0000050.1* was amplified using Phusion™ High-Fidelity DNA Polymerase (Thermo Fisher Scientific, Waltham, MA, USA) with primers specified in Table S1.

The insertion of the *EGT2* amplicons into pDONR221 P1-P4 entry vector carrying the attP1 and attP4 recombination sites was accomplished by BP reactions using the BP Clonase™ II enzyme mix (Thermo Fisher Scientific). The same enzyme was used for insertion of interaction candidates into pDONR221 P2R-P3 carrying the attP2 and attP3 recombination sites. Subsequently, entry clones were integrated with the corresponding destination vectors pFRETvr-2in1-NN or pFRETvr-2in1-NC. The reaction was catalyzed by LR Clonase™ II Mix (Thermo Fisher Scientific). Finally, we generated expression constructs containing the *EGT2* coding sequence either N- or C-terminally fused to tagRFP (EGT2-tagRFP and tagRFP-EGT2) and the coding sequence of interaction partners N-terminally fused to mVenus. All constructs were verified and transformed into Agrobacterium (*Agrobacterium tumefaciens*) strain AGI1.

Positive Agrobacterium clones were cultured in lysogeny broth medium with respective antibiotics until OD_{600} reach 0.8. Then, cells were precipitated and dissolved in 10 mM $MgCl_2$, 10 mM MES (2-morpholinoethanesulfonic acid), and 100 μM AS (Acetosyringone), and infiltrated into tobacco (*Nicotiana benthamiana*) leaves using a syringe. Transgene expression was analyzed using a Zeiss LSM 780 confocal microscopy system 3 d after infiltration. The fluorescence of tagRFP was excited at 543 nm using a helium neon laser with a laser power of 30%, and detected through the meta-channel at 579–633 nm (ChS1). mVenus and chloroplast autofluorescence were excited at 488 nm by the argon laser with a 10% laser power, emission of mVenus was detected at 517–553 nm. The emission of chloroplast autofluorescence was detected at 686–711 nm via the meta-channel (ChS2).

Bimolecular fluorescence complementation

The same entry vectors as used for the subcellular localization experiments were integrated with the corresponding destination vectors pBiFCt-2in1-NN or pBiFCt-2in1-NC for BiFC. Both destination vectors contained *tagRFP*, which was driven by the CaMV 35S promoter and used as a positive control for successful infiltration of tobacco cells. Finally, we generate expression constructs containing the *EGT2* coding sequence without stop codon (−TGA) N-terminally fused to the C-terminal part of YFP (EGT2 (−TGA)-cYFP) or the *EGT2* coding sequence with stop codon (+TGA) C-terminally fused to the C-terminal part of YFP (cYFP-EGT2 (+TAG)) and the coding sequence of the interaction partners C-terminally fused to the N-terminal part of YFP (nYFP-interaction partner (+TAG)). Constructs containing only the *EGT2* coding sequence either N- or C-terminally fused to cYFP were used to detect the autofluorescence of EGT2. Constructs containing the coding sequence of interaction partners C-terminally fused to nYFP and the coding sequence of *EGT2* with stop codon (+TAG) N-terminally fused to cYFP were used to detect the autofluorescence of interaction partners because cYFP will not be translated in this case. All constructs were verified and transformed into Agrobacterium strain AGI1. Tobacco infiltration and transgene expression analysis were conducted as described above. Excitation and detection of RFP, YFP (similar to mVenus), and chloroplast autofluorescence were performed as described above.

Results

Transcriptomic dynamics of three root zones of WT and *egt2* seminal roots upon gravistimulation

We investigated the transcriptomic dynamics in the root cap, the meristem, and the elongation zone (Fig. 1a) in seminal roots of WT seedlings and the hypergravitropic mutant *egt2* at 0, 3, 6, and 12 h after rotation by 90° (Fig. 1b) by RNA-seq (see the Materials and Methods section). Determination of the size of the different root zones is described in Fig. S1 and the material and methods section. We explored the transcriptomic relationship between genotypes, root zones, and duration of gravistimulation by a PCA (Fig. 1c). In the PCA plot, two components (PC1 and PC2) accounted for 91% of the total variance. The first component PC1 explained 74% of the overall variance and distinctly separated the samples of each root zone, indicating larger transcriptomic differences between root zones than between genotypes and time points (Fig. 1c).

Determination of genes responding to gravistimulation in seminal root zones

To identify genes responding to gravistimulation in barley roots, three pairwise comparisons were computed between control (0 h) and gravistimulated (3, 6, and 12 h) root samples for each of the three zones of WT roots. We determined DEGs using a FDR < 5% (Fig. 2a). In all three zones, longer gravitropic stimulation resulted in more DEGs (Fig. 2a; Table S2). The lowest number of identified genes at each time point was observed in the meristem (Fig. 2a). Only five genes were differentially regulated in the meristem (M) 12 h after rotation (Fig. 2a). Of 462 distinct DEGs in the root cap (RC), none was differentially expressed at all three time points after gravistimulation (Fig. 2b). Similarly, of 3173 distinct DEGs in the elongation zone (E), only the seven genes that were already induced 3 h after treatment were consistently regulated at all three time points (Fig. 2c). This suggests for both root zones, that most gravistimulated genes are specifically stimulated after a certain period of gravitropic bending (Fig. 2b,c). By investigating the expression dynamics of genes – whose homologs have been reported to play a role in regulating root gravitropism, we found that *HORVU.MOREX.r3.2HG0125600.1*, a homolog of *AtLZY2* and *AtLZY3* (Taniguchi *et al.*, 2017), and *HORVU.MOREX.r3.5HG0509060.1*, a homolog of *ZmCIPK15* (Schneider *et al.*, 2022), were significantly downregulated in the root cap after 12 h of gravistimulation (Table S2).

Expression dynamics of DEGs regulated by gravistimulation in seminal roots

To group genes with similar expression patterns over 12 h of rotation, we performed hierarchical clustering of all DEGs in the root cap and the elongation zone of WT roots. Hierarchical clustering classified 462 DEGs in the root cap into three clusters (Fig. S3a,b; Table S3) and 3173 DEGs in the elongation zone into nine clusters (Fig. S3c,d; Table S4) according to different patterns of up- and downregulation in the course of gravistimulation.

Gene Ontology term analyses assigned a variety of biological functions to the genes enriched in each cluster (Table S5). A number of enriched biological process terms related to cell wall were shared between different clusters in the elongation zone. For instance, the term 'plant-type cell wall organization' (GO:0009664); 'xyloglucan metabolic process' (GO:0010411); 'fucose metabolic process' (GO:0006004); and 'cellulose biosynthetic process' (GO:0030244) were shared between several clusters (Table S5b). In addition, the terms 'response to oxidative stress' (GO:0006979), 'hydrogen peroxide catabolic process'

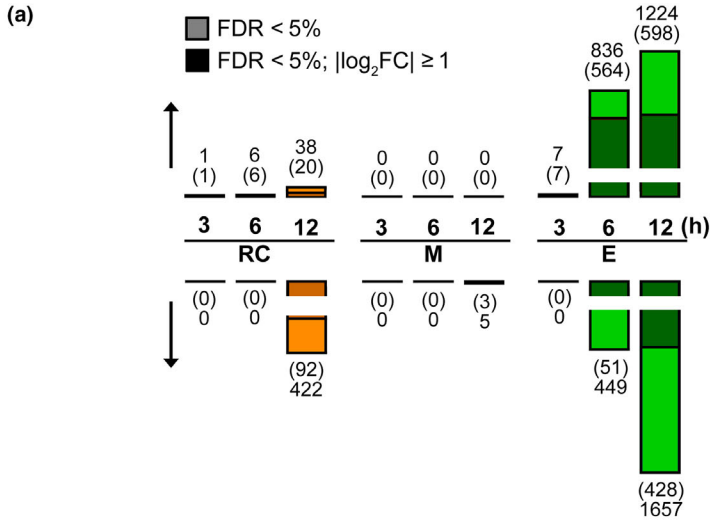

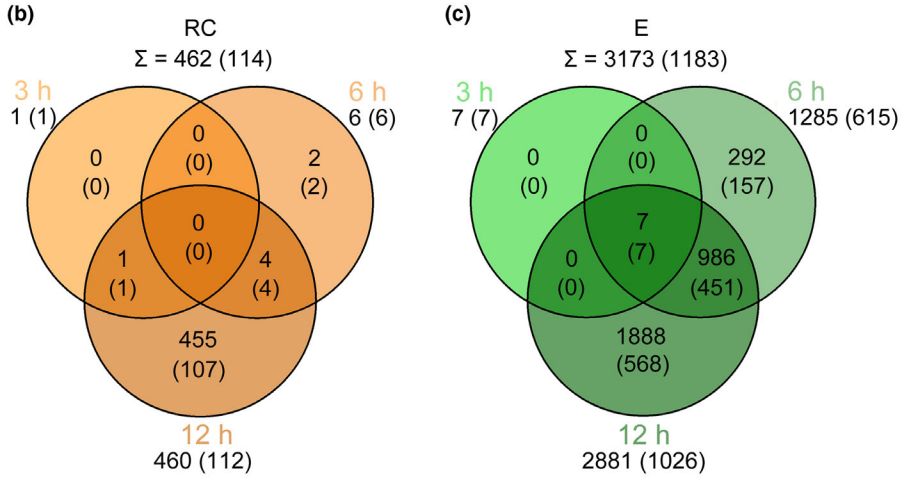

Fig. 2 Differential gene expression in gravistimulated wild-type (WT) roots. (a) Numbers of up- (↑) and downregulated (↓) genes determined by three pairwise comparisons between the root zones of WT vertically grown roots and the corresponding zone of WT gravistimulated roots. RC, root cap; M, meristem; E, elongation zone (light color and numbers without brackets, false discovery rate (FDR) < 5%; dark color and numbers in brackets, FDR < 5%, $\log_2$ fold change ($|\log_2 FC| \geq 1$). (b, c) Venn diagram of differentially regulated genes by gravistimulation in WT root cap (b) and elongation zone (c) (numbers without brackets, FDR < 5%; numbers in brackets, FDR < 5%, $|\log_2 FC| \geq 1$).

(GO:0042744), and 'protein phosphorylation' (GO:0006468) were significantly enriched in multiple clusters (Table S5b).

Determination of DEGs between gravistimulated roots of *egt2* and WT

Differential genes expression between *egt2* and WT was determined for each root zone by time point combination by computing 12 pairwise contrasts (Fig. 3a; Table S6). The root cap displayed 126 (Fig. 3b), the meristem 62 (Fig. 3c), and the elongation zone 2982 unique DEGs (Fig. 3d). In comparison with the WT, *EGT2* was downregulated in all three root zones of the *egt2* mutant at all four time points (Table S6).

Gene Ontology analyses revealed that 31 biological process terms were assigned to DEGs in the root cap (Table S7a). Among them, 'cytoplasmic microtubule organization' (GO:0031122), 'trichome branching' (GO:0010091), and 'plant-type cell wall biogenesis' (GO:0009832) were conserved among upregulated genes at all four time points (Table S7a). In the meristem, 17 GO terms were enriched (Table S7b). As in the root cap, the GO terms 'cytoplasmic microtubule organization' (GO:0031122), 'trichome branching' (GO:0010091), and 'plant-type cell wall biogenesis' (GO:0009832) were conserved among upregulated genes at all four time points in the meristem. In addition, 'cell growth' (GO:0016049) was conserved among upregulated genes while 'one-carbon metabolic process' (GO:0006730) was conserved among downregulated genes at all four time points (Table S7b). Finally, we identified 113 significantly enriched GO terms in the DEGs of the elongation zone (Table S7c). Among those, five GO terms were conserved among upregulated genes at 0, 3, and 6 h, while six GO terms were enriched among downregulated genes at 0 and 3 h, and among upregulated genes at 12 h (Table S7c).

Identification of genes regulated by gravity and by *EGT2*

To screen for genes, which are regulated by gravistimulation and *EGT2*, we compared DEGs responding to gravitropic stimulus with DEGs determined in *egt2* vs WT comparisons. We observed 13 intersecting genes in the root cap (Fig. 4a) and 1038 genes in the elongation zone (Fig. 4b). These genes are listed in Table S8. Among these genes, 12 of 13 in the root cap and 1027 of 1038 in

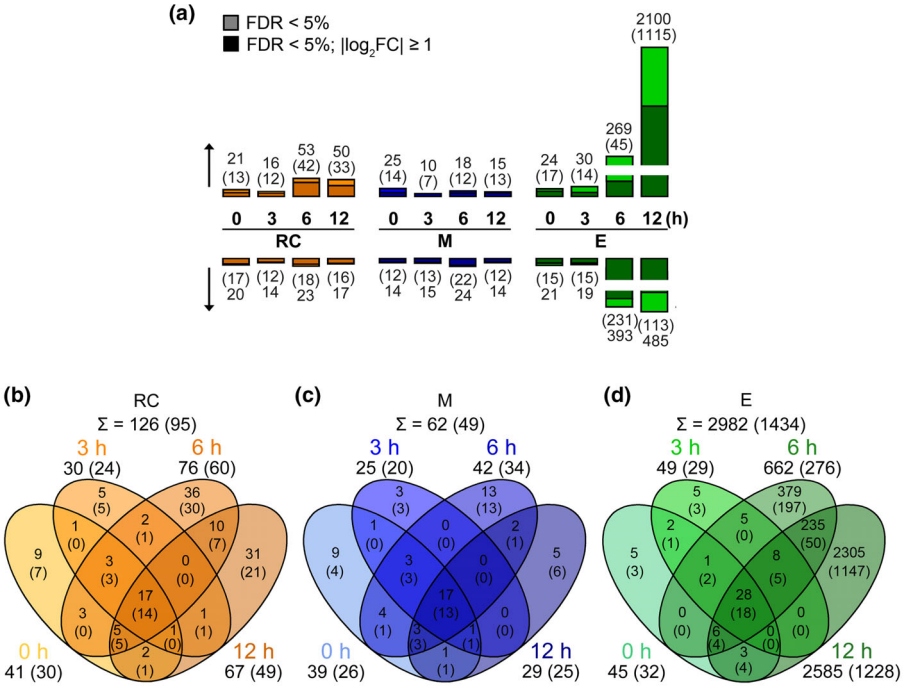

Fig. 3 Differential gene expression between *egt2* mutant and wild-type (WT). (a) Numbers of up- (↑) and downregulated (↓) genes identified by pairwise comparisons between the *egt2* mutant and WT for each of the three root zones: root cap (RC), meristem (M), and elongation zone (E) at each of the four time points: 0, 3, 6, and 12 h (light color and numbers without brackets, false discovery rate (FDR) < 5%; dark color and numbers in brackets, FDR < 5%, $\log_2$ fold change ($|\log_2 FC| \geq 1$). (b–d) Overlap of differentially expressed genes between the four time points in the root cap (b), the meristem (c), and the elongation zone (d) of *egt2* vs WT (numbers without brackets, FDR < 5%; numbers in brackets, FDR < 5%, $|\log_2 FC| \geq 1$).

the elongation zone showed opposite regulatory directions in WT time-course experiments and in *egt2* vs WT comparisons. No *EGT2*-regulated gene responding to gravistimulation was identified in the meristem. Of the gravity-regulated genes, 3% in the root cap and 33% in the elongation zone were also regulated by *EGT2*.

We conducted GO analyses for these intersected genes to reveal the biological processes in which *EGT2* might be involved to regulate root gravitropism. Three protein transmembrane transport-related and two mitochondrion-related GO terms were significantly enriched in intersected DEGs in the root cap (Fig. S4a). Of the 26 GO terms significantly enriched among the overlapping genes in the elongation zone, seven terms were associated with plant cell wall organization, four terms were related to protein processing, two terms were ROS-related, and two terms were associated with carbohydrate metabolic processes (Fig. S4b).

Identification of co-expression networks and their association with the traits genotype and time of gravistimulation

To reveal additional genes that are significantly associated with *EGT2* and gravistimulation in the root cap, meristem, and elongation zone of barley seminal roots, we performed a weighted gene co-expression network analysis (WGCNA). We constructed a co-expression network for the RNA sequencing data separately for each root zone to eliminate the effect of the large expression differences between the distinct root zones on the following analyses. This analysis identified 13 co-expression modules in the root cap, 21 in the meristem, and nine in the elongation zone (Fig. S5a–c). These modules were then correlated with the two genotypes (WT and *egt2*) and the time of gravistimulation (0, 3, 6, and 12 h). This resulted in nine modules that are strongly correlated (*) with at least one trait in the root cap (Fig. 5a), 14 in the meristem (Fig. 5b), and six in the elongation zone (Fig. 5c) with the module size ranging from 38 to 11 791 genes.

We determined two modules that were significantly correlated with genotype, and modules that displayed contrasting correlation values between WT and *egt2* at some time points in all three root zones (Fig. 5a–c). We performed GO analyses to identify overrepresented biological processes among genes in the three most strongly correlated modules in each root zone. The five most significantly enriched biological process terms in each module are shown in Fig. S5(d). Noticeably, 'plant-type cell wall organization' (GO:0009664), 'response to oxidative stress' (GO: 0006979), and 'hydrogen peroxide catabolic processes' (GO:0042744) were consistently identified in modules that significantly correlated with genotype in all three root zones (Fig. S5d). We compared genes associated with plant cell wall and ROS-related processes between the three root zones (Fig. 5d–f). Results showed that *HORVU.MOREX.r3.6HG0611780* and six genes encoding peroxidases were included in significantly correlated modules in all three root zones (Fig. 5d–f). All six genes encoding peroxidases were regulated by gravistimulation in the elongation zone, two of which were regulated by *EGT2* (Fig. 5g).

The module hub genes are defined as genes that are high connected with other genes in the module and have been shown to be closely correlated with biological processes. We determined hub genes in the three most strongly correlated modules in each root zone and surveyed their expression levels in WT gravistimulation time-course experiments and in *egt2* vs WT comparisons (Fig. S5e–g). Among them, *EGT2* was considered as a hub gene

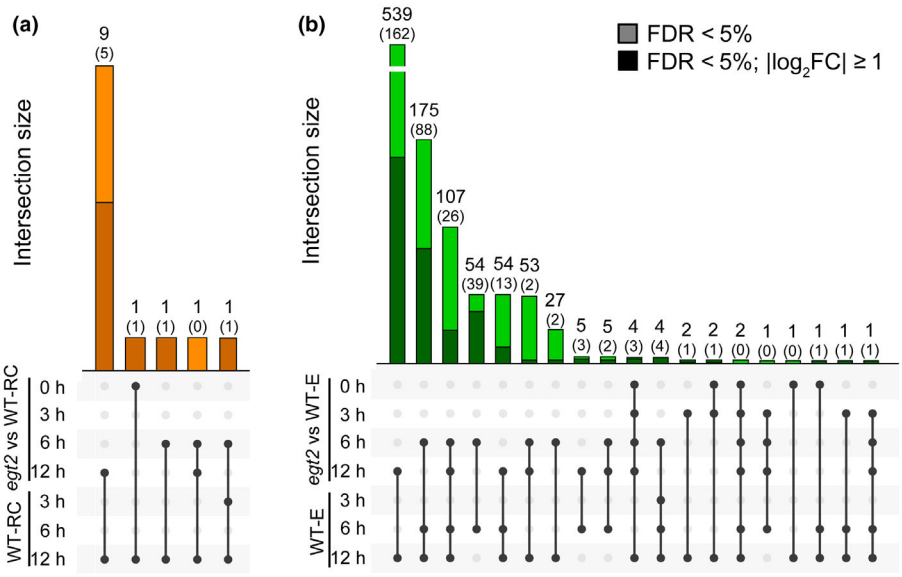

Fig. 4 Intersections between differentially expressed genes (DEGs) in the wild-type (WT) time-course experiment and in *egt2* vs WT comparisons. (a, b) Overlap of DEGs in the root cap (a) and elongation zone (b) of gravistimulated roots of the WT time-course and *egt2* vs WT comparisons (numbers without brackets, false discovery rate (FDR) < 5%; numbers in brackets, FDR < 5%, $\log_2$ fold change ($|\log_2 FC| \geq 1$).

in the midnightblue module in the meristem (Fig. S5f). All seven hub genes identified in this module displayed an *EGT2*-regulated while gravity-independent expression pattern (Fig. S5f). Hub genes identified in selected modules in the elongation zone were regulated by either gravity or *EGT2* in the elongation zone, seven of them were regulated by gravity and *EGT2* (Fig. S5g).

Identification of the interaction partners of EGT2 by a yeast-two-hybrid screening

To determine whether some of these DEGs are encoding for interaction partners of EGT2, we performed a yeast-two-hybrid screening. Two yeast-two-hybrid screens yielded 79 putative interaction partners of EGT2 that were confirmed by Sanger sequencing (Fig. S2c; Table S9). To validate this result in yeast cells, we tested the interaction between EGT2 and 23 putative interaction candidates by a one-on-one yeast-two-hybrid assay. The 23 interaction candidates included 21 candidates that were captured more than twice and two candidates encoded by DEGs in *egt2* vs WT comparisons (Fig. S2d; Table S9). Yeast cells co-transformed with EGT2 and the 23 selected interaction candidates survived and turned blue on high stringency selective medium (SD−Leu/−Trp/−His/−Ade + AbA + X-a-Gal), while yeast cells transformed with the empty control vector together with these 23 candidates could not grow on this medium (Fig. S2d). This suggests that all 23 selected interactions were positive in yeast cells (Fig. S2d), which confirmed the validity of the yeast-two-hybrid results.

Of all genes encoding putative interaction candidates, three genes were differentially expressed in the root cap and 24 in the elongation zone of gravity-stimulated WT roots. Moreover, 16 genes were differentially expressed in the elongation zone of the *egt2* mutant compared with WT (Fig. S2e; Table S9). Among those, genes encoding eight interaction partners were regulated by gravistimulation and *EGT2* (Table S9). Comparisons between the expected (= number of interaction candidates: number of annotated gene models × number of DEGs) and the observed number of interaction partners in each data set showed that more interaction partners were observed in the elongation zone of WT roots than expected after 6 and 12 h of rotation (Fig. S2e).

Validation of selected EGT2 interaction partners by BiFC

Five of eight interaction partners encoded by gravity and *EGT2*-regulated genes were independently surveyed via BiFC (Table S9). We first investigated the subcellular localization of EGT2 and the five interaction partners by fusing tagRFP to the N-terminus of EGT2 (Fig. 6a: tagRFP-EGT2) and fusing mVenus to the N-terminus of the interaction partners (Fig. 6a: mVenus-interaction partner). This experiment demonstrated that EGT2 and the four interaction candidates, HORVU.MOREX.r3.3HG0330120.1 (OMT), HORVU.MOREX.r3.7HG0709860.1 (PBP), HORVU.MOREX.r3.7HG0749870.1 (GXM), and HORVU.MOREX.r3.2HG0126380.1 (HMT) localized to the cytoplasm and the nucleus (Fig. 6a: results for mVenus-OMT, mVenus-GXM and mVenus-HMT). However, we were not able to detect the subcellular localization signal of HORVU.MOREX.r3.1HG0000050.1. For the BiFC assay, the four interaction candidates that also co-localized with EGT2 were C-terminally fused to the N-terminal fragment of YFP (Fig. 6b: nYFP-OMT, nYFP-GXM, nYFP-HMT), while EGT2 was either N-terminally (Fig. 6b: EGT2 (−TGA)-cYFP) or C-terminally (Fig. 6b: cYFP-EGT2 (+TGA)) fused to cYFP. We detected yellow fluorescence signals emitted by the interactions in tobacco epidermal cells infiltrated with constructs containing nYFP-OMT or nYFP-GXM and cYFP-EGT2 (+TGA) and the construct containing nYFP-HMT and EGT2 (−TGA)-cYFP (Fig. 6b). We did not detect a yellow fluorescence signal in tobacco epidermal cells infiltrated with constructs containing the coding sequence of EGT2 fused to cYFP (Fig. S6: cYFP-EGT2 (+TGA), EGT2 (−TGA)-cYFP) and the coding sequence of nYFP (Fig. S6). Nor did we detect a YFP signal in tobacco

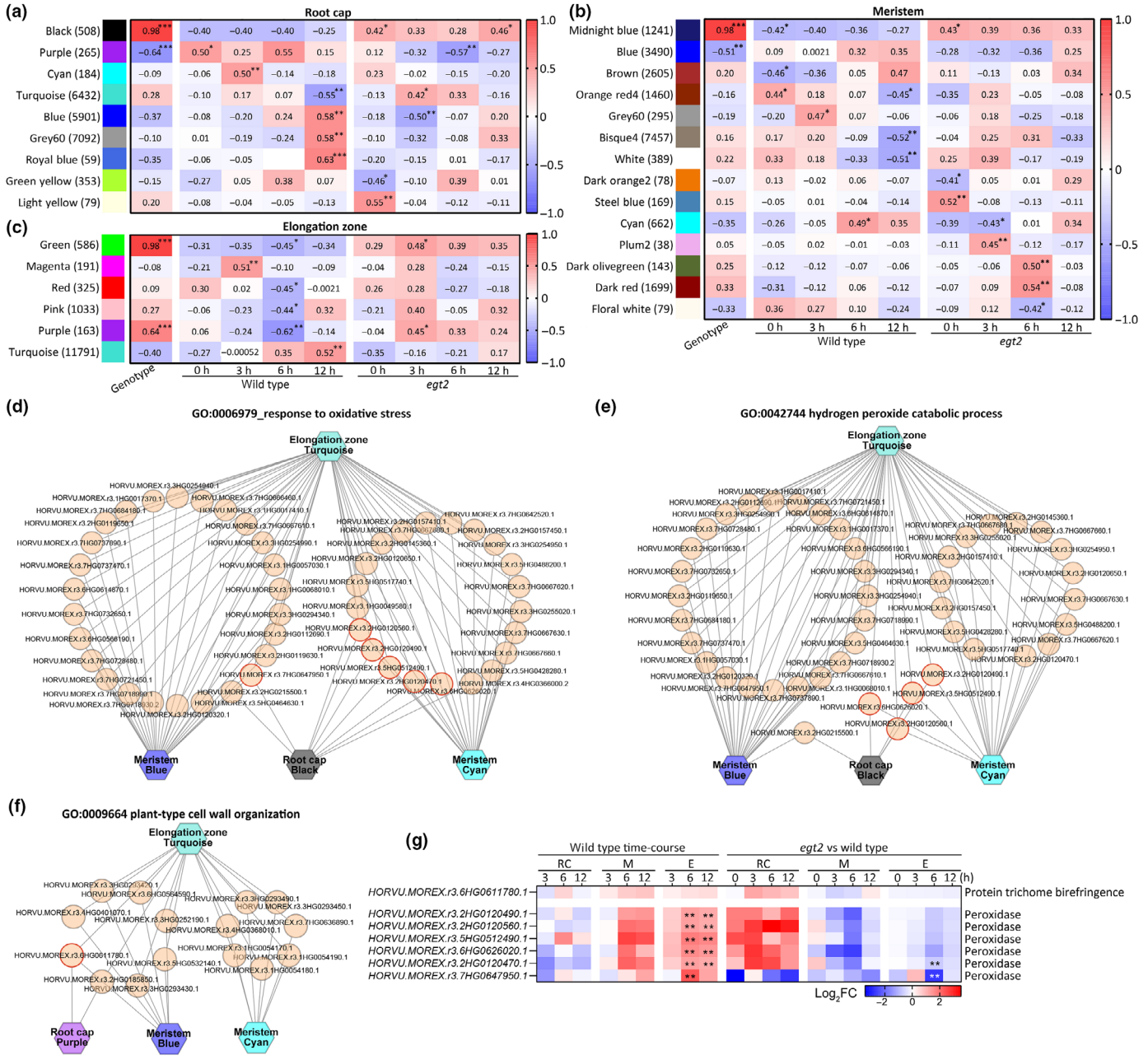

Fig. 5 Module-trait associations and genes assigned to plant cell wall and reactive oxygen species (ROS)-related processes in each selected module. (a–c) Module–trait relationships in the root cap (a), the meristem (b), and the elongation zone (c). The genotypes (WT and *egt2*) and time points (0, 3, 6 and 12 h) after gravistimulation are used as traits, each column corresponds to a different trait. Each row corresponds to the characteristic genes of the module. The relationship between the modules and traits is indicated in cell by Pearson's correlation coefficients. Asterisks indicate significant values calculated using the corPvalueStudent function: *, $P < 0.05$; **, $P < 0.01$; ***, $P < 0.001$. Cell color ranges from red (highly positive correlation) to blue (highly negative correlation). The number of genes contained in each module is indicated in brackets next to the module names. (d) Genes associated with 'response to oxidative stress'. (e) Genes associated with 'hydrogen peroxide catabolic process'. (f) Genes associated with 'plant-type cell wall organization'. (d–f) Hexagonal nodes represent modules, circle nodes in orange represent individual genes. Nodes encircled in dark orange represent genes determined in all three root zones. (g) The expression patterns of genes encircled in dark orange in (d–f) in the WT gravistimulation time-course experiments (WT time-course) and in the pairwise comparisons of *egt2* with WT (*egt2* vs WT). **, false discovery rate (FDR) < 5%.

epidermal cells infiltrated with constructs containing nYFP-OMT, nYFP-GXM, and nYFP-HMT together with the full-length coding sequence of EGT2 including a stop codon (+TGA) N-terminally fused to cYFP (Fig. S6: EGT2 (+TGA)-cYFP). The stop codon after EGT2 in this construct disables translation of cYFP. Remarkably, while OMT interaction with EGT2 was observed in the nucleus and in the cytoplasm (Fig. 6b) as expected from the subcellular localization experiments of these two proteins (Fig. 6a). By contrast, interaction of GXM and HMT with EGT2 occurred only in the nucleus (Fig. 6b), although these proteins are localized in the nucleus and cytoplasm (Fig. 6a).

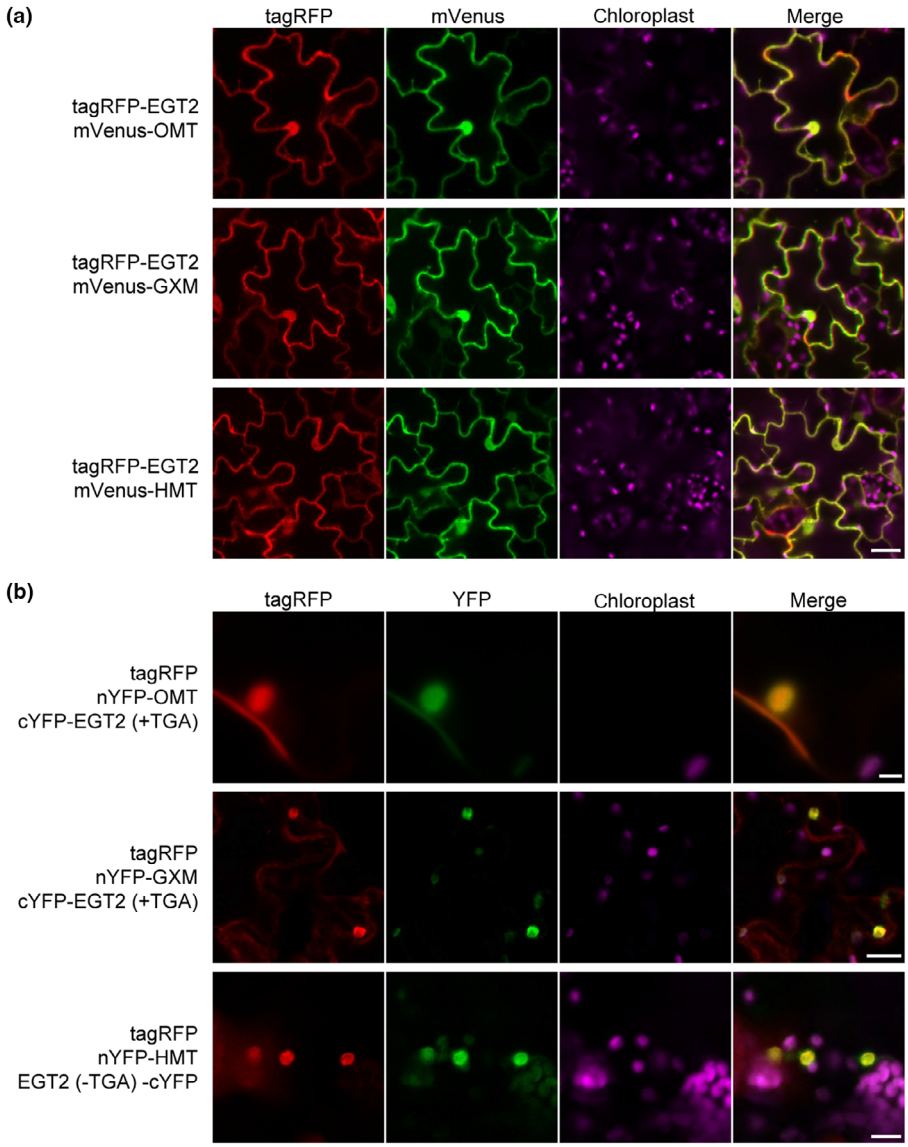

Fig. 6 Confirmation of interactions between EGT2 and other proteins. (a) Subcellular localization assay of EGT2 and interaction partners. tagRFP, red fluorescence; mVenus, yellow fluorescence. Bar, 50 μm. (b) Bimolecular fluorescence complementation assay of EGT2 and interaction partners. tagRFP, red fluorescence; mVenus, yellow fluorescence; nYFP, N-terminal part of YFP; cYFP, C-terminal part of YFP; EGT2 (+TGA), full-length coding sequence of EGT2; EGT2 (−TGA), coding sequence of EGT2 removed stop codon. Bars: (top) 10 μm; (middle) 50 μm; (bottom) 25 μm. (a, b) OMT, HORVU.MOREX.r3.3HG0330120.1; GXM, HORVU.MOREX.r3.7HG0749870.1; HMT, HORVU.MOREX.r3.2HG0126380.1; chloroplasts, autofluorescence of chloroplasts.

Discussion

Gravitropism modulates root system architecture by controlling the distribution of roots in different soil layers and thus their ability to absorb water and nutrients. Understanding the molecular mechanisms underlying root gravitropism will help to develop root ideotypes that can improve crop performance under unfavorable environmental conditions.

The root gravitropic response includes the perception of gravity signals mainly in the root cap, signal transduction through the meristem, and signal execution translating into a bending response in the elongation zone (Singh *et al.*, 2017; Su *et al.*, 2017; Nakamura *et al.*, 2019). We observed that the angle adjustment of WT barley roots was adjusted by 10° after 3 h of rotation and reached 30° (> 60% of the total adjusted angle) after 12 h of rotation (Fig. 1b; Kirschner *et al.*, 2021). In this study, we performed RNA-seq of the root cap, the meristem, and the elongation zone of WT barley roots before gravistimulation and 3, 6, and 12 h after reorientation of the roots by 90°. This experiment revealed transcriptomic variation in every step of gravitropic response at different time points. First, only a few DEGs were observed after 3 h of rotation in all three zones (Fig. 2a). This indicates that gravistimulation caused only little transcriptome adjustment at early stages of the experiment (Fig. 2b,c). Second, the elongation zone displayed by far the most DEGs (Fig. 2a,c), suggesting that gravitropic bending is subject to a more extensive transcriptomic regulation in the elongation zone than gravity perception in the root cap and signal transduction in the meristem.

Gene Ontology term analyses revealed the enrichment of a number of biological processes among the DEGs in the gravistimulated root cap and elongation zone. Gene Ontology terms related to ROS biosynthesis, cytoplasmic microtubule organization, plant transmembrane transport, carbohydrate metabolic, and calcium-mediated signaling were overrepresented in downregulated genes in root cap (Table S5a). These enriched GO

terms are in line with the notion that ROS (Krieger *et al.*, 2016), starch-related processes (Li *et al.*, 2020), dynamic actin-filament network (Hou *et al.*, 2003), and calcium (Bizet *et al.*, 2018) are involved in gravity sensing, which occurs primarily in root cap (Su *et al.*, 2020). In addition, the homolog of *AtLZY2* and *AtLZY3* and the homolog of *ZmCIPK15* were significantly downregulated in the root cap after 12 h of gravistimulation (Table S2). This is consistent with the role of *AtLZY2* and *AtLZY3* in root columella cells during gravitropic response and the function of *ZmCIPK15* in regulating maize root angles (Taniguchi *et al.*, 2017; Schneider *et al.*, 2022). In the elongation zone, seven cell wall, ROS, and protein phosphorylation-related terms were assigned to more than three gene clusters with DEG patterns (Table S5b). This is consistent with the observation that gravity changes lead to alterations in the shape of endodermal cells and in the transcript levels of genes associated with cell wall modifications (Johnson *et al.*, 2015, 2017). Moreover, cell wall-related processes are closely related to asymmetric cell elongation in the distal elongation zone of gravistimulated roots (Su *et al.*, 2017; Lešková *et al.*, 2020). It has also been demonstrated that gravistimulation induces an asymmetric distribution of ROS in the distal elongation zone of the root (higher in the lower flanks), which promotes root gravitropic bending (Krieger *et al.*, 2016). Furthermore, ROS production is also involved in regulating cell wall loosening and cell expansion (Liszkay *et al.*, 2004; Xiong *et al.*, 2015; Mabuchi *et al.*, 2018). Protein phosphorylation functions in mediating auxin biosynthesis, transport, and signaling, therefore playing a critical role in many auxin-related processes, including root gravitropism (Tan *et al.*, 2021).

In a previous study, we identified the barley mutant *egt2*, which shows enhanced root gravitropism (Kirschner *et al.*, 2021). RNA-seq of vertically grown roots showed that cell wall-related processes were affected in the mutant; however, nothing is known about the dynamics of the gravity response in regard to the role of EGT2 (Kirschner *et al.*, 2021). Here, we determined DEGs between different root zones of the gravistimulated roots of *egt2* and WT in a time-course experiment (Fig. 3). In the root cap, only 3% of gravity-responsive genes were regulated by *EGT2* (Fig. 4a), implying that *EGT2* might not play an important role in gravity perception in the root cap. This is in line with our previous observation that there was no significant difference in amyloplast content and their sedimentation rates between WT and *egt2* (Kirschner *et al.*, 2021). Similarly, there was no overlap between gravity-responsive genes and genes regulated by *EGT2* in the meristem suggesting that the role of *EGT2* in gravity signal transduction is not prominent on the transcriptomic level. In our previous study, we suggested that *EGT2* mediates gravity signal transduction at the protein level, further regulating the targets in the elongation zone to control the root gravitropism (Kirschner *et al.*, 2021). Consistently, in the elongation zone of *egt2*, gravistimulation induced the differential expression of thousands of *EGT2*-regulated genes (Fig. 3a,d). Intriguingly, > 1000 *EGT2*-regulated genes in the elongation zone were also regulated by gravistimulation in the WT roots (Fig. 4b). This implies that around one-third of gravity-responsive genes in the elongation zone of WT roots were regulated by *EGT2*, suggesting a critical role of *EGT2* in regulating root gravitropic bending. Plant cell wall organization and ROS-related GO terms that were assigned to these intersected genes in the elongation zone (Fig. S4b) support this hypothesis.

The *egt2* mutation results in an enhanced gravitropic response in barley roots, suggesting that *EGT2* might play a positive role in regulating antigravitropic offset (AGO), which counteracts gravitropism to regulate the root growth direction (Fig. 1b; Kawamoto *et al.*, 2020; Kirschner *et al.*, 2021; Fusi *et al.*, 2022). Based on this hypothesis, *EGT2* might suppress the expression of gravity-responsive genes that play a positive role in root gravitropism and induce the expression of gravity-responsive genes that negatively regulate root gravitropism. According to this hypothesis, mutation of *EGT2* would result in an opposite expression pattern of AGO-related genes in the *egt2* mutant than in the WT. Consistently, almost all of *EGT2*-regulated gravity-responsive genes were regulated in the opposite direction in the WT gravistimulation time-course experiment and in pairwise comparisons of *egt2* and WT roots (Table S7). This result supports the notion that *EGT2* mediates root gravitropism through the regulation of AGO and provides a number of candidate genes that might be involved in *EGT2*-depedent regulation of AGO, thus contributing to the understanding of the largely unknown mechanism of AGO.

Co-expression network analyses revealed that specific modules that have a strong correlation with genotype in all three root zones. These modules were in most cases contrastingly correlated with the gravitropic response of WT and *egt2* (Figs 5a–c, S5a–c). Genes in these modules are potential components involved in regulating gravitropic response and AGO (Fig. S5e–g; Kawamoto *et al.*, 2020; Fusi *et al.*, 2022). Moreover, modules correlated only with WT or *egt2* at some time point after gravistimulation might be involved in *EGT2*-independent or *EGT2*-dependent gravitropism, respectively. This result complements differential expression analyses, in particular for the root cap and the meristem where fewer gravity or *EGT2*-regulated genes were discovered (Figs 2, 3). In the elongation zone, many hub genes of significantly correlated modules were regulated by gravity and/or *EGT2* (Fig. S5g), which is in line with the differential expression analyses. Plant cell wall and ROS-related GO terms were assigned to modules strongly correlated with genotype in all three root zones (Fig. S5d). This is consistent with GO analyses of gravity and *EGT2*-regulated genes in the elongation zone (Fig. S4b), suggesting that plant cell wall and ROS-related processes might be involved in *EGT2*-controlled root gravitropic response. Moreover, six genes encoding peroxidases were present in significantly correlated modules in all three root zones (Fig. 5g). These results suggest that gravitropism regulation of *EGT2* might be similar to that of *EGT1*, which was proposed to control cell wall stiffness by regulating peroxidase and cell wall loosening-related enzymes, therefore mediating AGO (Fusi *et al.*, 2022).

Localization of EGT2 in the cytoplasm and nucleus was consistent with the predicted localization of its homologs in Arabidopsis (Denay *et al.*, 2017). As the only annotated domain in EGT2, the SAM domain is known as a protein–protein interaction domain in animals (Kim & Bowie, 2003). Recent studies on plant SAM

domain-containing proteins have provided initial insights into the interaction capabilities of the plant SAM domain (Murcha *et al.*, 2016; Sayou *et al.*, 2016). In the current study, we identified 79 proteins as putative interaction partners of EGT2 (Fig. S2c). The number of observed interaction candidates that responded to gravistimulation on basis of the transcriptome analyses was significantly higher than expected by chance (Fig. S2e), highlighting the role of EGT2 in root gravitropic response.

Bimolecular fluorescence complementation confirmed the interaction between EGT2 and three interaction candidates encoded by DEGs (Fig. 6). Two candidates were not confirmed, probably due to changes in protein structure caused by inappropriate terminal fusion to fluorescent proteins. Alternatively, the two proteins might be false-positive results of the yeast-two-hybrid experiment (Xing *et al.*, 2016). EGT2 fused with cYFP at the N-terminus (cYFP-EGT2 (+TGA)) displayed interaction with OMT and GXM, whereas EGT2 fused with cYFP at the C-terminus (EGT2 (−TGA)-cYFP) displayed interaction with HMT (Fig. 6b). This suggests that the interaction site of EGT2 with OMT or GXM might be different from that of EGT2 with HMT. None of the three independently confirmed proteins has been yet functionally characterized in barley. OMT is annotated as an '*O*-methyltransferase', while GXM is annotated as 'Glucuronoxylan 4-*O*-methyltransferase' and HMT is annotated as a heavy metal transport/detoxification superfamily protein.

Remarkably, while OMT interaction with EGT2 was observed in the nucleus and in the cytoplasm as expected from their subcellular localization, interaction of GXM and HMT with EGT2 occurred only in the nucleus, although these proteins are also localized in the nucleus and cytoplasm. One explanation for the confined interaction of GXM and HMT with EGT2 in the nucleus could be that their interaction needs a hypothetical co-factor that is present only in the nucleus but not the cytoplasm. Hence, the detailed function of these proteins in the determination of the setpoint angle of barley seminal roots by interacting with EGT2 remains to be investigated in future studies.

Acknowledgements

We would like to thank Andreas Meyer (University of Bonn) and Peng Yu (University of Bonn) for their discussions and suggestions on this project. We would also like to thank Helmut Rehkopf (University of Bonn) and Christa Schulz (University of Bonn) for their experimental support of this study. This work was funded by the Deutsche Forschungsgemeinschaft (DFG) grant HO2249/21-1 to FH. Open Access funding enabled and organized by Projekt DEAL.

Competing interests

None declared.

Author contributions

LG and FH conceived the experiments. LG performed the experiments, analyzed and interpreted the data and drafted the article. AK was involved in the bioinformatic analyses of RNA-seq data. MB was involved in the yeast-two-hybrid experiments. GKK and SS participated in data interpretation and revised the article. FH coordinated the study, participated in data interpretation and drafting of the article. All authors approved the final draft.

ORCID

Marcel Baer https://orcid.org/0000-0001-7708-7202
Li Guo https://orcid.org/0000-0003-0406-6966
Frank Hochholdinger https://orcid.org/0000-0002-5155-0884
Alina Klaus https://orcid.org/0000-0003-0805-2860
Silvio Salvi https://orcid.org/0000-0002-0338-8894

Data availability

RNA-seq data have been deposited in the SRA under accession no. PRJNA858009 (https://www.ncbi.nlm.nih.gov/bioproject/858009).

References

Alexa A, Rahnenführer J. 2022. *TOPGO: enrichment analysis for gene ontology.* R package v.2.50.0. [WWW document] URL https://bioconductor.org/packages/release/bioc/html/topGO.html [accessed 13 January 2023].

Baluška F, Mancuso S, Volkmann D, Barlow PW. 2010. Root apex transition zone: a signalling–response nexus in the root. *Trends in Plant Science* **15**: 402–408.

Benjamini Y, Hochberg Y. 1995. Controlling the false discovery rate: a practical and powerful approach to multiple testing. *Journal of the Royal Statistical Society: Series B (Methodological)* **57**: 289–300.

Bizet F, Pereda-Loth V, Chauvet H, Gérard J, Eche B, Girousse C, Courtade M, Perbal G, Legué V. 2018. Both gravistimulation onset and removal trigger an increase of cytoplasmic free calcium in statocytes of roots grown in microgravity. *Scientific Reports* **8**: 1–10.

Chen H, Boutros PC. 2011. VENNDIAGRAM: a package for the generation of highly-customizable Venn and Euler diagrams in R. *BMC Bioinformatics* **12**: 35.

Conway JR, Lex A, Gehlenborg N. 2017. UPSETR: an R package for the visualization of intersecting sets and their properties. *Bioinformatics* **33**: 2938–2940.

Denay G, Vachon G, Dumas R, Zubieta C, Parcy F. 2017. Plant SAM-domain proteins start to reveal their roles. *Trends in Plant Science* **22**: 718–725.

Eriksson S, Böhlenius H, Moritz T, Nilsson O. 2006. GA_4 is the active gibberellin in the regulation of *LEAFY* transcription and *Arabidopsis* floral initiation. *Plant Cell* **18**: 2172–2181.

Fusi R, Rosignoli S, Lou H, Sangiorgi G, Bovina R, Pattem JK, Borkar AN, Lombardi M, Forestan C, Milner SG *et al.* 2022. Root angle is controlled by *EGT1* in cereal crops employing an antigravitropic mechanism. *Proceedings of the National Academy of Sciences, USA* **119**: e2201350119.

Gietz RD, Schiestl RH, Willems AR, Woods RA. 1995. Studies on the transformation of intact yeast cells by the LiAc/SS-DNA/PEG procedure. *Yeast* **11**: 355–360.

Grefen C, Blatt MR. 2012. A 2in1 cloning system enables ratiometric bimolecular fluorescence complementation (rBiFC). *BioTechniques* **53**: 311–314.

Hollender CA, Pascal T, Tabb A, Hadiarto T, Srinivasan C, Wang W, Liu Z, Scorza R, Dardick C. 2018. Loss of a highly conserved sterile alpha motif domain gene (*WEEP*) results in pendulous branch growth in peach trees. *Proceedings of the National Academy of Sciences, USA* **115**: E4690–E4699.

Hou G, Mohamalawari DR, Blancaflor EB. 2003. Enhanced gravitropism of roots with a disrupted cap actin cytoskeleton. *Plant Physiology* **131**: 1360–1373.

Jiao Z, Du H, Chen S, Huang W, Ge L. 2021. *LAZY* gene family in plant gravitropism. *Frontiers in Plant Science* **11**: 2096.

Johnson CM, Subramanian A, Edelmann RE, Kiss JZ. 2015. Morphometric analyses of petioles of seedlings grown in a spaceflight experiment. *Journal of Plant Research* **128**: 1007–1016.

Johnson CM, Subramanian A, Pattathil S, Correll MJ, Kiss JZ. 2017. Comparative transcriptomics indicate changes in cell wall organization and stress response in seedlings during spaceflight. *American Journal of Botany* **104**: 1219–1231.

Johnson JM, Kohler AR, Haus MJ, Hollender CA. 2022. Arabidopsis *weep* mutants exhibit narrow root angles. *microPublication Biology*. doi: 10.17912/micropub.biology.000584.

Jones AM, Xuan Y, Xu M, Wang RS, Ho CH, Lalonde S, You CH, Sardi MI, Parsa SA, Smith-Valle E *et al.* 2014. Border control – a membrane-linked interactome of Arabidopsis. *Science* **344**: 711–716.

Kawamoto N, Kanbe Y, Nakamura M, Mori A, Terao Morita M. 2020. Gravity-sensing tissues for gravitropism are required for "anti-gravitropic" phenotypes of *lzy* multiple mutants in Arabidopsis. *Plants* **9**: 615.

Kim CA, Bowie JU. 2003. SAM domains: uniform structure, diversity of function. *Trends in Biochemical Sciences* **28**: 625–628.

Kirschner GK, Rosignoli S, Guo L, Vardanega I, Imani J, Altmüller J, Milner SG, Balzano R, Nagel KA, Pflugfelder D *et al.* 2021. *ENHANCED GRAVITROPISM 2* encodes a STERILE ALPHA MOTIF-containing protein that controls root growth angle in barley and wheat. *Proceedings of the National Academy of Sciences, USA* **118**: e2101526118.

Krieger G, Shkolnik D, Miller G, Fromm H. 2016. Reactive oxygen species tune root tropic responses. *Plant Physiology* **172**: 1209–1220.

Langfelder P, Horvath S. 2008. WGCNA: an R package for weighted correlation network analysis. *BMC Bioinformatics* **9**: 559.

Lešková A, Zvarík M, Araya T, Giehl RFH. 2020. Nickel toxicity targets cell wall-related processes and PIN2-mediated auxin transport to inhibit root elongation and gravitropic responses in Arabidopsis. *Plant and Cell Physiology* **61**: 519–535.

Li Y, Yuan W, Li L, Miao R, Dai H, Zhang J, Xu W. 2020. Light-dark modulates root hydrotropism associated with gravitropism by involving amyloplast response in Arabidopsis. *Cell Reports* **32**: 108198.

Liszkay A, Van Der Zalm E, Schopfer P. 2004. Production of reactive oxygen intermediates ($O_2^{\bullet-}$, H_2O_2, and $^{\bullet}OH$) by maize roots and their role in wall loosening and elongation growth. *Plant Physiology* **136**: 3114–3123.

Mabuchi K, Maki H, Itaya T, Suzuki T, Nomoto M, Sakaoka S, Morikami A, Higashiyama T, Tada Y, Busch W *et al.* 2018. MYB30 links ROS signaling, root cell elongation, and plant immune responses. *Proceedings of the National Academy of Sciences, USA* **115**: E4710–E4719.

Maechler M, Rousseeuw P, Struyf A, Hubert M, Hornik K. 2022. *CLUSTER: cluster analysis basics and extensions*. R package v.2.1.3. [WWW document] URL https://cran.r-project.org/web/packages/cluster/index.html [accessed 13 January 2023].

Mancuso S, Barlow PW, Volkmann D, Baluska F. 2006. Actin turnover-mediated gravity response in maize root apices. *Plant Signaling & Behavior* **1**: 52–58.

Mascher M, Wicker T, Jenkins J, Plott C, Lux T, Koh CS, Ens J, Gundlach H, Boston LB, Tulpová Z *et al.* 2021. Long-read sequence assembly: a technical evaluation in barley. *Plant Cell* **33**: 1888–1906.

Murcha MW, Kubiszewski-Jakubiak S, Teixeira PF, Gügel IL, Kmiec B, Narsai R, Ivanova A, Megel C, Schock A, Kraus S *et al.* 2016. Plant-specific preprotein and amino acid transporter proteins are required for tRNA import into mitochondria. *Plant Physiology* **172**: 2471–2490.

Nakamura M, Nishimura T, Morita MT. 2019. Gravity sensing and signal conversion in plant gravitropism. *Journal of Experimental Botany* **70**: 3495–3506.

Osthoff A, Donà dalle Rose P, Baldauf JA, Piepho H-P, Hochholdinger F. 2019. Transcriptomic reprogramming of barley seminal roots by combined water deficit and salt stress. *BMC Genomics* **20**: 1–14.

Qiao F, Bowie JU. 2005. The many faces of SAM. *Science's STKE* **2005**: re7.

Ray S, Chee L, Matson DR, Palermo NY, Bresnick EH, Hewitt KJ. 2020. Sterile alpha motif domain requirement for cellular signaling and survival. *Journal of Biological Chemistry* **295**: 7113–7125.

Ritchie ME, Phipson B, Wu D, Hu Y, Law CW, Shi W, Smyth GK. 2015. LIMMA powers differential expression analyses for RNA-sequencing and microarray studies. *Nucleic Acids Research* **43**: E47.

Robinson MD, McCarthy DJ, Smyth GK. 2010. EDGER: a BIOCONDUCTOR package for differential expression analysis of digital gene expression data. *Bioinformatics* **26**: 139–140.

Ronzier E, Corratgé-Faillie C, Sanchez F, Prado K, Brière C, Leonhardt N, Thibaud JB, Xiong TC. 2014. CPK13, a noncanonical Ca^{2+}-dependent protein kinase, specifically inhibits KAT2 and KAT1 shaker K^+ channels and reduces stomatal opening. *Plant Physiology* **166**: 314–326.

Sayou C, Nanao MH, Jamin M, Posé D, Thévenon E, Grégoire L, Tichtinsky G, Denay G, Ott F, Peirats Llobet M *et al.* 2016. A SAM oligomerization domain shapes the genomic binding landscape of the LEAFY transcription factor. *Nature Communications* **7**: 11222.

Schneider HM, Lor VSN, Hanlon MT, Perkins A, Kaeppler SM, Borkar AN, Bhosale R, Zhang X, Rodriguez J, Bucksch A *et al.* 2022. Root angle in maize influences nitrogen capture and is regulated by calcineurin B-like protein (CBL)-interacting serine/threonine-protein kinase 15 (ZmCIPK15). *Plant, Cell & Environment* **45**: 837–853.

Schultz J, Ponting CP, Hofmann K, Bork P. 1997. SAM as a protein interaction domain involved in developmental regulation. *Protein Science* **6**: 249–253.

Singh M, Gupta A, Laxmi A. 2017. Striking the right chord: signaling enigma during root gravitropism. *Frontiers in Plant Science* **8**: 1304.

Siriwardana NS, Lamb RS. 2012. The poetry of reproduction: the role of LEAFY in *Arabidopsis thaliana* flower formation. *International Journal of Developmental Biology* **56**: 207–221.

Su SH, Gibbs NM, Jancewicz AL, Masson PH. 2017. Molecular mechanisms of root gravitropism. *Current Biology* **27**: R964–R972.

Su SH, Keith MA, Masson PH. 2020. Gravity signaling in flowering plant roots. *Plants* **9**: 1–23.

Supek F, Bošnjak M, Škunca N, Šmuc T. 2011. REVIGO summarizes and visualizes long lists of gene ontology terms. *PLoS ONE* **6**: e21800.

Tan S, Luschnig C, Friml J. 2021. Pho-view of auxin: reversible protein phosphorylation in auxin biosynthesis, transport and signaling. *Molecular Plant* **14**: 151–165.

Taniguchi M, Furutani M, Nishimura T, Nakamura M, Fushita T, Iijima K, Baba K, Tanaka H, Toyota M, Tasaka M *et al.* 2017. The Arabidopsis LAZY1 family plays a key role in gravity signaling within statocytes and in branch angle control of roots and shoots. *Plant Cell* **29**: 1984–1999.

Verbelen JP, De Cnodder T, Le J, Vissenberg K, Baluška F. 2006. The root apex of *Arabidopsis thaliana* consists of four distinct zones of growth activities. *Plant Signaling & Behavior* **1**: 296–304.

Wolverton C, Mullen JL, Ishikawa H, Evans ML. 2002. Root gravitropism in response to a signal originating outside of the cap. *Planta* **215**: 153–157.

Xing S, Wallmeroth N, Berendzen KW, Grefen C. 2016. Techniques for the analysis of protein–protein interactions *in vivo*. *Plant Physiology* **171**: 727–758.

Xiong J, Yang Y, Fu G, Tao L. 2015. Novel roles of hydrogen peroxide (H_2O_2) in regulating pectin synthesis and demethylesterification in the cell wall of rice (*Oryza sativa*) root tips. *New Phytologist* **206**: 118–126.

Yamaguchi N. 2021. LEAFY, a pioneer transcription factor in plants: a mini-review. *Frontiers in Plant Science* **12**: 1274.

Zhang Y, Xiao G, Wang X, Zhang X, Friml J. 2019. Evolution of fast root gravitropism in seed plants. *Nature Communications* **10**: 3480.

Supporting Information

Additional Supporting Information may be found online in the Supporting Information section at the end of the article.

Fig. S1 Quantification of meristem length of wild-type and *egt2* before and after 6 or 10 h of gravistimulation.

Fig. S2 Overview of yeast-two-hybrid screening.

Fig. S3 Dynamics of the expression profiles of graviregulated genes.

Fig. S4 Enriched GO terms for gravity-regulated genes that are *EGT2* related.

Fig. S5 Co-expression analysis.

Fig. S6 Control experiments for bimolecular fluorescence complementation analyses of EGT2 and interaction candidates.

Table S1 List of oligonucleotide primers.

Table S2 Overview of differentially expressed genes (FDR < 5%) in gravistimulated wild-type roots in a time-course experiment.

Table S3 Hierarchical clustering analysis of differentially expressed genes (FDR < 5%) in the root cap of gravistimulated wild-type roots.

Table S4 Hierarchical clustering analysis of differentially expressed genes (FDR < 5%) in elongation zone of gravistimulated wild-type roots.

Table S5 Enriched biological process terms among differentially expressed genes (FDR < 5%) in the root cap and elongation zone of gravistimulated wild-type roots.

Table S6 Overview of genes differentially expressed between wild-type and *egt2* (FDR < 5%) in a gravistimulation time-course experiment.

Table S7 Enriched biological processes terms among genes differentially expressed between wild-type and *egt2* (FDR < 5%) root caps, meristems, and elongation zones after a gravistimulation time-course experiment.

Table S8 Overlapping genes among differentially expressed genes in the wild-type (WT) time-course experiment and *egt2* vs WT comparisons.

Table S9 Overview of the candidates interacting with EGT2 as identified by yeast-two-hybrid screening.

Please note: Wiley is not responsible for the content or functionality of any Supporting Information supplied by the authors. Any queries (other than missing material) should be directed to the *New Phytologist* Central Office.

General Discussion

The root setpoint angle is a major morphological trait of plants that determines the distribution of roots in soil and thus the ability of plants to absorb water and nutrients, and is therefore closely related to plant growth and development. This makes the root setpoint angle a potential target for crop breeding to improve crop resilience to unfavorable conditions (Uga *et al.*, 2015; Ober *et al.*, 2021). Gravitropism is one of the main internal mechanisms that determines the root setpoint angle of plants (Su *et al.*, 2020).

In this study, a novel barley mutant *enhanced root gravitropism 2* (*egt2*) was identified and the causative gene *EGT2*, a conserved regulator of root setpoint angle, was cloned (Chapter 2). To investigate the molecular networks in which *EGT2* is interwoven, a comparative tissue-specific transcriptome analysis of gravistimulated *egt2* and wild type roots was performed in a time-course experiment and interaction partners of EGT2 were determined (Chapter 3). In short, this study provides targets for root-based crop improvement by cloning and functionally characterizing *EGT2* involved in root gravitropic response and by identifying genes regulated by and interacting with EGT2.

4.1 The mutant *egt2* shows enhanced root gravitropism without displaying other morphological defects

In Chapter 2, we demonstrated that the *egt2* mutant forms a steeper root system at different developmental stages than wild type. However, we observed no differences in other root traits such as the number of seminal roots and root length between wild type and *egt2*, suggesting that the enhanced root gravitropism in *egt2* is not associated with general aspects of root growth. Analysis of root gravitropism by rotating vertically growing seedling by 90° showed that the root gravitropic bending of *egt2* was significantly faster and stronger than that of wild type. The adjusted angle of *egt2* away from the horizontal was about three times larger than that of the wild type, independent of root length variation. In addition, the structure and size of the root cap and the meristem of wild type and *egt2* were similar, and no differences in the quantity and sedimentation rate of amyloplasts was found in the root cap of wild type and *egt2*. These results suggest that gravity signal perception is undisrupted in *egt2*. In addition, wild type and *egt2* showed similar adjustments in root gravitropism and elongation in response to treatment with auxin (IAA) or the auxin transport inhibitor (NPA), suggesting that auxin response was not affected in *egt2*. All these phenotypes observed in *egt2* were similar to the barley mutant *enhanced gravitropism 1* (*egt1*; Fusi *et al.*, 2022). Nevertheless, *EGT2* encodes a sterile alpha

motif (SAM) domain-containing protein, while *EGT1* encodes a tubby-like F-box protein (Fusi *et al.*, 2022).

4.2 EGT2 is functionally conserved in dicotyledons and monocotyledons

To further validate the function of *EGT2*, we generated durum wheat double mutants with complete knockout of the wheat *EGT2* homologs. The roots of these mutants displayed a steeper root system similar to that of barley *egt2*, suggesting that *EGT2* is conserved in barley and wheat. The only functional domain predicted in EGT2 is the SAM domain, which is highly conserved between different plant species, including Arabidopsis. Therefore, it is likely that homologs of *EGT2* in dicotyledonous species also play a role in regulating gravitropic response. Consistently, the *WEEP* gene of peach (*Prunus persica*), a homolog of *EGT2*, is involved in regulating the direction of shoot growth (Hollender *et al.*, 2018). Based on the identification of the barley *EGT2* gene as regulator of root setpoint angle, the root phenotype of *weep* mutants of the Arabidopsis homolog was surveyed (Johnson *et al.*, 2022). Unlike the seminal roots of cereals, which mostly grow at a non-vertical root setpoint angles to forage for nutrients and water in the environment, the primary roots of Arabidopsis grow straight downward under natural conditions. This makes it difficult to observe phenotypes related to root setpoint angle of Arabidopsis primary roots. Nevertheless, *weep* mutants displayed a steeper lateral root angle and a narrower root system (Johnson *et al.*, 2022). Therefore, *EGT2* is likely to regulate root gravitropic response in both monocotyledons and dicotyledons, thereby governing the root setpoint angle. This makes *EGT2* a promising target for adjusting the root setpoint angles of different crop species to improve performance under varying growth conditions.

4.3 Gravistimulation primarily remodels the transcriptome of the elongation zone of wild type seminal roots

Root gravitropic response in flowering plants consists of three spatio-temporal steps, including gravity sensing mainly in the root cap, signal transduction from the root cap to the elongation zone and gravitropic bending in the elongation zone (Nakamura *et al.*, 2019). In Chapter 3, we analyzed the transcriptome plasticity in the root cap, the meristem and the elongation zone of gravistimulated wild type roots in a time-course experiment to reveal the transcriptomic variation in each step of gravitropic response. Principal component analysis (PCA) revealed that differences between the three root zones were greater than the differences between time points, which is in line with the notion that tissue identities are the main driver explaining transcriptome differences (Opitz *et al.*, 2016; Baldauf *et al.*, 2016).

Differential expression analyses revealed the highest number of differentially expressed genes in the elongation zone and the lowest in the meristem. This suggests that gravity signal transduction from the root cap to the elongation zone is not mediated at the transcriptional level, which is consistent with the fact that regulation of PIN transporters on protein level is critical for an appropriate gravitropic response (Zhang *et al.*, 2010; Retzer *et al.*, 2019; Ke *et al.*, 2021). The number of differentially expressed genes in the elongation zone (2881) was approximately seven times higher than that in the root cap (460), highlighting the importance of transcriptome remodeling in the elongation zone in response to gravity. Moreover, the number of differentially expressed genes in the root cap and the elongation zone gradually increased with the duration of gravitropic stimulation. 98% of differentially expressed genes in the root cap and 66% of differentially expressed genes in the elongation zone were induced only after 12 h of gravistimulation. However, root angle adjustment in gravistimulated roots was already visible after 3 h of gravistimulation (Chapter 2 and Chapter 3). This suggests that the early phases of gravitropism (within 3 h after gravitropic stimulation) are less dependent on transcriptional regulation than the later phases of gravitropism. Redistribution of auxin directed by reposition of PINs is a decisive event in the process of gravity signal perception and signal transduction, and phosphorylation of PINs controls their localization (Su *et al.*, 2017). Therefore, further analyses on the protein level will help to uncover the early processes of the root gravitropic response.

Gene Ontology (GO) assays revealed that some differentially expressed genes in the root cap are involved in gravity signal perception-related processes, including regulation of reactive oxygen species biosynthetic process, cytoplasmic microtubule organization, carbohydrate metabolic process and regulation of calcium-mediated signaling (Mugnai *et al.*, 2014; Krieger *et al.*, 2016; Singh *et al.*, 2017; Su *et al.*, 2020). Moreover, more than two hundred biological process terms were significantly enriched in differentially expressed genes in the elongation zone. Among them, cell wall organization, oxidative stress and protein phosphorylation are involved in root gravitropic bending (Su *et al.*, 2020; Fusi *et al.*, 2022). These data provide a list of candidate genes involved in different steps of gravitropic response by uncovering the tissue-specific transcriptome dynamics of barley seminal roots in response to gravistimulation. Analyzing expression patterns and GO associations allow future analyses to start not only with single genes of interest, but also with genes with specific biological functions to reveal the underlying molecular mechanisms of root gravitropic response.

4.4 *EGT2* likely plays a role in gravitropic signal transduction and is related to cell wall-related processes

Comparative transcriptome analyses of root zones between *egt2* and wild type provide new insights into the regulation of root gravitropism by *EGT2*. To this end, we first analyzed the transcriptomic differences between the root cap, the meristem and the elongation zone of vertically grown *egt2* and wild type roots in Chapter 2. Differentially expressed genes were determined by pairwise comparisons of *egt2* and wild type. GO analyses assigned biological process terms to differentially expressed genes in the elongation zone only, all of which were associated with the cell wall. This suggests that gravitropic bending in the elongation zone, which is achieved by asymmetrical cell elongation on the upper and lower side of gravistimulated roots (Su *et al.*, 2020), is likely to be differentially regulated in *egt2*. However, since this data was obtained from vertically grown roots, the regulation of graviregulated genes by *EGT2* remains unclear.

Therefore, graviregulated genes associated with *EGT2* were determined by comparing them with *EGT2* regulated genes upon gravistimulation (Chapter 3). Of the graviregulated genes in the elongation zone determined in the wild type gravistimulation time-course experiment, more than one thousand were regulated by *EGT2*. This represents more than one-third of the total number of gravity-regulated genes in the elongation zone, which supports the important role of *EGT2* in regulating root gravitropic bending. Many GO terms related to biological processes associated with cell wall, ROS and protein modification were significantly enriched in genes regulated by both gravistimulation and *EGT2* in the elongation zone. This provides possible clues to explore the molecular function of *EGT2*. GO term analysis of gravity- and *EGT2*-regulated genes in the root cap suggested that these genes were likely to be associated with intracellular transmembrane transport, which is important for signal transduction from the root cap to the elongation zone (Strohm *et al.*, 2012). Nevertheless, the low proportion of graviregulated genes in the root cap regulated by *EGT2* and the absence of such genes determined in the meristem suggest a less prominent role of *EGT2* in gravity signal transduction at the transcriptomic level. Furthermore, co-expression network analyses revealed that in all three root zones, plant cell wall- and ROS-related biological process terms were consistently enriched in modules strongly correlated with genotype and/or gravistimulation time point. These two processes interplay and are involved in the regulation of signal transduction and gravitropic bending response (Pennell, 1998; Krieger *et al.*, 2016; Su *et al.*, 2017; Janků *et al.*, 2019). Therefore, it is likely that *EGT2* functions on the protein level in signal transduction to further regulate root gravitropic bending by mediating plant cell wall organization and ROS

metabolism. This hypothesis is also supported by previous results that *EGT2* was expressed ubiquitously in the root tip (Chapter 2).

The only annotated domain in EGT2 is the SAM domain, which has been shown to have multiple functions in mammals and might be involved in oligomerization or RNA binding in plants (Schultz *et al.*, 1997; Kim & Bowie, 2003; Denay *et al.*, 2017). In a combination of yeast-two-hybrid and bimolecular fluorescence complementation (BiFC) assays, three interaction partners of EGT2 encoding by gravity- and *EGT2*-regulated genes were identified. The functions of these three interacting partners are predicted to be related to cell wall organization and the catalytic action of flavonoids. Flavonoids have been shown to be involved in regulation of root gravitropic response and polar auxin transport by ethylene (Buer *et al.*, 2006; Santelia *et al.*, 2008). This strengthens the hypothesis that *EGT2* plays a role in signal transduction and regulates root gravitropic bending. Nevertheless, further experiments on cell wall organization and flavonoid action in the *egt2* mutant are required.

4.5 Future perspectives

This study identified *EGT2*, a novel regulator of root setpoint angle control in barley, and extended the knowledge of root zone-specific transcriptomic remodeling in response to gravistimulation. Based on the results of the present study, the following experiments could be considered in the future: To begin with, measuring flavonoid content and investigating the cell wall structure and stiffness in wild type and *egt2* roots would allow confirming the putative function of the interaction partners of EGT2 and thus the function of *EGT2*. Secondly, creating mutants for graviregulated genes determined in this study would accelerate the identification of candidate genes involved in regulating root setpoint angle. Furthermore, comparing the phytohormone content of *egt2* and wild type roots before and after gravistimulation would provide support for the role of phytohormones in *EGT2*-regulated root gravitropic response. Confirmation of graviregulated phytohormones-related genes involved in root gravitropism would generate reporter genes for further studies. Moreover, investigation of the accumulation, localization, and phosphorylation of PIN proteins in *egt2* and wild type roots could help to understand the regulation of auxin transport by *EGT2*. In addition, exploring the function of genes that were significantly differentially expressed in *egt2* would provide opportunities to discover other roles of *EGT2* besides the regulation of root setpoint angle. Finally, systematic analysis of SAM-domain containing proteins in crops would provide new insights into their roles and offer novel candidates for reshaping root structure in other species.

4.6 References

Baldauf JA, Marcon C, Paschold A, Hochholdinger F. (2016). Nonsyntenic genes drive tissue-specific dynamics of differential, nonadditive, and allelic expression patterns in maize hybrids. *Plant Physiology*, 171, 1144–1155.

Buer CS, Sukumar P, Muday GK. (2006). Ethylene modulates flavonoid accumulation and gravitropic responses in roots of Arabidopsis. *Plant Physiology*, 140, 1384–1396.

Denay G, Vachon G, Dumas R, Zubieta C, Parcy F. (2017). Plant SAM-domain proteins start to reveal their roles. *Trends in Plant Science*, 22, 718–725.

Fusi R, Rosignoli S, Lou H, Sangiorgi G, Bovina R, Pattem JK, Borkar AN, Lombardi M, Forestan C, Milner SG, Davis JL, Lale A, Kirschner GK, Swarup R, Tassinari A, Pandey BK, York LM, Atkinson BS, Sturrock CJ, Mooney SJ, Hochholdinger F, Tucker MR, Himmelbach A, Stein N, Mascher M, Nagel KA, De Gara L, Simmonds J, Uauy C, Tuberosa R, Lynch JP, Yakubov GE, Bennett MJ, Bhosale R, Salvi S. (2022). Root angle is controlled by *EGT1* in cereal crops employing an antigravitropic mechanism. *Proceedings of the National Academy of Sciences*, 119, e2201350119.

Hollender CA, Pascal T, Tabb A, Hadiarto T, Srinivasan C, Wang W, Liu Z, Scorza R, Dardick C. (2018). Loss of a highly conserved sterile alpha motif domain gene (*WEEP*) results in pendulous branch growth in peach trees. *Proceedings of the National Academy of Sciences of the United States of America*, 115, E4690–E4699.

Janků M, Luhová L, Petřivalský M. (2019). On the origin and fate of reactive oxygen species in plant cell compartments. *Antioxidants (Basel)*, 8, 105.

Johnson JM, Kohler AR, Haus MJ, Hollender CA. (2022). Arabidopsis *weep* mutants exhibit narrow root angles. *microPublication Biology*. 10.17912/micropub.biology.000584.

Ke M, Ma Z, Wang D, Sun Y, Wen C, Huang D, Chen Z, Yang L, Tan S, Li R, Friml J, Miao Y, Chen X. (2021). Salicylic acid regulates PIN2 auxin transporter hyperclustering and root gravitropic growth via Remorin-dependent lipid nanodomain organisation in *Arabidopsis thaliana*. *New Phytologist*, 229, 963–978.

Kim CA, Bowie JU. (2003). SAM domains: uniform structure, diversity of function. *Trends in Biochemical Sciences*, 28, 625–628.

Konstantinova N, Korbei B, Luschnig C. (2021). Auxin and root gravitropism: addressing basic cellular processes by exploiting a defined growth response. *International Journal of*

Molecular Sciences, 22, 1–20.

Krieger G, Shkolnik D, Miller G, Fromm H. (2016). Reactive oxygen species tune root tropic responses. *Plant Physiology*, 172, 1209–1220.

Lueck JD, Yoon JS, Perales-Puchalt A, Mackey AL, Infield DT, Behlke MA, Pope MR, Weiner DB, Skach WR, McCray PB, Ahern CA. (2019). Engineered transfer RNAs for suppression of premature termination codons. *Nature Communications*, 10, 822.

Mugnai S, Pandolfi C, Masi E, Azzarello E, Monetti E, Comparini D, Voigt B, Volkmann D, Mancuso S. (2014). Oxidative stress and NO signalling in the root apex as an early response to changes in gravity conditions. *BioMed Research International*, 2014, 834134.

Nakamura M, Nishimura T, Morita MT. (2019). Gravity sensing and signal conversion in plant gravitropism. *Journal of Experimental Botany*, 70, 3495–3506.

Ober ES, Alahmad S, Cockram J, Forestan C, Hickey LT, Kant J, Maccaferri M, Marr E, Milner M, Pinto F, Rambla C, Reynolds M, Salvi S, Sciara G, Snowdon RJ, Thomelin P, Tuberosa R, Uauy C, Voss-Fels KP, Wallington E, Watt M. (2021). Wheat root systems as a breeding target for climate resilience. *Theoretical and Applied Genetics*,134, 1645–1662.

Opitz N, Marcon C, Paschold A, Malik WA, Lithio A, Brandt R, Piepho HP, Nettleton D, Hochholdinger F. (2016). Extensive tissue-specific transcriptomic plasticity in maize primary roots upon water deficit. *Journal of Experimental Botany*, 67, 1095–1107.

Pennell R. **(1998)**. Cell walls: structures and signals. *Current Opinion in Plant Biology*, 1, 504–510.

Retzer K, Akhmanova M, Konstantinova N, Malínská K, Leitner J, Petrášek J, Luschnig C. (2019). Brassinosteroid signaling delimits root gravitropism via sorting of the Arabidopsis PIN2 auxin transporter. *Nature Communications*, 10, 1–15.

Santelia D, Henrichs S, Vincenzetti V, Sauer M, Bigler L, Klein M, Bailly A, Lee Y, Friml J, Geisler M, Martinoia E. (2008). Flavonoids redirect PIN-mediated polar auxin fluxes during root gravitropic responses. *Journal of Biological Chemistry*, 283, 31218–31226.

Schultz J, Ponting CP, Hofmann K, Bork P. (1997). SAM as a protein interaction domain involved in developmental regulation. *Protein Science*, 6, 249–253.

Singh M, Gupta A, Laxmi A. (2017). Striking the right chord: Signaling enigma during root gravitropism. *Frontiers in Plant Science*, 8, 1304.

Strohm AK, Baldwin KL, Masson PH. (2012). Multiple roles for membrane-associated

protein trafficking and signaling in gravitropism. *Frontiers in Plant Science*, 3, 274.

Su SH, Gibbs NM, Jancewicz AL, Masson PH. (2017). Molecular mechanisms of root gravitropism. *Current Biology*, 27, R964–R972.

Su SH, Keith MA, Masson PH. (2020). Gravity signaling in flowering plant roots. *Plants*, 9, 1–23.

Uga Y, Kitomi Y, Ishikawa S, Yano M. (2015). Genetic improvement for root growth angle to enhance crop production. *Breeding Science*, 65, 111–119.

Zhang J, Nodzyński T, Pěnčík A, Rolčík J, Friml J. (2010). PIN phosphorylation is sufficient to mediate PIN polarity and direct auxin transport. *Proceedings of the National Academy of Sciences of the United States of America*, 107, 918–922.

Appendix

Supplementary Figures for Chapter 2

Title: *ENHANCED GRAVITROPISM 2* encodes a STERILE ALPHA MOTIF–containing protein that controls root growth angle in barley and wheat

Kirschner GK, Rosignoli S, **Guo L**, Vardanega I, Imani J, Altmüller J, Milner SG, Balzano R, Nagel KA, Pflugfelder D, Forestan C, Bovina R, Koller R, Stöcker TG, Mascher M, Simmonds J, Uauy C, Schoof H, Tuberosa R, Salvi S, Hochholdinger F

The supplementary tables for Chapter 2 are attached to this thesis as online supplement on a CD-ROM.

Supplementary Figure 1: **Root phenotype of *egt2-1***

A Wild type and *egt2-1* roots grown on paper sheets, 14 days after germination (DAG). Scale bar: 2 cm. **B** Number of seminal roots 7 DAG; n = 40 per genotype in one experiment. **C** Root length 14 DAG; n = 8-9 per genotype in two independent experiments. **D** Root length after rotation; n = 32 in three independent experiments; compare Figure 1G; standard deviation is depicted; two-tailed t-test did not show any significant differences between the genotypes at respective time points; all measurements were normalized to the starting length of the roots at time point 0. **E** Magnetic resonance imaging (MRI) pictures of wild type and *egt2-1* roots grown in soil for 7 DAG. Scale bar: 2 cm. **F** Root angle of roots grown in soil for 3 DAG and captured by MRI (see D); n = 17-18 per genotype; two-tailed t-test, ** $p<$ 0.01.

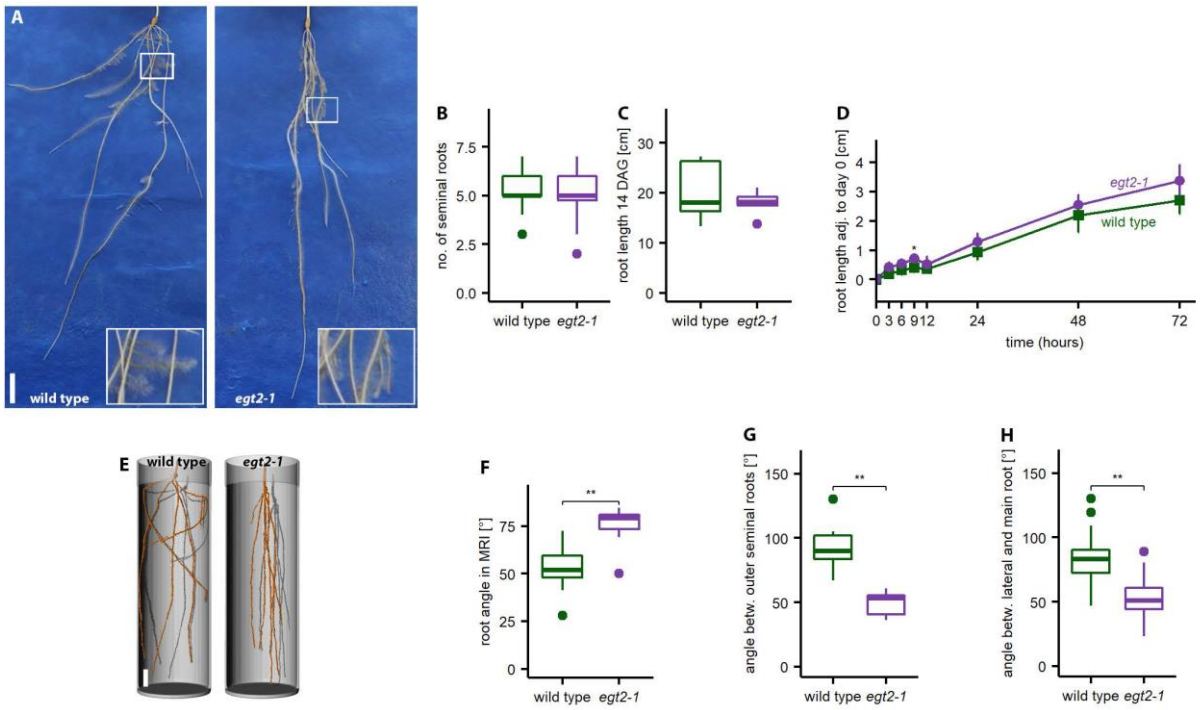

Supplementary Figure 2: **Meristem phenotype of *egt2-1* resembles the wild type phenotype**

A Root meristem of wild type and *egt2-1* 7 DAG; arrow heads mark transition to elongation zone. Scale bar: 200 µm. **B** Wild type and *egt2-1* root cap 7 DAG. Scale bar: 50 µm; brightness adjusted in magnification. **C** Quantification of meristem length 7 DAG; n = 15-20 roots per genotype; two-tailed t-test does not show any significant difference. **D** Lateral roots of wild type and *egt2-1* plants 14 DAG stained by mPS-PI staining. Scale bar: 50 µm. **E** Root caps of wild type and *egt2-1* plants 7 DAG, after 180° rotation at the indicated time points, starch granules stained with Lugol staining. Scale bar: 20 µm. **F** Quantification of the starch granule distance to the former distal or new lower cell wall, measured from the center of the starch granules, n = 4-9 plants per time point, 6-10 cells of a size of 25-40 µm were measured per root.

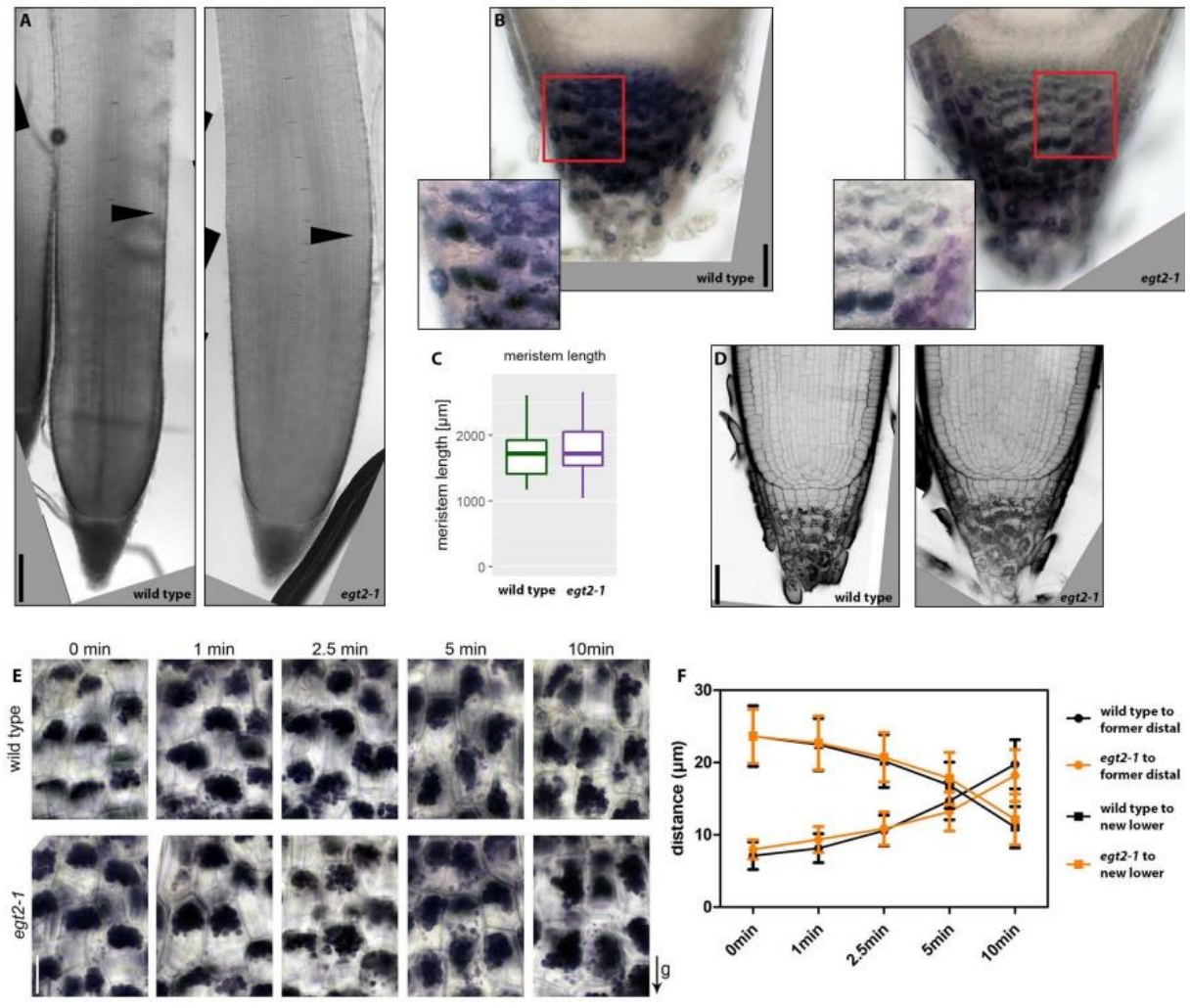

Supplementary Figure 3: ***egt2-1*** **mutant and wild type react similarly to auxin treatment**

A, **C**, **E**, **G**, **I**, **K** Angle of the root tip after indicated treatment and rotation for 90° (at time point 0). **B**, **D**, **F**, **H**, **J**, **L** Length of the roots after indicated treatment and rotation for 90° (at time point 0); phytohormone treated plants were compared to the mock-treated plants of the same genotype at the respective time points by a two-tailed t-test, * $p< 0.05$; ** $p< 0.01$ and *** $p< 0.001$; standard deviation is depicted; to account for the different starting angles of the roots, all measurements were normalized to the starting angle/length of the roots at time point 0. **A**, **B** 1 nM IAA treatment, **C**, **D** 10 nM IAA treatment. **E**, **F** 100 nM IAA treatment. **G**, **H** 10 nM NPA treatment. **I**, **J** 100 nM NPA treatment**K**, **L** 1 µM NPA treatment. n = 4 plants per genotype and treatment in two independent experiments for all phytohormone concentrations.

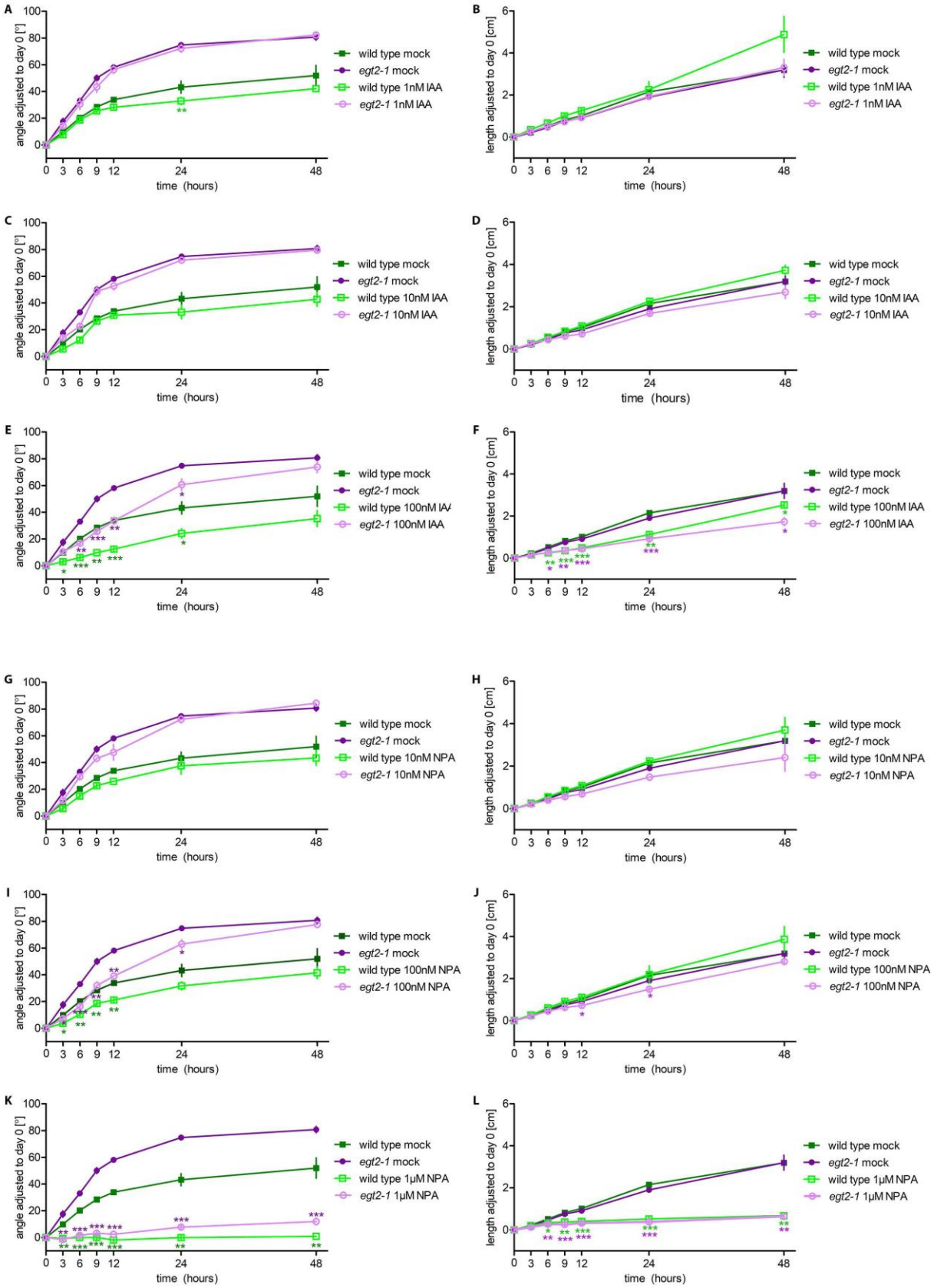
A
angle adjusted to day 0 [°]
time (hours)
wild type mock
egt2-1 mock
wild type 1nM IAA
egt2-1 1nM IAA
B
length adjusted to day 0 [cm]
time (hours)
wild type mock
egt2-1 mock
wild type 1nM IAA
egt2-1 1nM IAA
C
angle adjusted to day 0 [°]
time (hours)
wild type mock
egt2-1 mock
wild type 10nM IAA
egt2-1 10nM IAA
D
length adjusted to day 0 [cm]
time (hours)
wid type mock
egt2-1 mock
wild type 10nM IAA
egt2-1 10nM IAA
E
angle adjusted to day 0 [°]
time (hours)
wild type mock
egt2-1 mock
wild type 100nM IAA
egt2-1 100nM IAA
F
length adjusted to day 0 [cm]
time (hours)
wild type mock
egt2-1 mock
wild type 100nM IAA
egt2-1 100nM IAA
G
angle adjusted to day 0 [°]
time (hours)
wild type mock
egt2-1 mock
wild type 10nM NPA
egt2-1 10nM NPA
H
length adjusted to day 0 [cm]
time (hours)
wild type mock
egt2-1 mock
wild type 10nM NPA
egt2-1 10nM NPA
I
angle adjusted to day 0 [°]
time (hours)
wild type mock
egt2-1 mock
wild type 100nM NPA
egt2-1 100nM NPA
J
length adjusted to day 0 [cm]
time (hours)
wild type mock
egt2-1 mock
wild type 100nM NPA
egt2-1 100nM NPA
K
angle adjusted to day 0 [°]
time (hours)
wild type mock
egt2-1 mock
wild type 1µM NPA
egt2-1 1µM NPA
L
length adjusted to day 0 [cm]
time (hours)
wild type mock
egt2-1 mock
wild type 1µM NPA
egt2-1 1µM NPA

Supplementary Figure 4: **CRISPR/Cas9 induced mutation in *EGT2* and conserved function in wheat**

A Gene model of *EGT2* and partial DNA sequence; arrow marks translation start site; purple boxes mark the CRISPR target sites; in the *egt2-2* mutant line, CRISPR/Cas induced a deletion between the target sites as depicted. **B** Protein structure of EGT2 with the SAM domain from amino acid 172 - 225; protein alignment of EGT2, AtSAM5 (At3g07760) and peach WEEP (Prupe. 3G200700) in the SAM region. **C** Root length 7 DAG, two-tailed t-test does not show a significant difference (p<0.05). n = 15-17 in two independent experiments. **D** Wild type GP and *egt2-2* lateral roots 14 DAG. Scale bar: 1 cm. **E** Root tip angle after rotation; plants 5 DAG were rotated by 90° (time 0) and the root tip angle was measured over time; n = 20 per genotype in two independent experiments; the two genotypes were compared between each other at the respective time points by a two-tailed t-test and no significant difference was detected; standard deviation is depicted; to account for the different starting angles of the roots, all measurements were normalized to the starting angle of the roots at time 0. **F** Root length after rotation as described in D; n = 20 per genotype in two independent experiments. **G** Area enclosed by the first three seminal root of wild type (WT/WT) and *egt2* (*mut/mut*) wheat seedling at 7 DAG; n = 16 and 35 for wild type and mutant, respectively. **H** Number of seminal roots of wild type (WT/WT) and egt2 (mut/mut) wheat seedling at 7 DAG; n = 18 and 39 for wild type and mutant, respectively. **I** Length of the first three seminal root in wild type (WT/WT) and *egt2* (*mut/mut*) wheat seedling at 7 DAG; n = 16 and 35 for wild type and mutant, respectively. Wheat plants analyzed in **G**, **H** and **I** were derived from two independent segregating populations; the two genotypes were compared by a two-tailed t-test (* p< 0.05, ns = no significant difference).

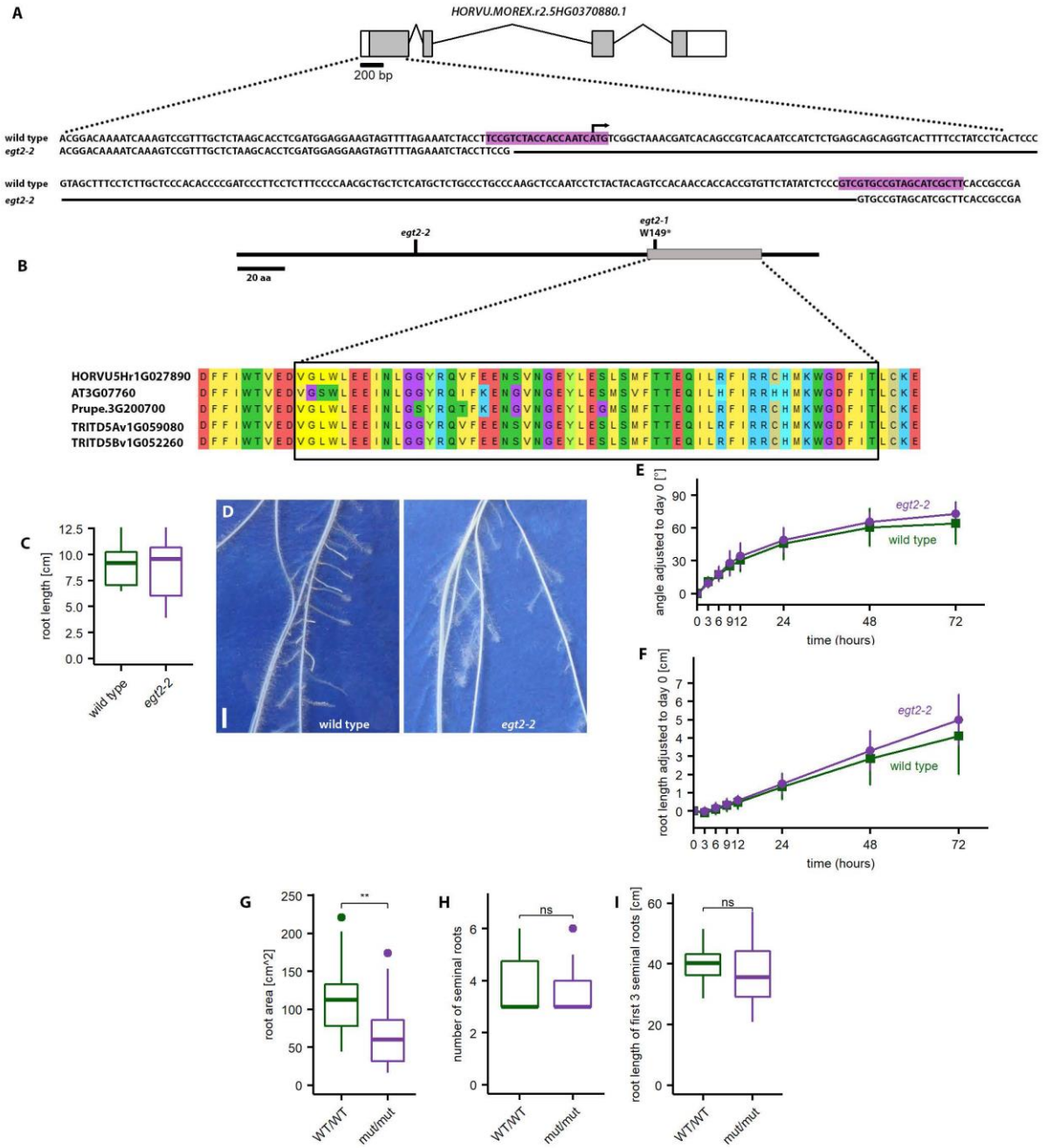
A
HORVU.MOREX.r2.5HG0370880.1
200 bp
wild type
egt2-2
B
egt2-2
egt2-1
W149*
20 aa
HORVU5Hr1G027890
AT3G07760
Prupe.3G200700
TRITD5Av1G059080
TRITD5Bv1G052260
C
root length [cm]
wild type
egt2-2
D
wild type
egt2-2
E
angle adjusted to day 0 [°]
time (hours)
F
root length adjusted to day 0 [cm]
time (hours)
G
root area [cm^2]
**
WT/WT
mut/mut
H
number of seminal roots
ns
I
root length of first 3 seminal roots [cm]
ns

Supplementary Figure 5: **LCM samples A** Representative picture of rotated root before tissue dissection by laser capture microdissection (LCM). Scale bar: 300 µm. **B** Representative picture of root before and after tissue dissection by LCM for RNA-seq. Scale bar: 300 µm.

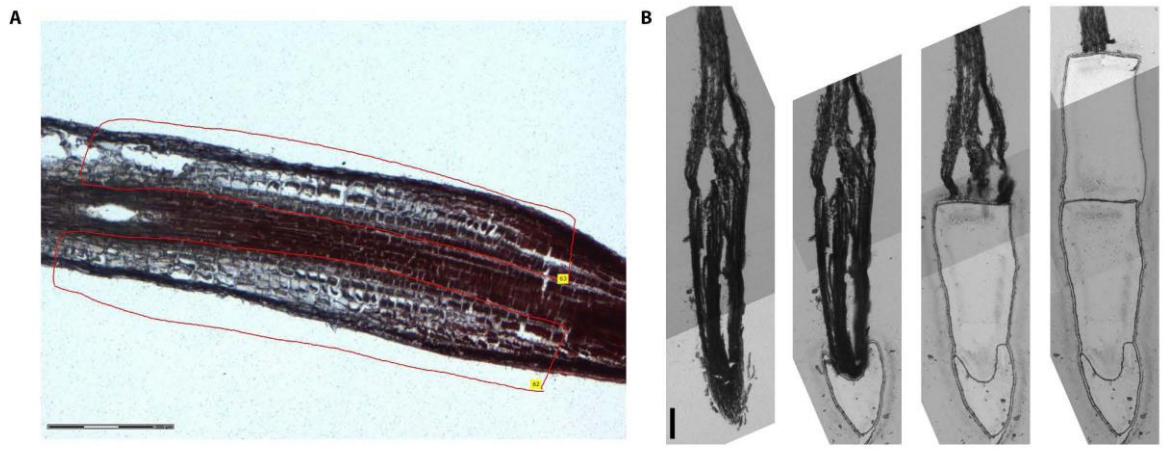

Supplementary Figure 6: **Phylogenetic tree of EGT2 and related proteins**

Species abbreviations: AT: *Arabidopsis thaliana*; BGIOS: *Oryza sativa Indica*; BRADI: *Brachypodium distachyon*; Os: *Oryza sativa Japonica*; PRUPE: *Prunus persica*; SORBI: *Sorghum bicolor*; Traes: *Triticum aestivum*; TRITD: *Triticum durum*; Zm: *Zea mays*.

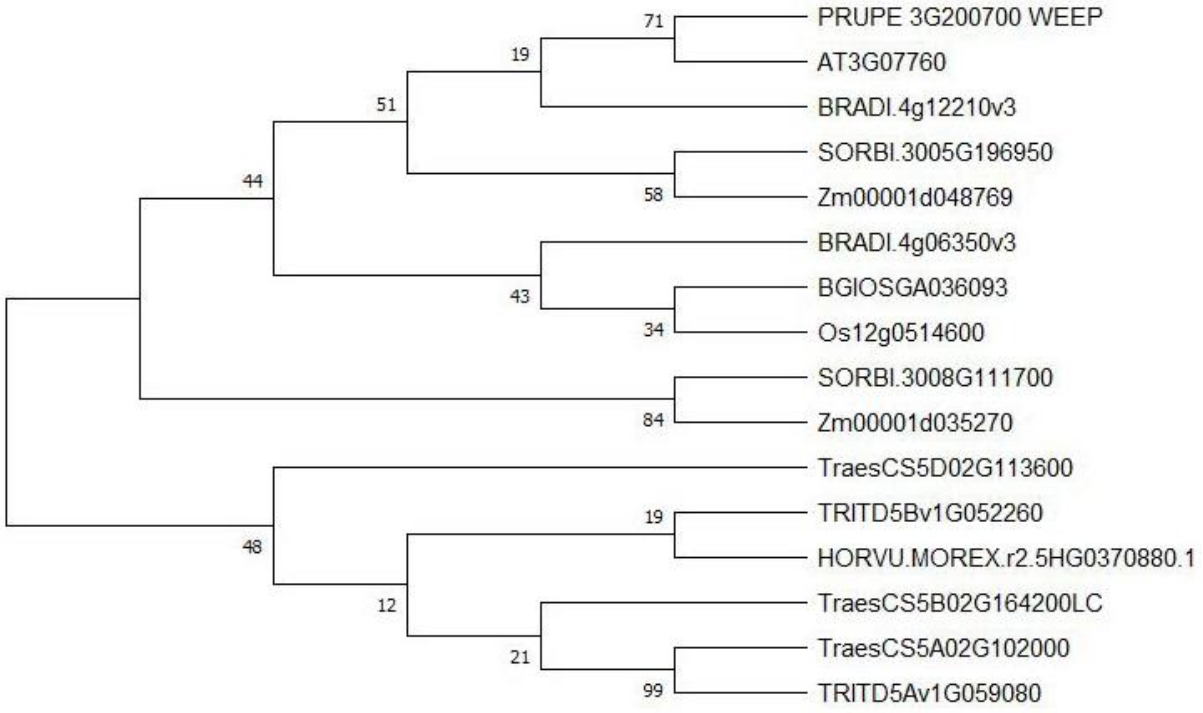

Supplementary Figure 7: **Heat map of differentially expressed genes (FDR <5%, $log_2FC \geq |1|$) between wild-type and *egt2-1* in root cap, root meristem and elongation zone**

Average of log1p of FPM (fragments per million mapped fragments) normalized counts of four biological replicates of the respective genotype and tissue is shown in blue scale.

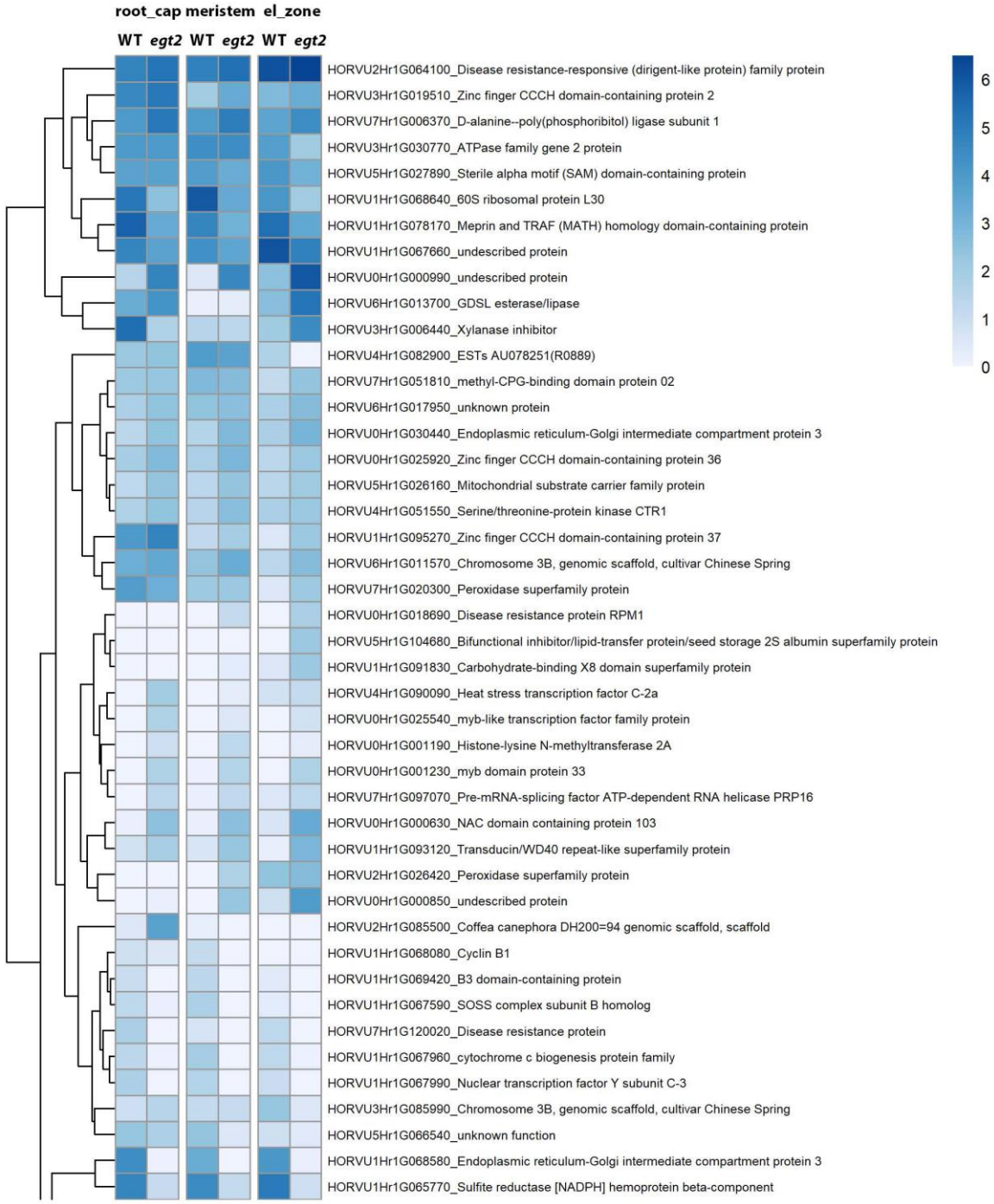

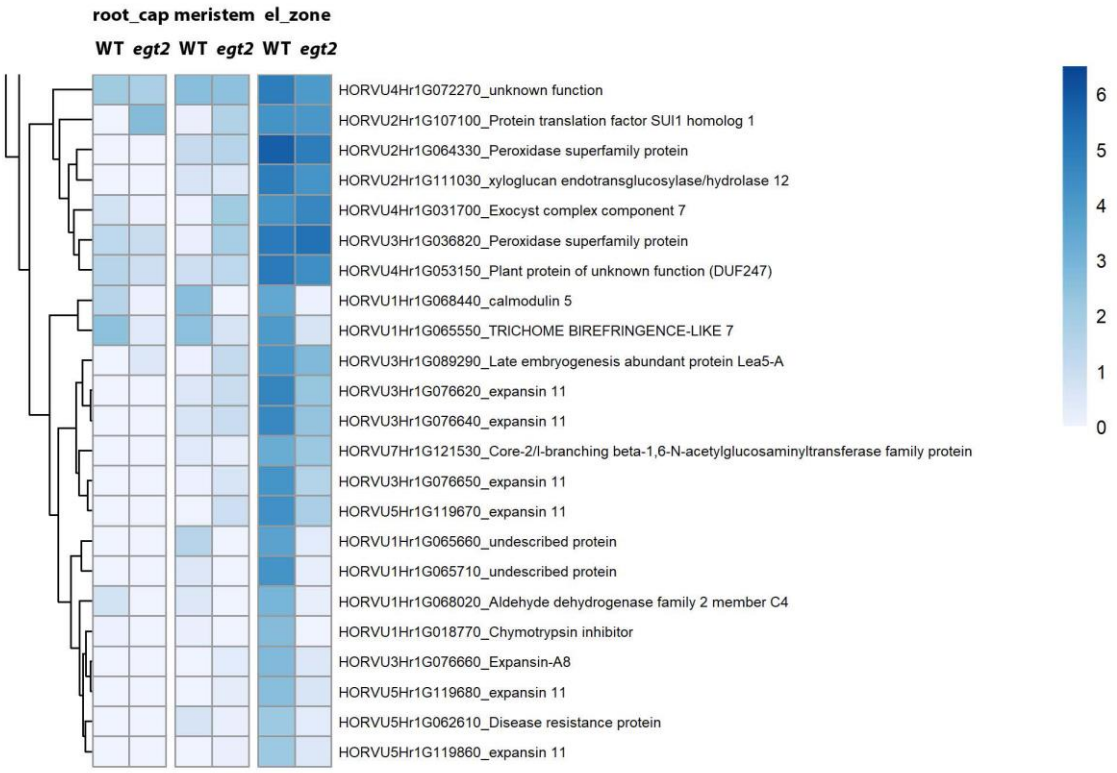
root_cap meristem el_zone
WT egt2 WT egt2 WT egt2
HORVU4Hr1G072270_unknown function
HORVU2Hr1G107100_Protein translation factor SUI1 homolog 1
HORVU2Hr1G064330_Peroxidase superfamily protein
HORVU2Hr1G111030_xyloglucan endotransglucosylase/hydrolase 12
HORVU4Hr1G031700_Exocyst complex component 7
HORVU3Hr1G036820_Peroxidase superfamily protein
HORVU4Hr1G053150_Plant protein of unknown function (DUF247)
HORVU1Hr1G068440_calmodulin 5
HORVU1Hr1G065550_TRICHOME BIREFRINGENCE-LIKE 7
HORVU3Hr1G089290_Late embryogenesis abundant protein Lea5-A
HORVU3Hr1G076620_expansin 11
HORVU3Hr1G076640_expansin 11
HORVU7Hr1G121530_Core-2/I-branching beta-1,6-N-acetylglucosaminyltransferase family protein
HORVU3Hr1G076650_expansin 11
HORVU5Hr1G119670_expansin 11
HORVU1Hr1G065660_undescribed protein
HORVU1Hr1G065710_undescribed protein
HORVU1Hr1G068020_Aldehyde dehydrogenase family 2 member C4
HORVU1Hr1G018770_Chymotrypsin inhibitor
HORVU3Hr1G076660_Expansin-A8
HORVU5Hr1G119680_expansin 11
HORVU5Hr1G062610_Disease resistance protein
HORVU5Hr1G119860_expansin 11
6
5
4
3
2
1
0

Supplementary Figure 8: **Expression of expansins**.

A Fpm normalized expression values of the expansins differentially expressed in the gene set; padj is depicted with * $p< 0.05$, ** $p< 0.01$; RC: root cap, M: meristem, EZ: elongation zone. **B** qRT-PCR of *EGT2* expression in meristem and elongation zone without rotation as control to Figure 3B. **C** qRT-PCR of *HORVU3Hr1G076640* expression in meristem and elongation zone after rotation of 90°. **D** qRT-PCR of *HORVU5Hr1G119670* expression in meristem and elongation zone after rotation of 90°. **E** qRT-PCR of *HORVU5Hr1G119680* expression in meristem and elongation zone after rotation of 90°. F qRT-PCR of *HORVU5Hr1G119860* expression in meristem and elongation zone after rotation of 90°. **G** qRT-PCR of *HORVU3Hr1G076660* expression in meristem and elongation zone after rotation of 90°. **B-E** All gene expression values are normalized to *Tubulin* (*HORVU.MOREX.r3.1HG0082050.1*). Significant differences were determined by two-tailed t-tests: * $p< 0.05$, ** $p<0.01$

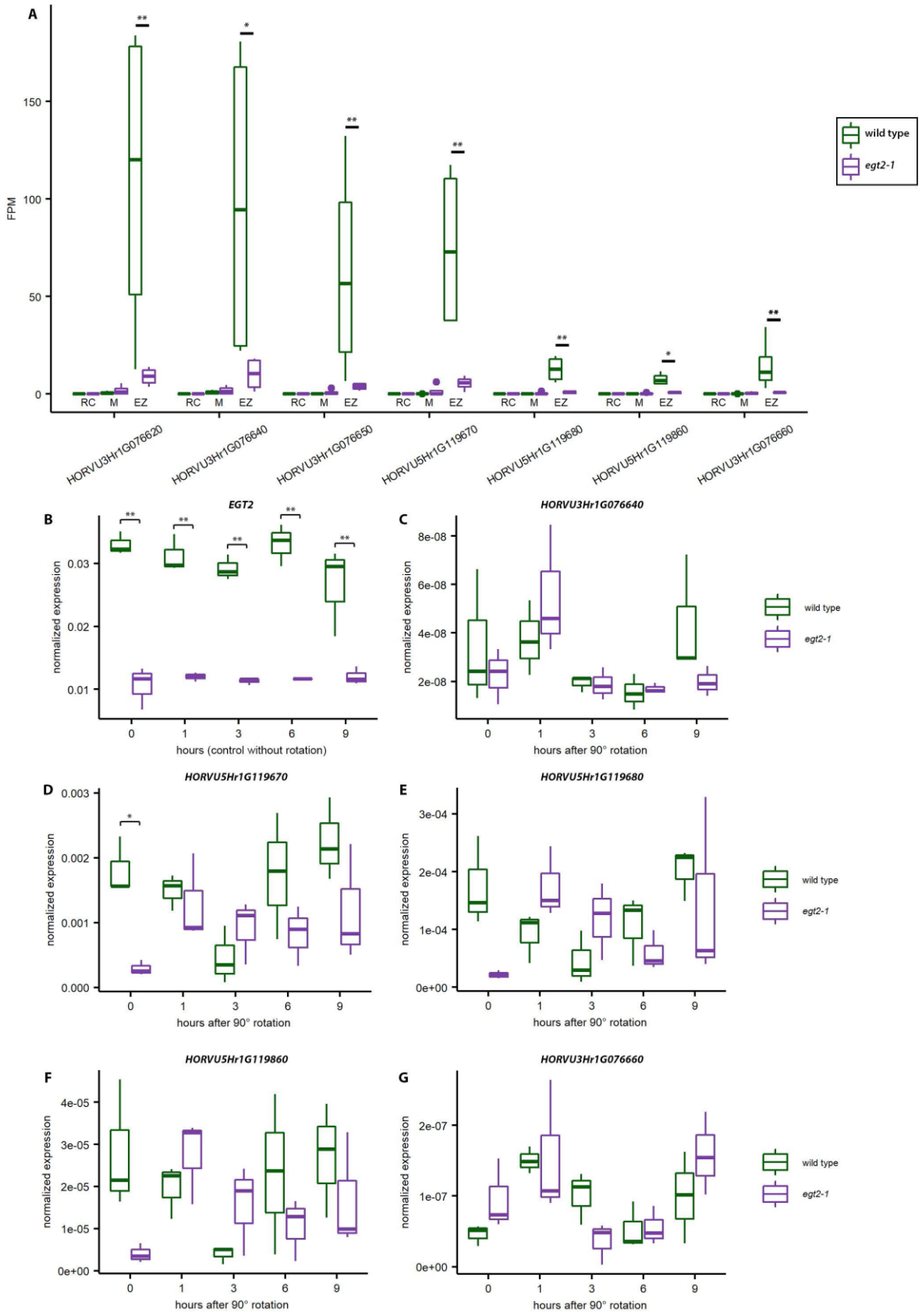
A
FPM
150
100
50
0
RC M EZ
HORVU3Hr1G076620
HORVU3Hr1G076640
HORVU3Hr1G076650
HORVU5Hr1G119670
HORVU5Hr1G119680
HORVU5Hr1G119860
HORVU3Hr1G076660
wild type
egt2-1
B
EGT2
normalized expression
hours (control without rotation)
C
HORVU3Hr1G076640
hours after 90° rotation
D
HORVU5Hr1G119670
E
HORVU5Hr1G119680
F
HORVU5Hr1G119860
G
HORVU3Hr1G076660

Supporting Information for Chapter 3

Title: ENHANCED GRAVITROPISM 2 coordinates molecular adaptations to gravistimulation in the elongation zone of barley roots

Li Guo, Alina Klaus, Marcel Baer, Gwendolyn K. Kirschner, Silvio Salvi, and Frank Hochholdinger

The supporting information tables for Chapter 3 are attached to this thesis as online supplement on a CD-ROM.

Fig. S1: Quantification of meristem length of wild type (WT) and *egt2* before and after 6 h or 10 h of gravistimulation.

(V): vertically grown samples; (R): rotated samples. n = 11-19 per genotype by time point combination.

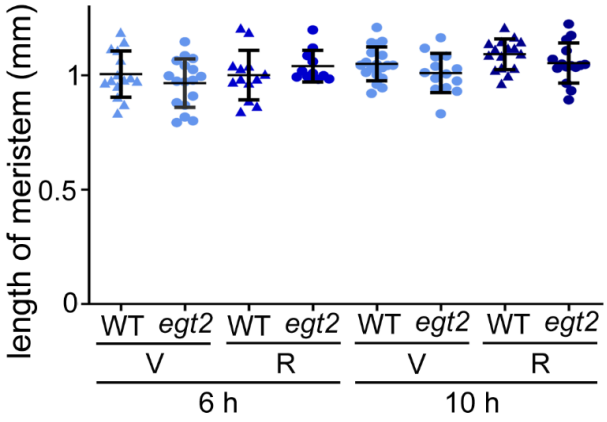

Fig. S2: Overview of yeast-two-hybrid screening.

a. Toxicity testing of EGT2.

b. Autoactivation testing of EGT2.

c. Numbers of interaction partners identified by two screens.

d. Confirmation of the interaction between EGT2 (BD-EGT2) and the 23 interaction partners (AD-prey) by one-on-one yeast-two-hybrid assays. Co-transformation with each of the AD-preys and pGBKT7 (BD) was used as a negative control. OMT: HORVU.MOREX.r3.3HG0330120.1; GTF: HORVU.MOREX.r3.7HG0736300.1.

c-d. Co-transformation of BD-53 and AD-T was shown as positive control, co-transformation of BD-lam and AD-T was shown as negative control,

e. Numbers of expected interaction partners and observed interaction candidates in differentially expressed genes. Fisher's exact test, *, $p < 0.05$; **, $p < 0.01$.

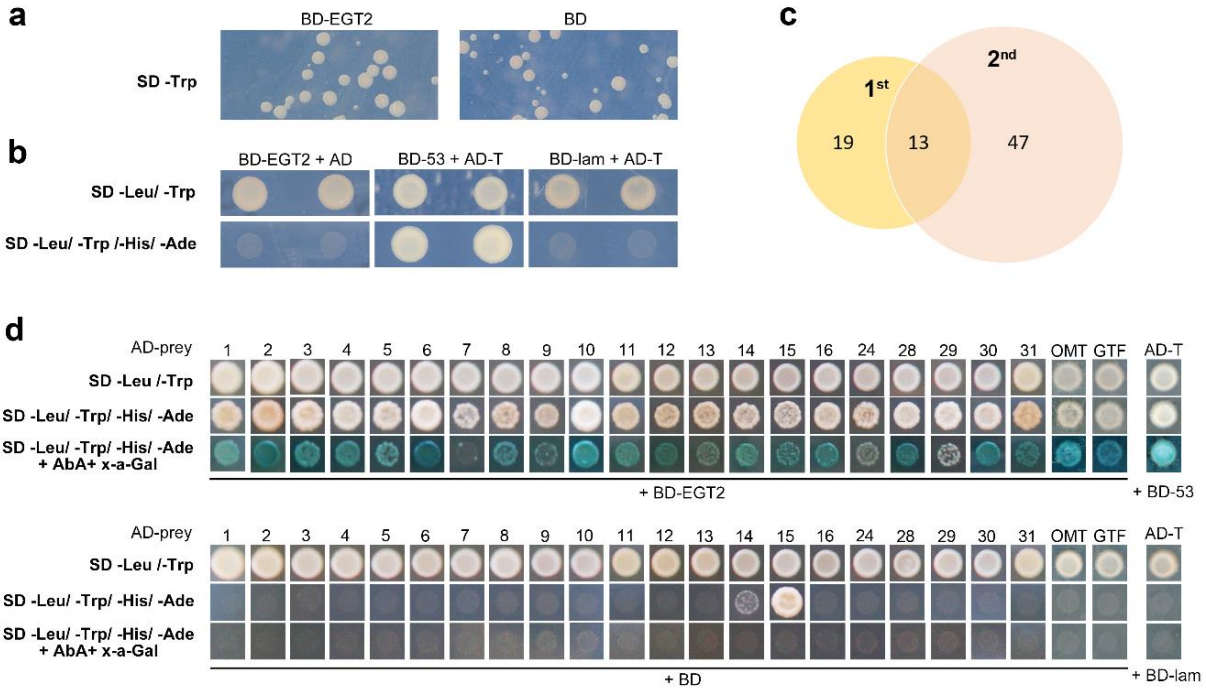
a
BD-EGT2
BD
SD -Trp
b
BD-EGT2 + AD
BD-53 + AD-T
BD-lam + AD-T
SD -Leu/ -Trp
SD -Leu/ -Trp /-His/ -Ade
c
1st
2nd
19
13
47
d
AD-prey
1 2 3 4 5 6 7 8 9 10 11 12 13 14 15 16 24 28 29 30 31 OMT GTF AD-T
SD -Leu /-Trp
SD -Leu/ -Trp/ -His/ -Ade
SD -Leu/ -Trp/ -His/ -Ade + AbA+ x-a-Gal
+ BD-EGT2
+ BD-53
+ BD
+ BD-lam

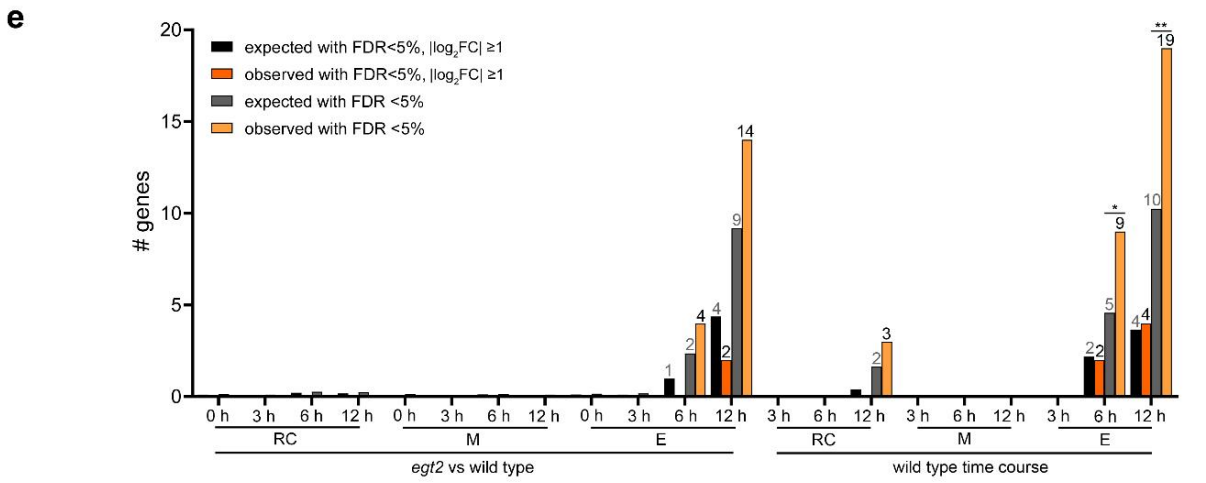
e
expected with FDR<5%, |log2FC| ≥1
observed with FDR<5%, |log2FC| ≥1
expected with FDR <5%
observed with FDR <5%
genes
0 h 3 h 6 h 12 h
RC
M
E
egt2 vs wild type
wild type time course

Fig. S3: **Dynamics of the expression profiles of graviregulated genes**.

a-d Hierarchical clustering analyses of differentially expressed genes in root cap (a and b) and elongation zone (c and d) of gravistimulated wild type roots.

a and **c** Observed expression patterns of differentially expressed genes during 12 h of gravistimulation. Numbers of genes assigned to each cluster are shown (numbers without brackets: FDR <5%; numbers in brackets: FDR <5%, $|\log_2 FC| \geq 1$).

b and **d** Heatmap of differentially expressed genes (FDR <5%) based on average expression values.

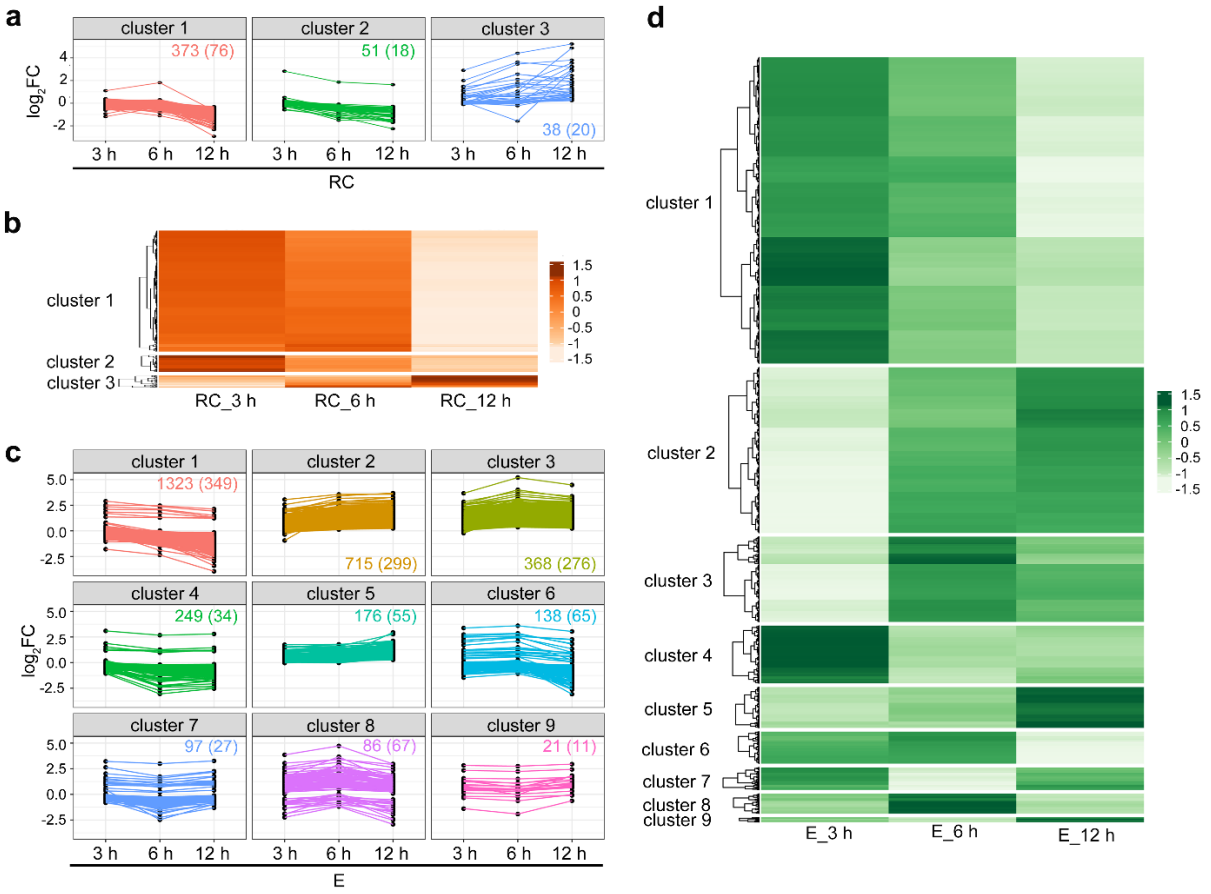

Fig. S4: Enriched GO terms for gravity regulated genes that are *EGT2* related.

a-b Significantly enriched GO terms among intersected differentially expressed genes (FDR <5%) in root cap (a) and elongation zone (b).

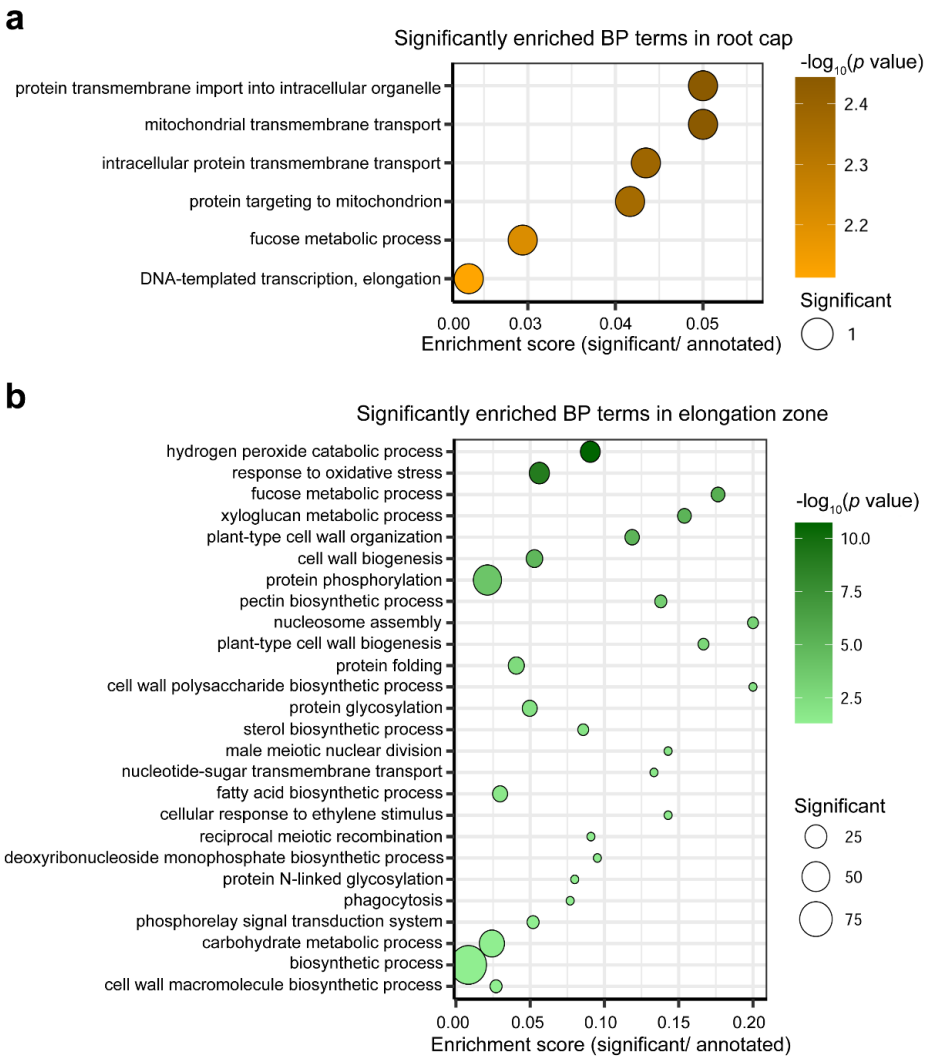

Fig. S5: Co-expression analyses.

a-c Module-trait relationships in the root cap (a), the meristem (b) and the elongation zone (c). The genotypes (wily type and *egt2*) and time points (0, 3, 6 and 12 h) after gravistimulation are used as traits, each column corresponds to a different trait. Each row corresponds to the characteristic genes of the module. The relationship between the modules and traits is indicated in cell by Pearson correlation coefficients. Numbers in brackets indicate significant levels. Cell color ranges from red (highly positive correlation) to blue (highly negative correction).

d Gene ontology analyses of genes in selected significantly correlated modules in the root cap, the meristem and the elongation zone. The five most significantly enriched biological process terms of each module are shown. Hexagonal nodes represent modules, circle nodes represent individual GO terms. Numbers in hexagonal indicate the total number of significantly enriched biological process terms in corresponding module. The size of circle nodes indicates the ratio of the number of genes associated with each GO term to the total number of genes annotated for corresponding term.

e-g The expression patterns of hub genes of the black, the purple and the blue modules in the root cap (RC; e), the midnightblue, the blue and cyan modules in the meristem (M; f), and the green, purple and turquoise modules in the elongation zone (E; g) in the WT gravistimulation time-course experiments (wild type time-course) and in the comparisons of *egt2* with wild type (*egt2* vs wild type). **, FDR<5%.

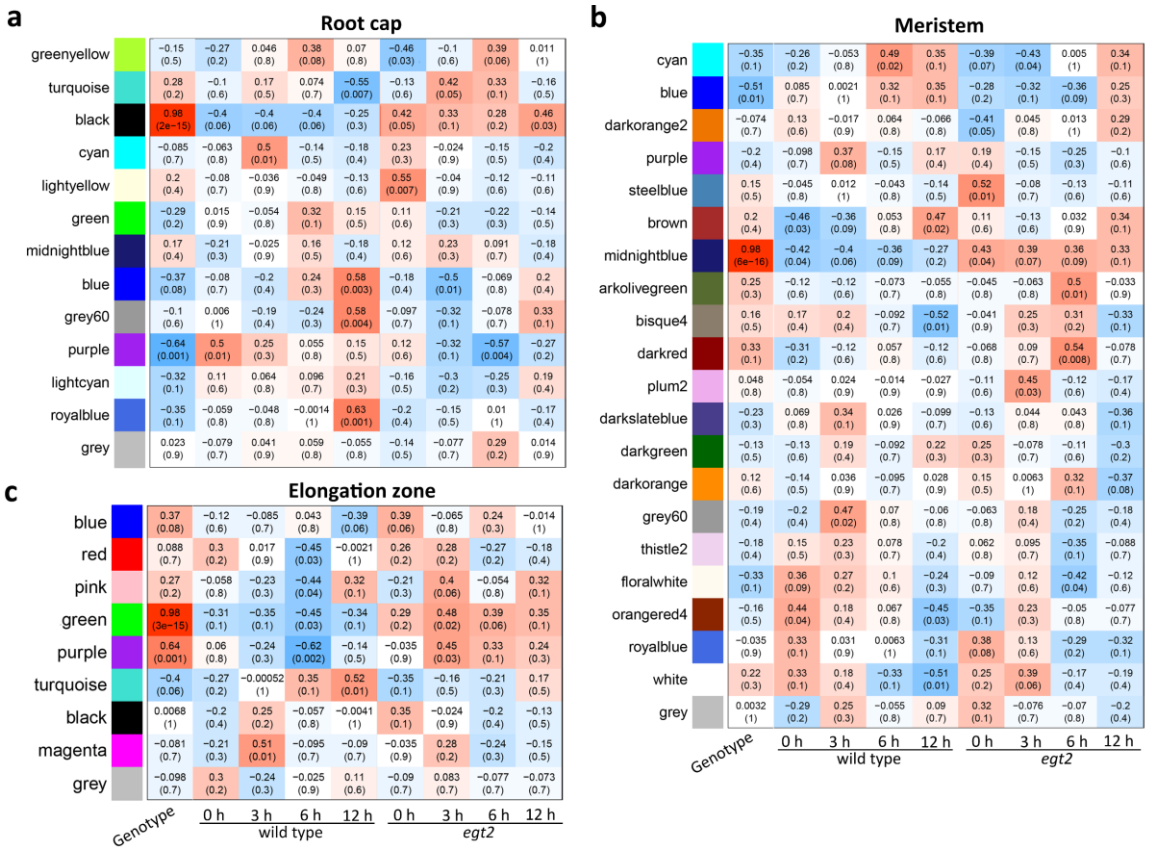

Fig. S5 Continued.

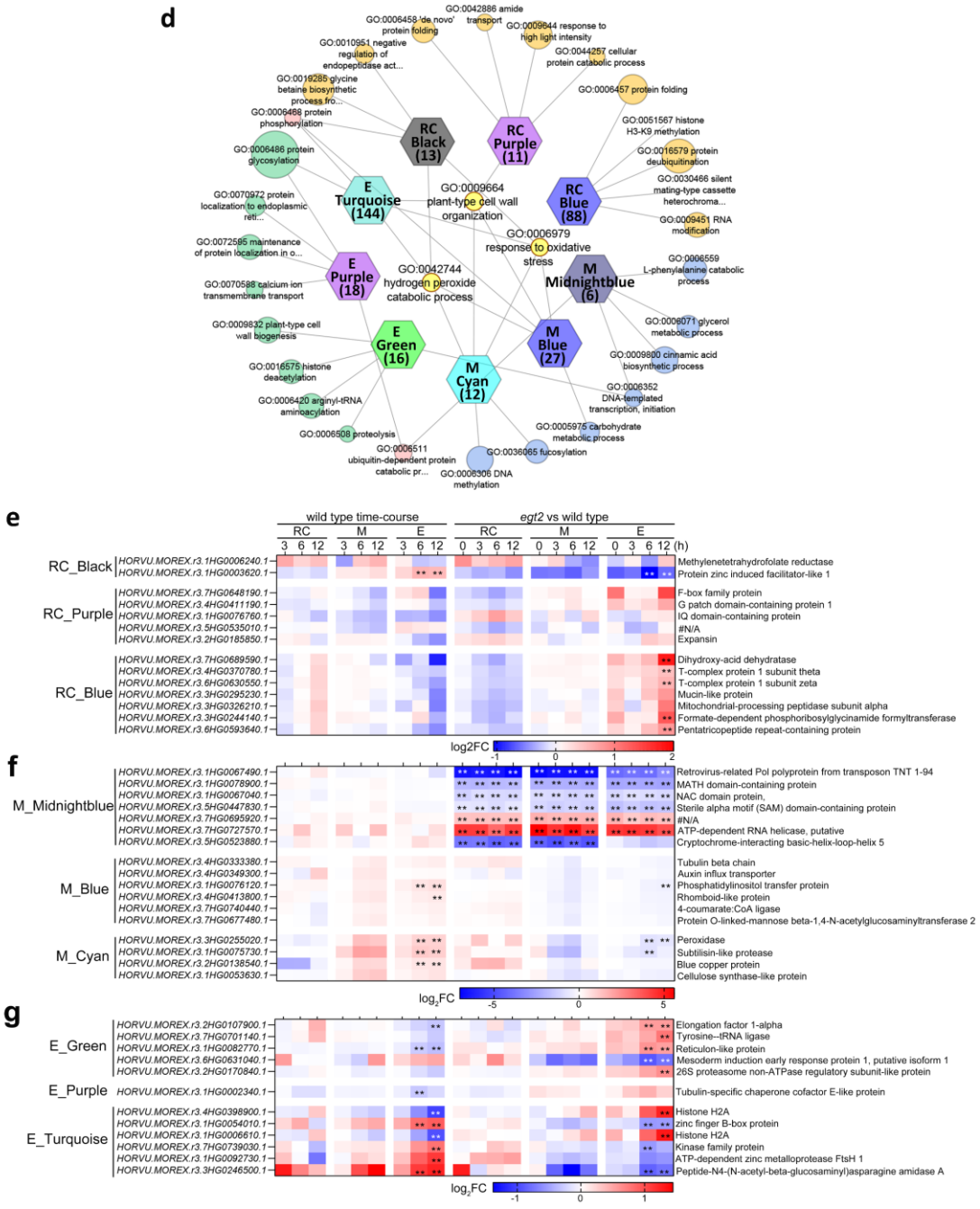

Fig. S6: Control experiments for bimolecular fluorescence complementation analyses of EGT2 and interaction candidates.

tagRFP: red fluorescence; YFP: yellow fluorescence; chloroplasts: auto-fluorescence of chloroplasts. nYFP: N-terminal part of YFP; cYFP: C-terminal part of YFP. EGT2 (+TGA): full-length coding sequence of EGT2; EGT2 (-TGA): coding sequence of EGT2 removed stop codon.

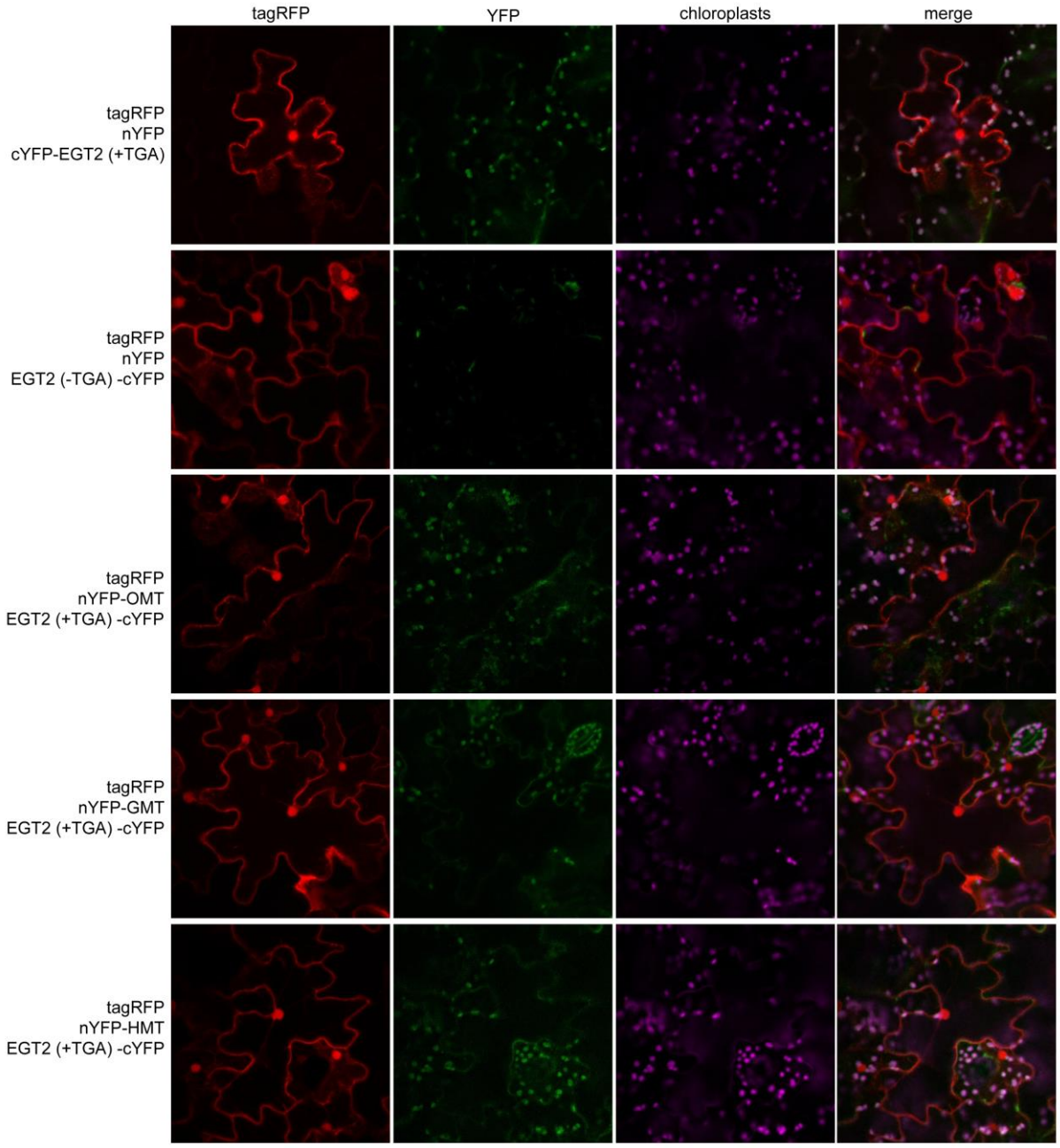

Acknowledgements

Firstly, I would like to sincerely thank Dr. Changzheng Xu for introducing me to Frank, which made everything here possible.

I am extremely grateful to my supervisor Prof. Dr. Frank Hochholdinger for providing me this wonderful opportunity to work on an interesting project about barley root development in this group, for his constant patience and support as well as his professional and helpful suggestions. Every discussion with Frank makes me learn something new and think more. I also greatly appreciate the opportunities to travel and present my work at conferences.

Sincere thanks to my second supervisor, Prof. Dr. Andreas Meyer, who provided me with valuable advice to think about my results in different directions and to come up with new ideas. I am also very grateful to Prof. Dr. Claudia Knief and Prof. Dr. Gabriel Schaaf for accepting my request to be in the committee. I would also like to thank the Bonn International Graduate School (BIGS) - Land and Food for advanced learning opportunities.

Many thanks also to our collaborators, especially Prof. Dr. Silvio Salvi and Serena Rosignoli (University of Bologna, Italy) for their close collaboration and thought-provoking scientific discussions.

Sincere thanks to all lab mates of the CFG and CS groups for their help and suggestions and for the enjoyable and scientific atmosphere of the group:

- Thank to Caro, Jutta, Micha, Yaping, Zhihui, Xiaoming, Verena, Alejandra, Mauritz, Marion, Danning, Liuyang, Boagang, Junwen, Ling, Zamiga. Many thanks to Marcel, Alina, Yan, Annika, Luca, Anna-Lena and José for their help and support with my experiments and other things.
- I would also like to sincerely thank Gwen for her patience and care in helping me to get to know the project and the lab during the first months of my PhD program.
- My sincere thank also goes to Peng, who always encouraged me and gave me many helpful suggestions when my experiments did not go well and I was frustrated.
- Thanks to Helmut, Britta, Christa, Claudia, Alexa and Selina for their valued technical support.
- Thanks to Christine Jessen and Ellen Kreitz for their administrative support.

Last but most importantly, I would like to sincerely thank my family and friends, especially my parents, my sister and brother in law, my niece and Qinglin for their constant support and care. This helps me to get rid of my bad moods and be more positive and energetic about life and work.

Publications

Kirschner GK*, Rosignoli S*, **Guo L***, Vardanega I, Imani J, Altmüller J, Milner SG, Balzano R, Nagel KA, Pflugfelder D, Forestan C, Bovina R, Koller R, Stöcker TG, Mascher M, Simmonds J, Uauy C, Schoof H, Tuberosa R, Salvi S, Hochholdinger F. (2021). *ENHANCED GRAVITROPISM 2* encodes a STERILE ALPHA MOTIF-containing protein that controls root growth angle in barley and wheat. ***Proceedings of the National Academy of Sciences of the United States of America*** 118. https://doi.org/10.1073/pnas.2101526118 (*: co-first authors)

Li Guo, Alina Klaus, Marcel Baer, Gwendolyn K. Kirschner, Silvio Salvi, and Frank Hochholdinger. (2023). ENHANCED GRAVITROPISM 2 coordinates molecular adaptations to gravistimulation in the elongation zone of barley roots. ***New Phytologist*** 237. https://doi.org/10.1111/nph.18717

Conference Participation

Li Guo, Alina Klaus, Marcel Baer, Gwendolyn K. Kirschner, Silvio Salvi, and Frank Hochholdinger. (2022). Identification of gravity regulated genes that encode direct interaction partners of barley ENHANCED GRAVITROPISM 2. 13th International Barley Genetics Symposium (IBGS13), July 3-7, 2022. Riga, Latvia (*Poster Presentation* and Flash & Dash *Oral Presentation*).

Li Guo & Frank Hochholdinger. (2022). *ENHANCED GRAVITROPISM 2* coordinates molecular adaptations to gravistimulation in the elongation zone of barley roots. Botanik-Tagung - International Conference of the German Society for Plant Sciences. Aug 28-Sep 1, 2022. University of Bonn, Germany (*Poster Presentation*).